corewind

Public design and FAST models of the two 15MW floater-turbine concepts

USTUTT/UPC/COBRA/ESTYCO/DTU

April 2020

Disclaimer:

This project has received funding from the European Union's Horizon 2020 Research and Innovation programme under grant agreement No 815083.

Project details:

Duration:
1 Sep 2019 - 28 Feb 2023
Grant agreement:
No: 815083

Document information

Deliverable number	D1.3
Deliverable name	Public design and FAST models of the two 15MW floater-turbine concepts
Reviewed by	V. Arramounet (Innosea), Friedemann Borisade (RAMBOLL)
Date	04.2020
Work Package and Task	1.3
Lead Beneficiary for this Deliverable	USTUTT

Authors

Name	Organisation	E-mail
Mohammad Youssef Mahfouz	USTUTT	mahfouz@ifb.uni-stuttgart.de
Mohammad Salari	USTUTT	salari@ifb.uni-stuttgart.de
Sergio Hernández	ESTEYCO	sergio.hernandez@esteyco.com
Fernando Vigara	ESTEYCO	fernando.vigara@esteyco.com
Climent Molins	UPC	climent.molins@upc.edu
Pau Trubat	UPC	pau.trubat.casal@upc.edu
Henrik Bredmose	DTU	hbre@dtu.dk
Antonio Pegalajar-Jurado	DTU	ampj@dtu.dk

Version control

Version	Date	Author	Description of Changes
Version 2	[2020-04-29]	Mohammad Youssef Mahfouz	Refinements and quality check
Version 1	[2020-04-08]	Mohammad Youssef Mahfouz	

Table of contents

Executive Summary

We present two floating OpenFAST models for the WindCrete spar and the ActiveFloat semi-submersible. The floaters are designed for the IEA Wind 15MW reference wind turbine. Moreover, Ultimate Limit State (ULS) load cases are selected for the mooring and dynamic cable design in COREWIND.

Both floaters and the changes needed in the numerical models to couple the floaters and the turbine are introduced. This includes the mooring system and the modified wind turbine control settings. The detailed structure of both models is explained, including hydrodynamics, mooring system, tower and modifications to the controller properties.

A preliminary verification of the models is done and the results are shown. The simulated responses are as expected and generally within the design limitations. The load cases include static offsets checks, natural frequencies, a step wind test and a subset of the IEC design load cases (1.3, 1.6, 2.1 and 6.1). The load cases are used to check the controller performance, as well as to check the dynamic response of the models in normal and severe environmental conditions. The OpenFAST models of both floaters will be available for free public download.

1 Introduction and objective

1.1 Introduction

This report introduces two new floating wind turbine configurations, both based on the new IEA Wind 15 MW reference wind turbine. The two floaters are a spar and a semi-submersible. The report is structured in the following way: First the new 15 MW turbine is introduced. Then the load cases are defined. Afterwards, the structural design and hydrodynamic properties of the spar platform, WindCrete, is introduced. Then the model demonstration of the design is done using OpenFAST model. Afterwards, the structural design and the hydrodynamic properties of the semi-submersible floater, Activefloat, is introduced. Finally, model demonstration of the Activefloat is done using OpenFAST similar as for WindCrete.

1.2 Objective

The goal of this report is to create and demonstrate two OpenFAST models for 15MW floating wind turbine on a spar and a semi-submersible floaters, and to have a preliminary verification of the models' performance. These models will be used afterwards through COREWIND, for optimization of mooring lines and cable to achieve the main project's goal of decreasing the LCOE of floating wind turbines.

2 Reference wind turbine

2.1 Wind turbine

The two floater concepts developed in COREWIND have been designed to support the IEA Wind 15 MW reference wind turbine [1, 2] shown in Figure 2-1. The key parameters of the turbine are given in Table 2-1. As it is clear in Figure 2-1 the reference turbine is an offshore turbine on a monopile structure. This means that the tower of the turbine will be adapted for each floater design. The tower height, tower thickness and tower mass is different for each model. The tower properties for the floaters are defines in sections 5.2.1 and 6.2 for WindCrete and Activefloat respectively.

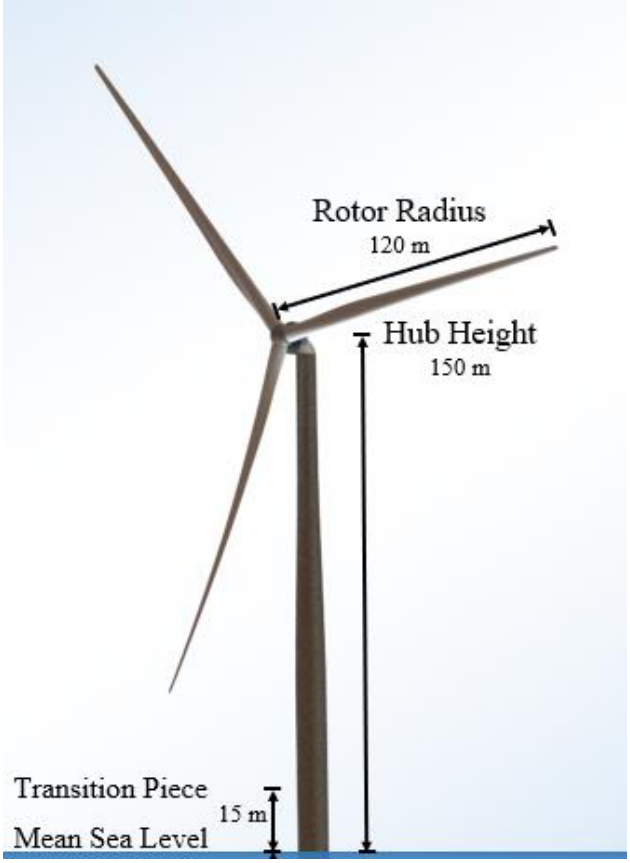

Figure 2-1: The IEA Wind 15MW reference wind turbine (Figure adapted from [1])

Table 2-1: Key properties of the IEA Wind 15MW reference wind turbine [1]

Rated power (MW)	15	Turbine class	IEC Class 1B
Cut-in wind speed (m/s)	3	Cut-out wind speed (m/s)	25
Rated wind speed (m/s)	10.59	Rated thrust (MN)	2.4
Rotor diameter (m)	240	Hub height above sea level (m)	150
Minimum rotor speed (rpm)	5.0	Maximum rotor speed (rpm)	7.56
Blade mass (t)	65	Rotor-nacelle assembly mass (t)	1017

2.2 Controller

It is well known that the wind turbine controller affects the dynamics of floating offshore wind turbines. Therefore the controller properties (such as gains) need to be designed for each floating concept to avoid the so-called “platform pitch instability” (see, for example, [3]).

In the power production mode of the IEA Wind 15 MW wind turbine, the controller provides a combination of variable speed generator torque control and collective blade pitch control. For below rated the variable speed generator torque controller ensures an optimal operation to achieve the maximum power. On the other hand, when the turbine operates at rated power or alternatively at rated torque, the collective pitch controller

regulates the rotor speed. In this report's simulations, the collective pitch controller aims to make the turbine work at constant power above rated wind speed.

The controller used here is a slightly modified version of the provided NREL Reference OpenSource Controller (ROSCO), which can be found in [4] . The ROSCO controller uses a Bladed-style controller DISCON interface. After compiling the controller, which is developed in Fortran, it can be configured/tuned using a single control setting parameter file [4]. For both the variable speed (VS) torque controller and the blade pitch controller, there are different parameters which can be set and tuned. The adopted baseline controller in [4] is originally developed for the NREL 5 MW and the DTU 10 MW reference wind turbines for which a tuning was needed to make it usable for the floating wind turbine. For the case of IEA Wind 15 MW, installed on WindCrete and ActiveFloat platforms, a tuning of the Proportional Integral (PI) gains for the collective pitch controller (CPC) was enough to achieve stability for the above rated region. Note that the PI controller for collective pitch uses a gain-scheduling method, with collective blade pitch as the scheduling parameter, to deal with different sensitivities of aerodynamic torque to pitch angle at different wind speeds [5].

More details on the controller adaptation for the floating wind turbine with WindCrete and ActiveFloat platforms can be found in sections 5.5 and 6.5, respectively.

2.3 Model accessibility

Further details of the IEA Wind 15 MW reference wind turbine on the monopile structure, including the OpenFAST and HAWC2 models, are available at the IEA Wind Task 37 GitHub https://github.com/IEAWindTask37/IEA-15-240-RWT. Details on the accessibility to the two OpenFAST models described in this report are given in Section 7.

3 Modelling approach

The numerical models described in this report were implemented in the open-source aero-hydro-servo-elastic tool OpenFAST v2.1 [6] For the present work, the OpenFAST bottom-fixed IEA 15 MW wind turbine has been adapted to the two floating concepts. This means that new input files for tower, controller, hydrodynamics and mooring system have been prepared. The reference frame used in both models uses the FAST convention reference frames.

3.1 Approach for hydrodynamic modelling

Hydrodynamic loads on the two floaters have been included as described below.

3.1.1 First-order hydrodynamic loads

When modelling a floating wind turbine in an aero-hydro-servo-elastic tool, it is common practice to compute the hydrodynamic properties (such as radiation added mass and damping, hydrostatics and wave excitation forces) in a radiation-diffraction solver (e.g. WAMIT [7] or ANSYS AQWA [8]). These frequency-dependent hydrodynamic properties are typically included in the time-domain equations of motion through the Cummins equation [9]. Further details on the radiation-diffraction theory and its coupling to OpenFAST can be found in [10] and [11], respectively.

3.1.2 Viscous effects

Viscous effects, which are not captured by potential-flow radiation-diffraction solvers, are usually included in the numerical model by means of the drag term in the Morison equation [12]. This term, which depends on the relative velocity between the wave particles and the floating structure, introduces both forcing and damping. An alternative approach to model viscous effects is to replace the Morison drag term by global linear and/or

quadratic damping matrices lumped at the flotation point. These matrices are often obtained experimentally or with higher-fidelity models such as computational fluid dynamics (CFD). This approach, however, neglects the forcing part of the Morison equation. In some cases, and especially when comparing to physical test results, a combination of Morison drag and lumped damping matrices is chosen to represent viscous effects on the floater (see, for example, [13]).

3.1.3 Second-order hydrodynamic loads

Second-order hydrodynamic loads occur at the sum and the difference frequencies of the linear wave spectrum. Although they are in magnitude smaller than linear loads, they are likely to excite the floater natural frequencies and cause fatigue for some components, e.g. the mooring system. Second-order hydrodynamic effects are often calculated in a radiation-diffraction solver in the form of Quadratic Transfer Functions (QTFs), and are coupled to the aero-hydro-servo-elastic model through a double sum over the range of frequencies [14].

3.2 Approach for mooring lines modelling

For the present models, the mooring systems are modelled with MoorDyn [15], a lumped-mass dynamic mooring model that captures dynamic effects such as line mass inertia, buoyancy, seabed contact and hydrodynamic forces on the line in still water. MoorDyn also allows modelling of multi-segmented mooring lines, including clump weights and buoyancy elements.

4 Load cases selection

The floating platforms are designed to fulfill the design constraints indicated in the Design Basis in [16] for the Canary Island site.

The main characteristics of the site are presented in the following table.

Table 4-1 - Canary Island Site. Key environmental parameters

Site Environmental key parameters	
Depth (m)	200.00
Vref at 135 m (m/s)	40.68
Wind speed 10-min at 135 m (m/s)	12.26
Hs (Tr=50-y) (m)	5.11
Tp (Hs=5.11 m) (s)	9.0 - 11.0
Most probable Hs (m)	1.50

4.1 Excursion and acceleration limits

The excursion and acceleration limits in Table 4-2 are the limits compared to the responses shown later in sections 5.6 and 6.6.

Table 4-2: Excursion and acceleration limits

Limit for	Windcrete	Activefloat
OPERATION		
Yaw (10 min. max)	<15º	
Yaw (10 min. std)	<3º	
Pitch (max.)	[-5.5º, +5.5º]	[-5.0º, +5.0º]
Pitch (10 min. average)	[-4.0º, +4.0º]	[-2.0º, +2.0º]

Roll (max.)	[-3.5º, +3.5º]	[-2.0º, +2.0º]
Pitch (10 min. std)	<1º	
Roll (10 min. std)	<1º	<0.4º
IDLING CONDITION		
Pitch (10 min. average)	[-5º, +5º]	
Pitch (10 min. max)	[-7º, +7º]	
EMERGENCY STOP		
Max. pitch	[-15º, +15º]	

EXCURSION RESTRICTIONS	
Horizontal offset (alarm limit) (mean during operation)	15 m
Horizontal offset (WTG shutdown). Maximum during parked conditions	30 m

ACCELERATIONS LIMITS		
Operation (acc. XY / acc. Z)	2.8 m/s^2 (0.28g)	1.85 m/s^2 (0.18 g)
Survival (acc. XY / acc. Z)	3.5 m/s^2 (0.35g)	2.94 m/s^2 (0.3 g)

4.2 Models preliminary verification

Representative load cases were selected to check the time and frequency domain responses of both floating systems. First, decay tests were done to identify the natural frequencies of the floaters in surge, heave, pitch and yaw platform degree of freedom. Results are checked with provided design values from the substructure designers. They are followed by free decay simulations of the tower in both fore-aft and side to side degrees of freedom, during this decay test all other degrees of freedom were not blocked. The goal is to make sure that the tower's natural frequency is higher than the 3P frequency. Moreover, the equilibrium state of the floaters is evaluated in the absence of wind and wave. Afterwards, simulations of regular waves in the absence of wind are done. The controller performance was checked through running a step wind simulation. The step wind simulation starts at 3m/s and increases 1m/s every 200s to reach 25m/s, then decreases again 1m/s every 200s till it gets back to 3m/s. Finally, representative cases of DLCs 1.3, 1.6, 2.1, and 6.1 [17] were carried on to check the performance of the floating wind turbine at different sea states, wind turbulence and sudden grid loss.

The values for extreme wind and waves as well as the wind-wave relationships were chosen based on values from [16] for the Gran Canaria site. The turbulence class was chosen following the turbine's class shown in [1]. Pierson-Moskowitz spectrum is used to model the irregular waves while including the effect of second order waves and forces at irregular sea states.

Table 4-3: Load cases used for models verification

Name	Duration [s]	Waves	Wind [m/s]	Turbine
Surge decay	1500	-	-	Parked
Heave decay	1500	-	-	Parked
Pitch decay	1500	-	-	Parked

Yaw decay	1500	-	-	Parked
Tower decay	1500	-	-	Parked
Static equilibrium	1500	-	-	Parked
Regular Waves	1500	Regular H_s = 2 m, T_p = 6 s	-	Parked
Step wind	9200	-	Steady wind; 3-25-3 m/s	Operational Active control
DLC1.3	5400	Irregular; Hs=2m, Tp=6s	Turbulent ETM; 8, 10.5, 16, 20, 25 m/s	Operational Active control
DLC1.6	5400	Irregular; Hs=5.11m, Tp=9s	Turbulent NTM; 8, 10.5, 16, 20, 25 m/s	Operational Active control
DLC2.1	600	Irregular; Hs=2m, Tp=6s	Turbulent NTM; 20 m/s	Grid loss Shutdown control
DLC6.1	5400	Irregular; Hs=5.11m, Tp=9s	Turbulent EWM50; 41.2 m/s	Idling Active control

4.3 Load cases for mooring design

ULS load cases are selected for the mooring and dynamic cable design within Task 2.2. DLC 6.1 and 6.2 are studied for this specific purpose as they generate large platform offsets and dynamic motions. Studied DLC characteristics are provided in Table 4-4 below.

Mooring and cable design will be done for the three sites Gran Canaria, West of Barra and Morro Bay.

Table 4-4 Load cases used for mooring & dynamic cable design

Name	Wind	Waves	Wind & Wave misalignment	Current	Water level	Turbine	Duration
DLC 6.1	EWM turbulent wind (TI 11%) 50 years return period	ESS Irregular waves 50 years return period 6 wave seeds	-30°, 0° & 30°	ECM 50 years return period	EWLR	Parked -8°, 0 & 8° yaw misalignment	3600s

DLC 6.2	EWM turbulent wind (TI 11%) 50 years return period	ESS Irregular waves 50 years return period 6 wave seeds	-30°, 0° & 30°	ECM 50 years return period	EWLR	Parked -150°, -120°, -90°, -60°, 30°, 0°, 30°, 60°, 90°, 120°, 150° & 180° yaw misalignment	3600s

5 WindCrete spar floater FAST model

5.1 Platform design

The design of the WindCrete platform is based on a first static predesign to assess the main platform characteristics in order to verify the design basis. The predesign basis are to present a static pitch due to the maximum thrust force of the turbine less than 4 deg., and the natural motions periods of the platform, in heave, pitch and roll to have a value above 30s. Moreover, the relations of draft, diameter and thickness of the substructure and tower ensures the structural response of the platform and the disposition of the reinforcement steel and the posttensioning.

The hub height of the platform is adjusted to 135 m above sea level, which is lower than the IEA-15MW which is set to 150m, according to the following constraints referred to Gran Canaria location based on IEC 61400-3-2 standard [18]: 1) Access platform to be out of the reach of the 50-years wave crest; 2) Minimum air gap of 20% of Hs or 1.50 meters, whichever is larger; 3) Hub height to be 6 meters plus the semi-rotor diameter. The 6 meters allowance is for an operating crane located at the access platform. The tower height is 129.495 m in order to have a hub height of 135 m.

The tower in the WindCrete design is a tapered cylinder made of concrete with a constant thickness of 0.4m. The tower base, which is defined at the mean sea level (MSL), has a diameter of 13.2m, and the top tower diameter of 6.5m is the same as the IEA design, to ensure the connection with the wind turbine.

The substructure consists of a tapered transition piece of 10m length, a cylindrical spar of 135.7m length and a hemisphere of 9.3m radius at the bottom of the substructure. Then, the total draft of the platform is 155m. The cylindrical spar has a diameter of 18.6m and the tapered transition piece has a top diameter of 13.2 and a bottom diameter of 18.6m. The Figure 5-1 shows a sketch of the WindCrete with its main dimensions in meters. The origin of the reference system used in the WindCrete description and its mooring system is set at the MSL, in the intersection with the WindCrete axis of symmetry, that coincides with the tower base on its undisplaced position.

The required hydrostatic stiffness in the pitch/roll degree of freedom is achieved by adding a solid aggregate ballast at the platform keel with a bulk density of 2500 kg/m3. The internal height of the ballast is of 44.15m from the keel. In Figure 5-1 the aggregate ballast is colored in brown.

The Table 5-1 shows the main characteristics of the WindCrete platform, including tower and substructure with the ballast. The Table 5-2 shows the hydrostatic properties of the buoy and the expected natural periods using approximated values of the added mass terms, the mass of a hemisphere at the bottom for the heave motion and the inertia produced by the displaced volume for pitch/roll motion.

Regarding the static pitch for the rated wind, a static mean pitch of 3.2 deg is expected for a mean thrust of 2.376E+03 kN and accounting the favorable action of the center of mass of the wind turbine, which is located in windward direction.

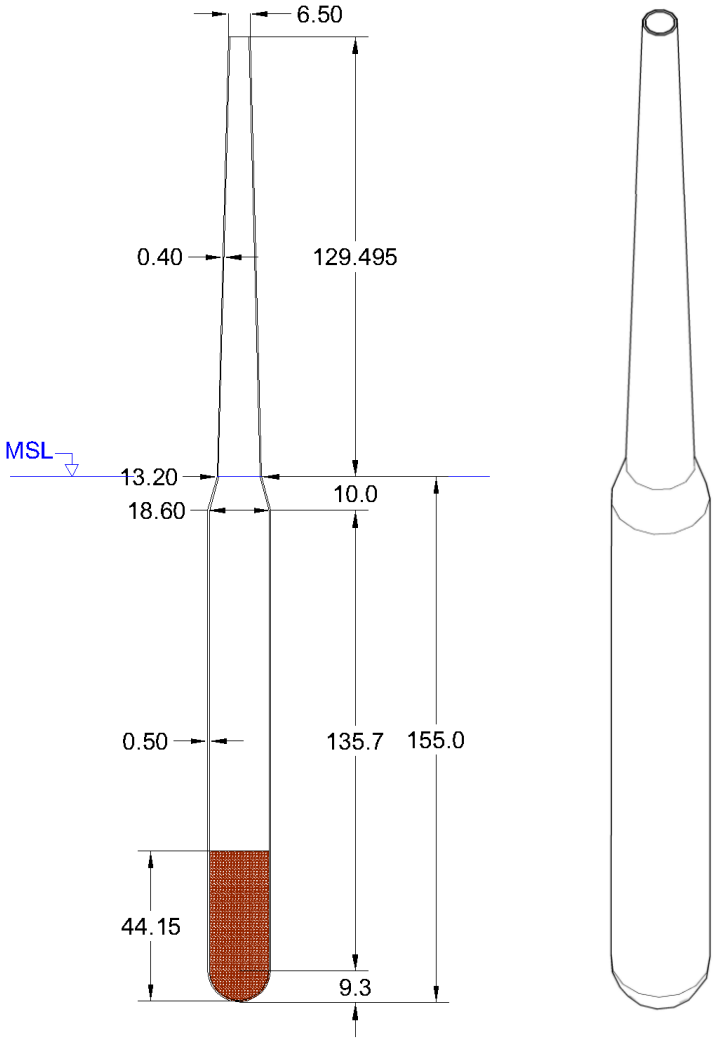

Figure 5-1: WindCrete sketch (values in meters)

Table 5-1: WindCrete main properties

WindCrete Properties	
Mass [kg]	3.9805e+07
Center of Mass (CM) Height [m]	-98.41
Ixx [kg·m^2] from CM	1.5536e+11
Iyy [kg·m^2] from CM	1.5536e+11
Izz [kg·m^2] from CM	1.9025e+09

Table 5-2: WindCrete hydrostatic properties

WindCrete Hydrostatic Properties	
Displacement [m3]	4.054e+04
Center of Buoyancy Height [m]	-77.29
C_{33} [N/m]	1.3746e+06
C_{44} [N·m/rad] from [0;0;0]	-3.1463e+10
C_{55} [N·m/rad] from [0;0;0]	-3.1463e+10
A_{33} [kg] from CM	1.727e+06
A_{55} [kg·m^2] from CM	8.964e+10
T_3 [s]	35
T_5 [s]	41

5.2 FAST model

In order to model the WindCrete platform in FAST, the tower and the substructure have to be defined separately. The tower base height set in the WindCrete FAST model preserves the tower base height of the monopile model to support the IEA-15 MW reference wind turbine. However, the tower height is reduced to 129.495m as explained in section 5.2.1. Then, in the WindCrete FAST model the lower part of the tower is included in the substructure. The Figure 5-2 shows a sketch of the separation between the tower and substructure modeled in FAST.

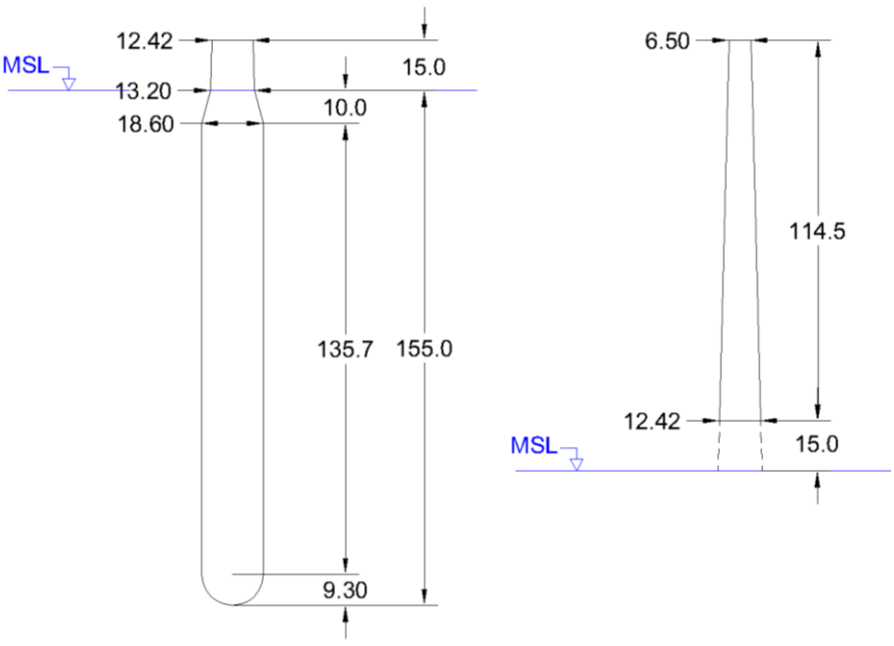

Figure 5-2: FAST Substructure and Tower (values in meters)

5.2.1 Tower

The elastic tower model in FAST is discretized in 20 sections from the bottom to the top. The physical properties of each node based on the tower height fraction are shown in Table 5-3. The overall stiffness of the tower ensures a stiff-stiff behavior against the 1P and 3P rotor frequencies.

Table 5-3: Physical properties of WIndCrete Tower

Height Fraction [u]	Tower Mass Density [kg/m]	Tower FA Bending Stiffness [Nm^2]	Tower SS Bending Stiffness [Nm^2]
0	3.776194E+04	9.918269E+12	9.918269E+12
0.05	3.683203E+04	9.203955E+12	9.203955E+12
0.1	3.590212E+04	8.524801E+12	8.524801E+12
0.15	3.497221E+04	7.879919E+12	7.879919E+12
0.2	3.404230E+04	7.268423E+12	7.268423E+12
0.25	3.311239E+04	6.689423E+12	6.689423E+12
0.3	3.218248E+04	6.142033E+12	6.142033E+12
0.35	3.125256E+04	5.625365E+12	5.625365E+12
0.4	3.032265E+04	5.138531E+12	5.138531E+12
0.45	2.939274E+04	4.680643E+12	4.680643E+12
0.5	2.846283E+04	4.250814E+12	4.250814E+12
0.55	2.753292E+04	3.848156E+12	3.848156E+12
0.6	2.660301E+04	3.471781E+12	3.471781E+12
0.65	2.567310E+04	3.120801E+12	3.120801E+12
0.7	2.474318E+04	2.794330E+12	2.794330E+12
0.75	2.381327E+04	2.491478E+12	2.491478E+12
0.8	2.288336E+04	2.211359E+12	2.211359E+12
0.85	2.195345E+04	1.953085E+12	1.953085E+12
0.9	2.102354E+04	1.715768E+12	1.715768E+12
0.95	2.009363E+04	1.498520E+12	1.498520E+12
1	1.916372E+04	1.300453E+12	1.300453E+12

To compute the aerodynamics loads on the tower, its diameter is defined every 10 meters, which leads to 13 points tower discretization. Table 5-4 shows the relation with the tower elevation and the tower diameter at each point.

Table 5-4: Aerodyn tower sections

Tower Elevation [m]	Tower Diameter [m]	Cd
15	12.42	1
25	11.90	1
35	11.39	1
45	10.89	1
55	10.35	1

65	9.83	1
75	9.32	1
85	8.80	1
95	8.28	1
105	7.77	1
115	7.25	1
125	6.73	1
129.495	6.5	1

5.2.2 Substructure

The substructure in FAST is modeled as a rigid body defined by its properties from the center of mass of the floater. The Table 5-5 shows the properties of the FAST WindCrete substructure including the ballast.

Table 5-5: WindCrete Substructure FAST properties

WindCrete Substructure FAST properties	
Total mass [kg]	3.655e+07
Concrete mass [kg]	1.148e+07
Ballast mass [kg]	2.507e+07
Center of Mass (CM) Height [m]	-113.08
Ixx [kg·m^2] from WindCrete Substructure CM	5.590e+10
Iyy [kg·m^2] from WindCrete Substructure CM	5.590e+10
Izz [kg·m^2] from WindCrete Substructure CM	1.828e+09

5.3 Hydrodynamic model

The hydrodynamics of the WindCrete spar model are inertia dominated and the potential flow (PF) theory is applicable. Then, the PF model is applied for the wave inertia hydrodynamic forces, wave diffraction effect and radiation. The WAMIT files, which are needed for the HydroDyn module, are derived by converting the ANSYS-AQWA potential-flow solution outputs to WAMIT output files format. The linear potential flow problem is solved with the platform in its equilibrium position, with a draft of 155m. The reference point is located at [0;0;0], which is the intersection between the platform axis and the MSL.

Moreover, drag forces are applied through the Morison equation that is included to account for viscous forces.

5.3.1 First order hydrodynamics

The first order hydrodynamic waves forces are assessed through the PF solution from ANSYS-AQWA. Figure 5-3 shows the wave excitation force and moment per unit amplitude for the WindCrete. The results are presented using the number of each degree of freedom: 1 for the x, 2 for y, 3 for z, 4 for the rotation in x, 5 for the rotation in y and 6 for the rotation in z.

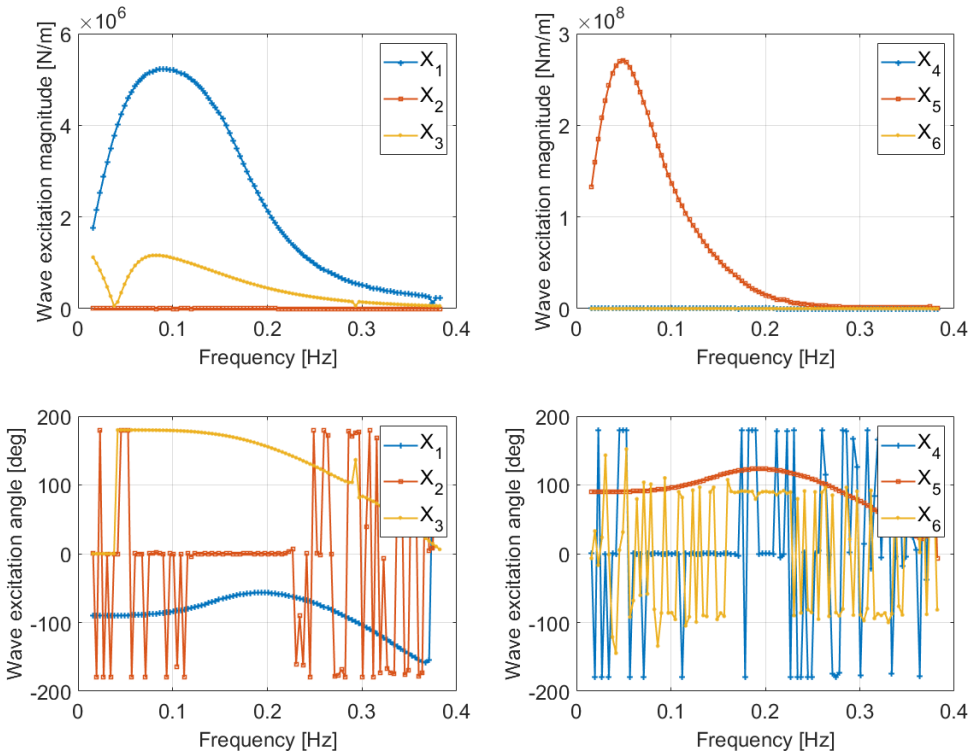

Figure 5-3: WindCrete first order wave excitation forces and moments computed with ANSYS-AQWA (Results for 0º wave heading direction

5.3.2 Radiation solution

The radiation solution of the potential flow problem is shown in Figure 5-5 .Moreover, the added mass matrix at infinite frequency is shown in Eq. (5.1) in kg for the ij = {11, 22 and 33} terms, in kg.m for the ij {15, 24, 51 and 42} terms and in kg.m^2 for the ij = {44, 55, and 66} terms.

$$A_\infty = \begin{bmatrix} 3.7354e+07 & 0 & 0 & 0 & -2.9637e+09 & 0 \\ 0 & 3.7354e+07 & 0 & 2.9637e+09 & 0 & 0 \\ 0 & 0 & 1.2657e+06 & 0 & 0 & 0 \\ 0 & 2.9637e+09 & 0 & 2.9156e+11 & 0 & 0 \\ -2.9637e+09 & 0 & 0 & 0 & 2.9156e+11 & 0 \\ 0 & 0 & 0 & 0 & 0 & 9.3145e+01 \end{bmatrix} \quad \textbf{(5.1)}$$

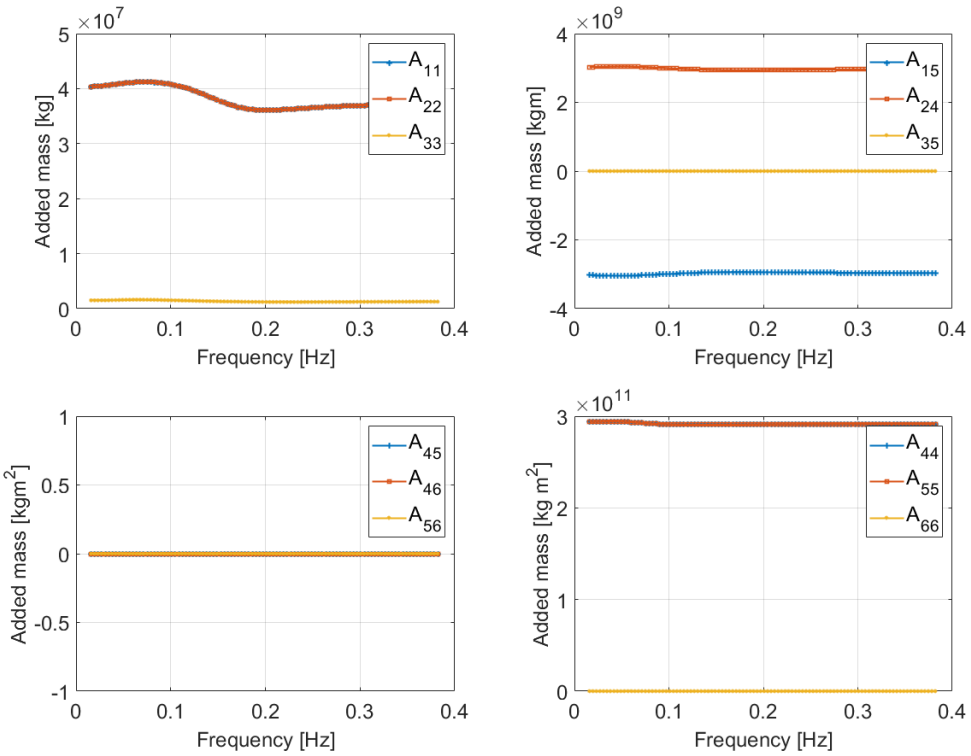

Figure 5-4: WindCrete hydrodynamic added mass from ANSYS-AQWA

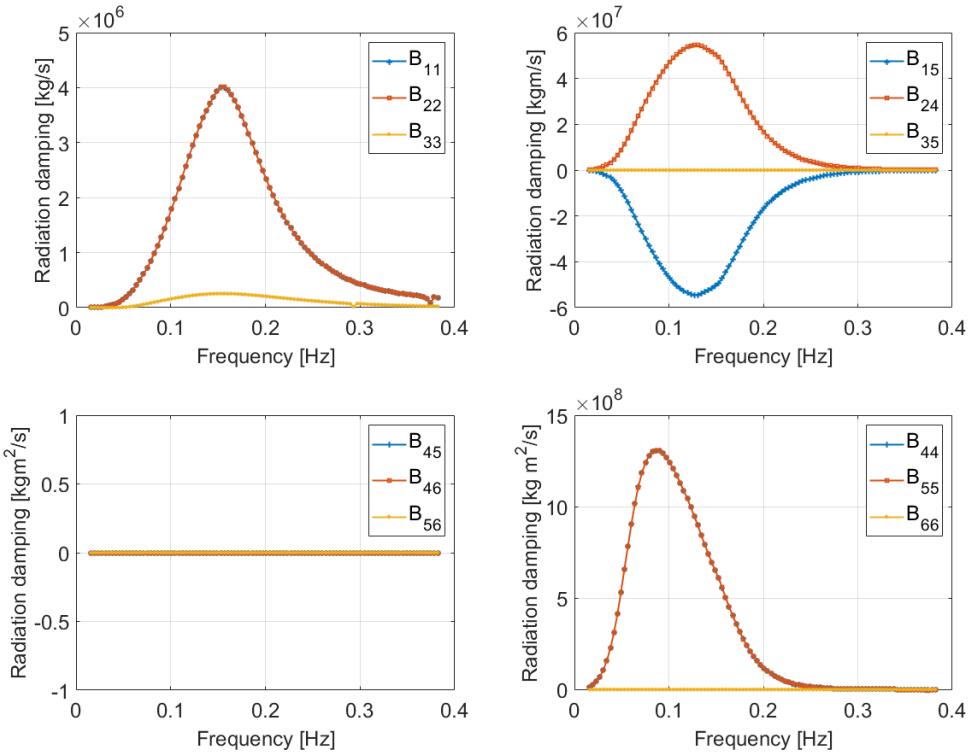

Figure 5-5: WindCrete hydrodynamic potential damping from ANSYS-AQWA

5.3.3 Viscous forces

The viscous forces are modelled using the drag term of the Morison equation in the FAST Hydrodyn model. The viscous forces are applied at the transverse motion of the substructure and at the bottom of the cylinder in the vertical motion.

The transverse drag coefficient is set to 0.7, constant in all the length of the submerged substructure. The value of the drag coefficient is a commonly used value in the literature [19], and was obtained in the scale experiments of the 5MW WindCrete platform [20].

The axial drag coefficient is set to 0.2 due to low resistance produced by the hemispheric bottom section. The value is estimated from the lower bound of the drag coefficients of cylindrical bodies in axial flow with streamlined head forms [21] as shown in Figure 5-6.

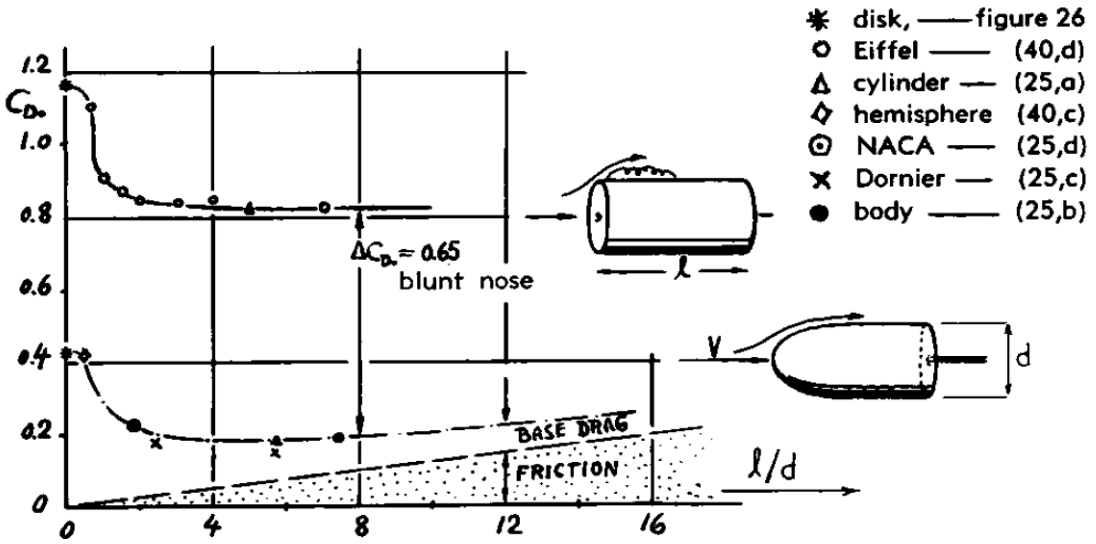

Figure 5-6: Drag coefficients for cylindrical bodies in axial flow [21]

5.3.4 Second order forces

The second order forces are related to the wave's nonlinear effects which can excite the low frequency motions of the platform, mainly the surge and sway. These loads are proportional to the wave amplitude squared and they are related to the effect of a pair of waves with different frequencies. An AQWA diffraction analysis can calculate the two contributions to this type of loads, difference frequencies and sum frequencies terms.

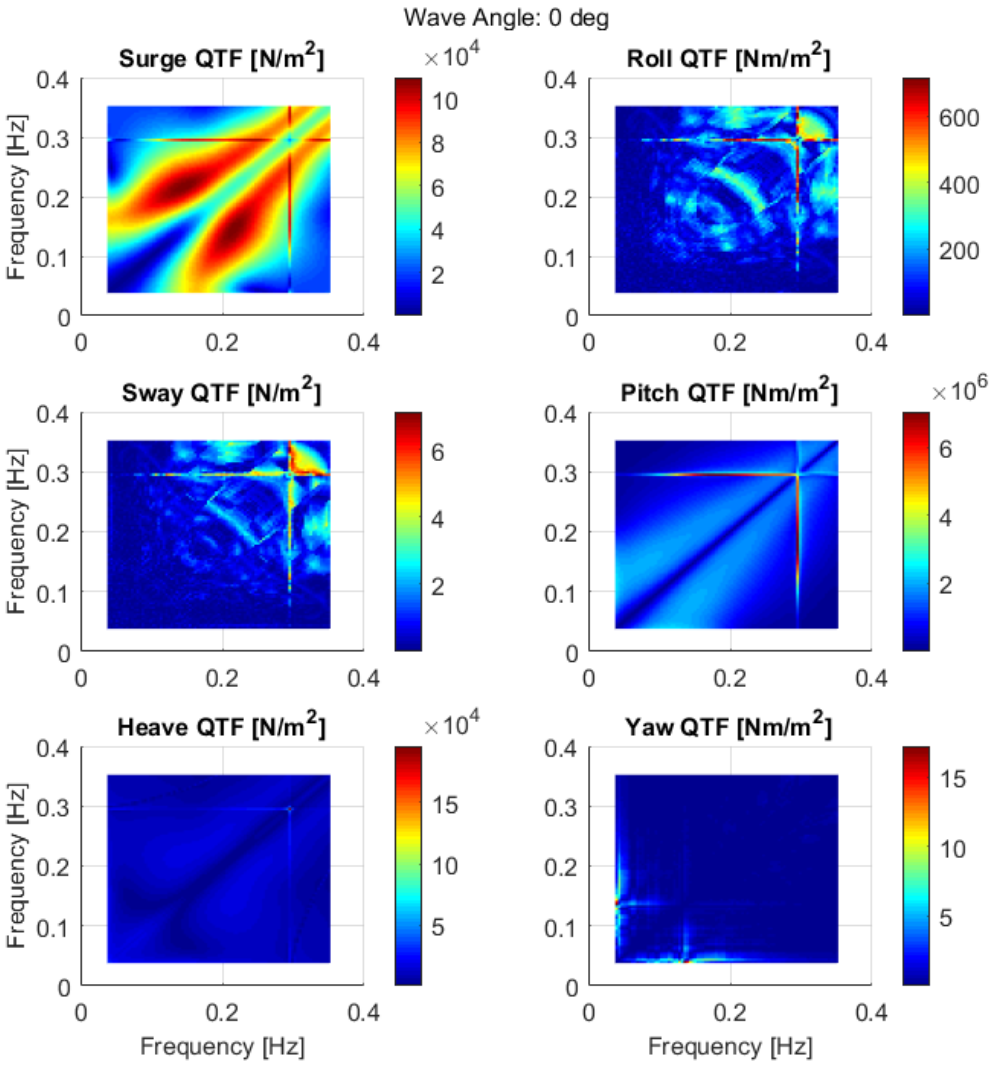

Figure 5-7: Difference Quadratic Transfer unction (QTF) for wave direction = 0 deg

5.4 Mooring line model

The mooring line model is a preliminary design set for the WindCrete placed in the Gran Canaria island location in a 200m water depth. The aim of the predesign is to withstand the external forces, the wind and the waves, and to provide enough stiffness to the system. However, the system is not verified against the ULS and FLS because this is not the aim of this report. The mooring line system design will be optimized further through COREWIND in Work Package 2. The mooring lines are modelled with MoorDyn FAST module.

The mooring system is designed as a three single catenary mooring shape line composed by one type of chain. At the top of the mooring system, the lines are equipped with the crowfoot system (delta connection) to provide enough yaw stiffness to the platform. Moreover, the mooring system is intended to avoid uplifting forces at the anchor. The fairleads are located at a 90m depth and the radius to anchor is set to 600m. The length of the main line is of 565m, and the length of the delta lines is of 50m. The physical properties of the chain and its hydrodynamic coefficients are presented in Table 5-6. The position of the fairleads and the anchors for each mooring line are shown in Table 5-7. The mooring system is designed in order to provide a stiffness to the surge

and yaw DOFs that ensures a surge and yaw natural periods about 80 and 10 seconds, respectively. The surge stiffness is of 5.0523e+05 N/m and the yaw stiffness is of 5.1545e+08 N·m/rad. These stiffnesses lead to a surge natural period of about 82 s and a yaw natural period of about 12s. The Figure 5-8 shows the surge, sway and heave forces of the mooring system against a surge motion of the platform.

Table 5-6: Chain characteristics

Parameter	Value
Nominal diameter [mm]	160
Dry mass per meter length [kg/m]	561.25
Stiffness EA [N]	2.3040e+09
Main line length [m]	565
Delta line length [m]	50

Table 5-7: Mooring system anchors and fairlead location

Line #	Anchor coordinates [m]			Fairlead coordinates[m]		
	X	Y	Z	X	Y	Z
1	-600	0.0	-200	-4.65	8.05	-90.0
				-4.65	-8.05	-90.0
2	300	-519.61	-200	-4.65	-8.05	-90.0
				9.3	0.0	-90.0
3	300	519.61	-200	9.3	0.0	-90.0
				-4.65	8.05	-90.0

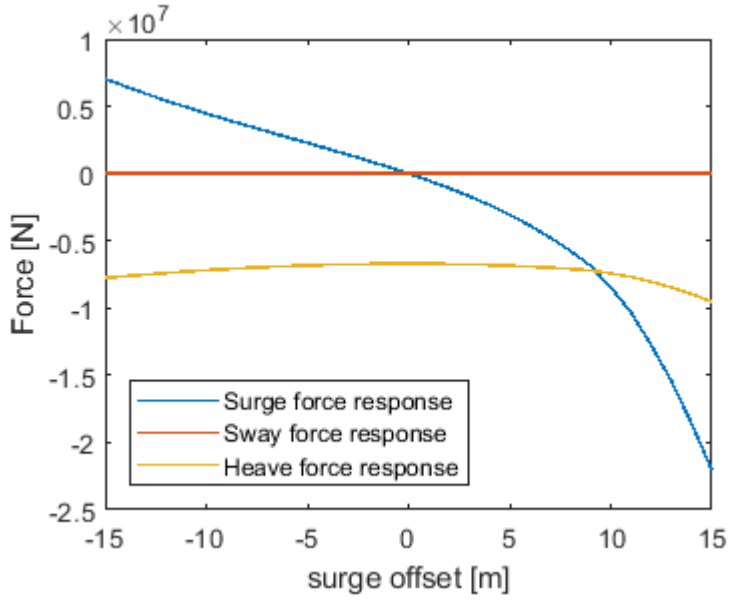

Figure 5-8: Mooring system response against surge motion

5.5 Controller adaptation

As it has been mentioned in the section 2.2, an adaptation of the baseline controller ROSCO [4], which is originally developed for an onshore wind turbine, was needed for the turbine installed on a floating platform. We started with the adaptation of the controller for the WindCrete platform to achieve stability and acceptable performance in the entire power production regions.

We noticed that the original collective pitch PI controller failed to achieve stability for some constant wind speeds above rated. As a first try we tuned the controller gains for the operating point corresponding to wind speed 13 m/s. The tuning was based on the well-known Ziegler–Nichols tuning method. After tuning the gains for this point an update of the vectors of K_p and K_I for other operating points is carried out. Based on the Ziegler-Nichols method for PI controller tuning we first chose an integral gain k_i equal zero, and then we increase the proportional gain k_p until we reach the ultimate gain at which the closed loop system is on its stability limit. This can be checked by plotting the generator speed for a constant wind v_0 = 13 m/s and see for which proportional gain the generator speed oscillates stable and with constant amplitude. We then select the proportional and integral gains for this operating point, i.e. $k_{p_{new}}^{13}$ and $k_{i_{new}}^{13}$ as follows:

$$k_{p_{new}}^{13} = 0.45\, k_{ul} = -0.2804$$

$$k_{i_{new}}^{13} = 0.54 \frac{k_{ul}}{T} = -0.0070$$

in which k_{ul} is the ultimate gain, and T is the oscillation period of the generator speed at ultimate gain, see the following plot.

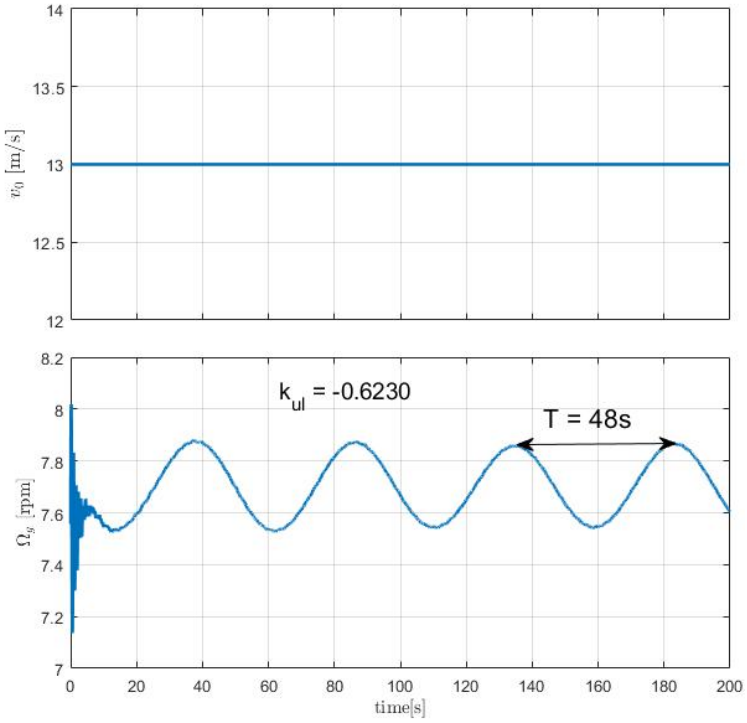

Figure 5-9: Tuning the PI controller gain for the operating point corresponding to v0=13m/s using Zeigler-Nichols method

We then compare this obtained PI gains with the original ones at the same operating point and apply the same scaling to all the PI gains of gain-scheduling controller for other operating points overrated:

$$d_{k_p} = \frac{k_{p_{new}}^{13}}{k_{p_{original}}^{13}}$$

$$d_{k_i} = \frac{k_{i_{new}}^{13}}{k_{i_{original}}^{13}}$$

$$K_{P_{new}} = d_{k_p} . K_{p_{original}} \ , \qquad K_{i_{new}} = d_{k_i} . K_{i_{original}}$$

In the above equations, $k_{p_{original}}^{13}$ and $k_{i_{original}}^{13}$ are the original proportional and integral gains corresponding to wind speed 13 m/s and $k_{p_{new}}^{13}$ and $k_{i_{new}}^{13}$ are the tuned ones as before. d_{k_p} and d_{k_i} are the calculated scales which can be used to find the new vectors of PI gains $K_{P_{new}}$ and $K_{i_{new}}$ for all operating points for overrated from the original proportional and integral vectors $K_{p_{original}}$ and $K_{i_{original}}$. The following figures show the tuned gains comparing to the original ones.

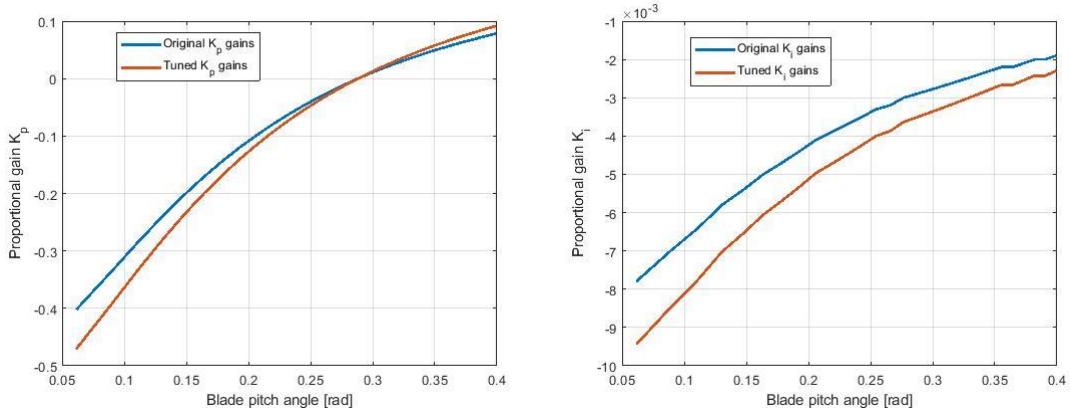

Figure 5-10: Tuned gains of the PI controller comparing to the original ones, scheduled over the blade pitch angle

A preliminary check for the controller performance can be seen in Figure 5-13 and Figure 6-14 for WindCrete and ActiveFloat respectively. Here we should mention that an optimization of the controller for the entire of the power production operating points is scheduled for the future.

5.6 Simulation results

Simulations shown in Table 4-3 are done to identify the system properties. We will show the outputs of these simulations in the following sections for WindCrete floater.

5.6.1 Static Equilibrium

First, we ran a static equilibrium simulation to identify the offsets in heave pitch and surge in the absence of wind and waves. The goal is to make sure that the system is balanced and the global mass and net buoyancy match each other.

The offsets especially in pitch and surge are because the CG of the tower top mass has an offset from the tower axis.

Table 5-8: Offsets of the platform in the 6 DOFs at sea water level

Surge [m]	Sway [m]	Heave [m]	Roll [deg]	Pitch [deg]	Yaw [deg]
-1.01	0.0	- 0.16	0.0	-0.64	0.0

5.6.2 Free Decays

We then ran decay tests for surge, heave, pitch and yaw DOFs. We managed to calculate the natural frequencies of these DOFs and are listed in Table 5-9. For every DOF an initial displacement was introduced, and the system was left to oscillate freely in the absence of wind and wave. The mooring lines were attached to the system during all decay simulations.

The Figure 5-11 and Figure 5-12 show the free decay tests for the surge and heave response of the WindCrete. In Figure 5-11 the surge motion does not follow a simple decay system because the surge motion is coupled with the pitch motion since the platform reference node at [0,0,0] does not correspond to the center of rotations of the platform.

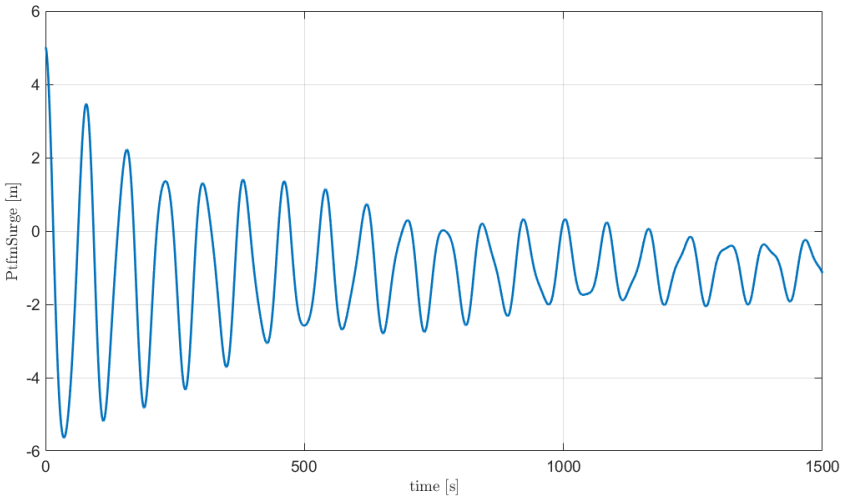

Figure 5-11: Surge decay of WindCrete floater

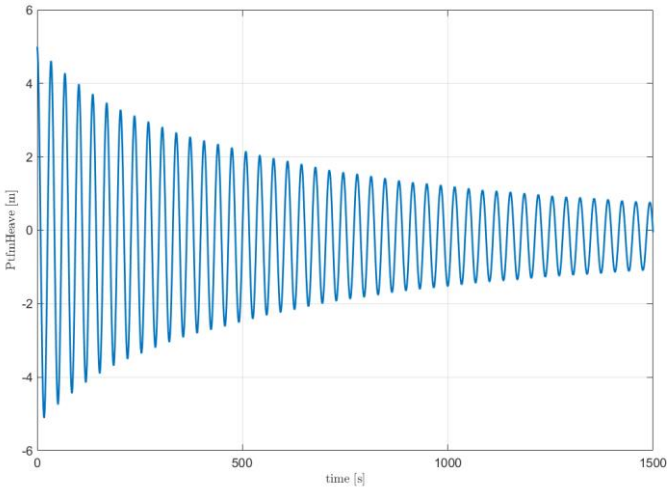

Figure 5-12: Heave decay of WindCrete floater

Table 5-9: WindCrete's natural frequencies in surge, heave, pitch and yaw

	Surge	Heave	Pitch	Yaw
Frequency [Hz]	0.01221	0.03052	0.02441	0.09155
Period [s]	81.9	32.77	40.97	10.92

Moreover, we also did tower decay test for in both side to side and fore-aft DOFs, for the floating moored configuration. The decay test is performed by imposing an initial tower-top displacement in the ElastoDyn FAST file of the floating WindCrete model. The goal is to check that the tower's natural frequencies lie outside the 1P and 3P frequencies, to avoid resonance between the tower and the blade. From [1], the 1P frequency range of [0.0833 to 0.1260] Hz and a 3P range of [0.25 to 0.378] Hz is set as reference. The tower side to side and fore-aft natural frequencies are shown in Table 5-10. The tower's frequencies are outside the 1P and 3P frequencies range.

Table 5-10: WindCrete's tower natural frequencies (first modes)

Tower side to side [Hz]	Tower fore-aft [Hz]
0.5127	0.4944

5.6.3 Step Wind

We used step wind field of steady wind velocities, in the absence of waves to check the controller's performance. The wind field started at 3m/s and increased, with 1m/s step, till 25m/s then back to 3m/s also with 1m/s step. The duration of the step is 200s for every wind speed.

Figure 5-13 shows that the controller is performing properly for all degrees of freedom except for heave. Every time the wind speed increases all degrees of freedom starts oscillating with their natural frequency until they reach the steady state. However, for heave there is a low decay ratio in the simulation. The reason for such oscillation may be coming from the limited heave damping of the platform in the linear region for low heave amplitudes when the movement is centimetric. Successive steps in the wind speed introduce pitch changes which simultaneously induce variation of the vertical loads due to the thrust of the wind turbine. That excitation is not completely damped in the 200 seconds between each wind step (that is less than 9 cycles for that vibration).

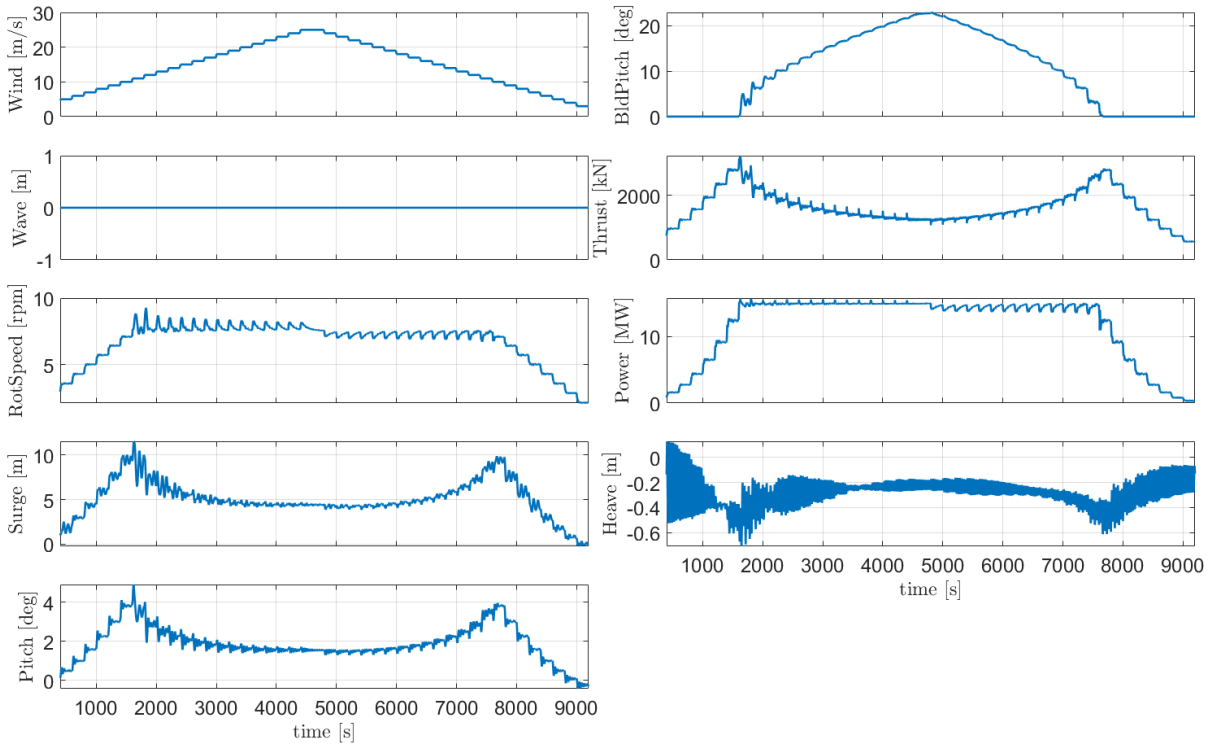

Figure 5-13: Timeseries response of WindCrete to stepwind

5.6.4 Regular waves

The next and last step for the WindCrete system identification is regular wave simulation. In the absence of wind, we simulated the floating wind turbine with the regular waves of height (H) = 2m and period (T) of 6s. These wave characteristics were taken from the Gran Canaria site characteristics in [16].

The time series for the floating response is shown in Figure 5-14. The turbine response is stable for all degrees of freedom. The thrust force shown in the figure is the force along the shaft of the turbine (including inertia effects), because of this the thrust is not equal to zero.

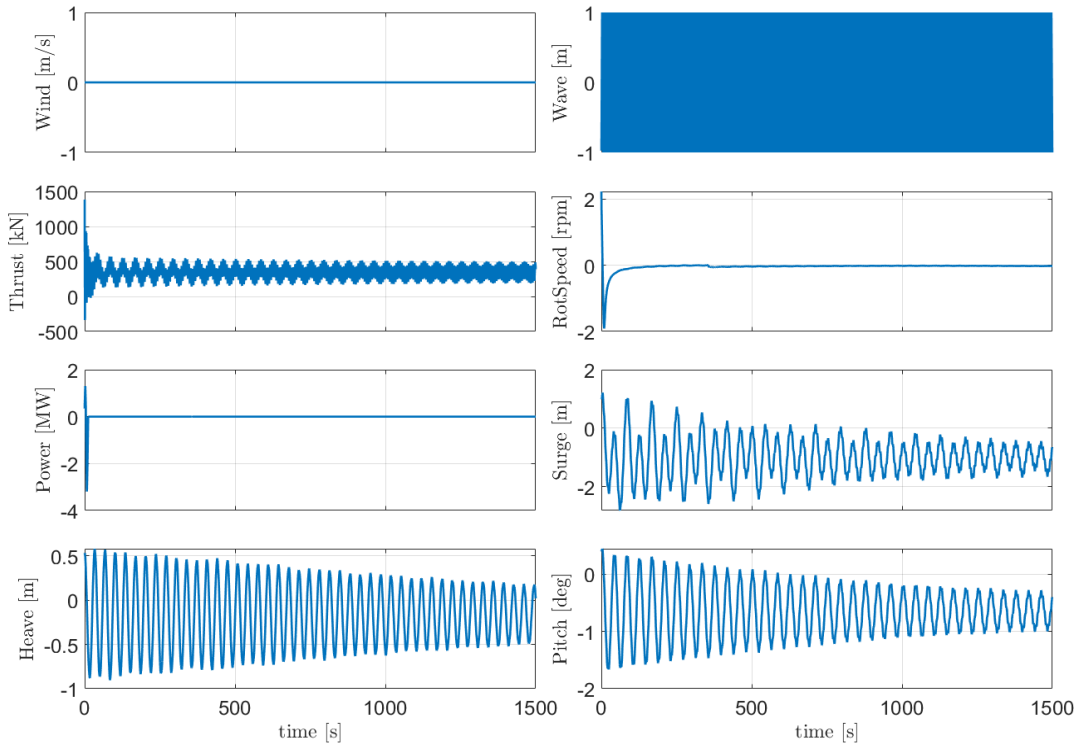

Figure 5-14: Timeseries response of WindCrete floater for regular waves

After checking the outputs of regular wave of H=2m and T=6s, it was surprising that the response at the wave frequency was not very visible. Therefore, we ran simulations with Morison-based hydrodynamics and compared them to the potential flow simulations. The goal was to check that the potential flow hydrodynamic model was correctly included in the simulations. We ran a regular wave simulation with H=10m and T=10s, in the absence of wind. Figure 5-15 shows the comparison, and as expected, the two models show similar responses except for heave, where the potential flow model causes a larger response due to the low axial hydrodynamic coefficient for the Morison-based model. We therefore concluded that the low response to hydrodynamic loads was not related to a modelling issue, but instead to the large inertia of the physical system.

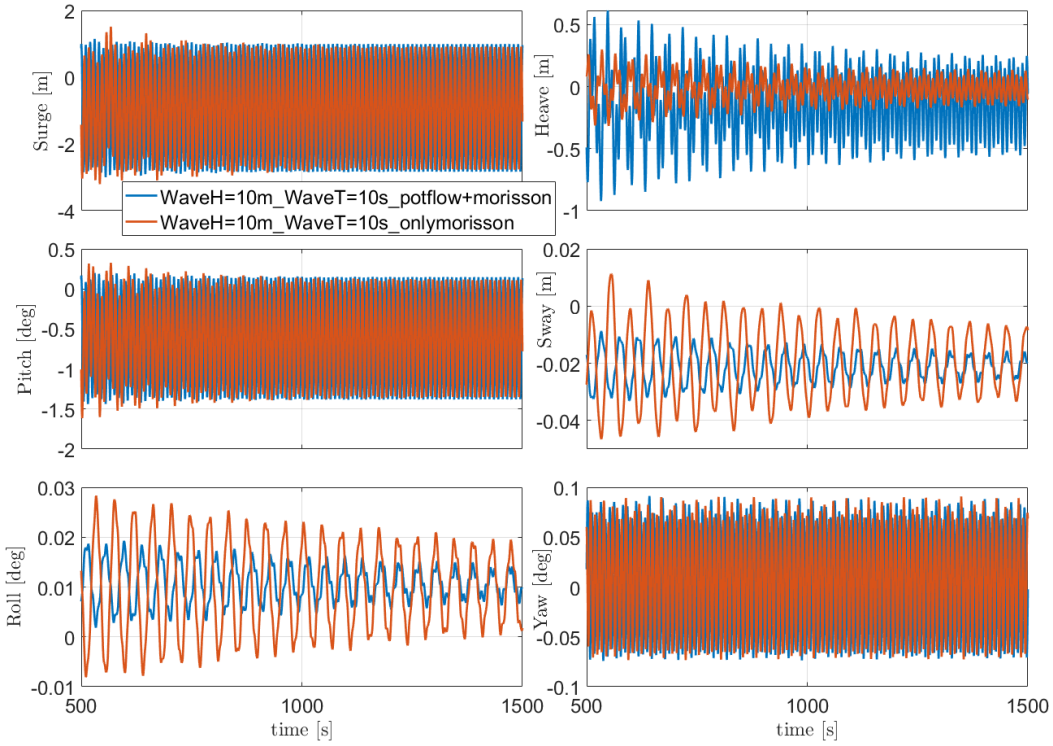

Figure 5-15: Comparison of the time series response of WindCrete with and without potential flow included

5.6.5 Extreme turbulence wind and stochastic waves (DLC 1.3)

The next simulation carried out is DLC 1.3 [1], with an extreme turbulent wind field for wind speeds (8, 10.5, 16, 20, 25) m/s and stochastic wave of (Hs=2m, and Tp=6s). The first 1800s were excluded from the PSD analysis, to make sure there are no transient conditions. The second order wave forces are taken into consideration, by taking the difference QTF into account. We decided to use only the difference QTF as it is the most relevant for our system due to the low natural frequencies of the floater and the mooring system. The Figures in this section are only at windspeed 10.5m/s. The rest of the simulations can be seen in the Appendix.

In general, the turbine acts as expected. The motion ranges are compared to the operation ranges defined in [16]. There are minor deviations for some motion ranges which are underlined in the following table. The main motions of the platform are found in the low frequency range due to the large wind forces and the extreme turbulence as shown in Figure 5-17. As previously discussed, the response to wave loads is small compared to the wind-induced response, because of the relatively mild sea conditions at the location, the wind turbine size and the large inertia of the system.

Table 5-11: WindCrete's motion ranges (underlined values have higher values than the limits introduced in Table 4-2)

	Yaw maximum [deg]	Yaw average [deg]	Pitch maximum [deg]	Pitch average [deg]	Roll maximum [deg]	Roll average [deg]
8 m/s	2.619	0.167	5.587	2.352	1.031	0.162
10.5 m/s	3.632	0.481	6.194	3.087	1.6401	0.258

16 m/s	4.276	0.355	4.159	1.752	2.119	0.310
20 m/s	5.996	0.643	5.090	1.422	3.835	0.402
25 m/s	7.312	0.816	4.79	1.335	4.357	0.515

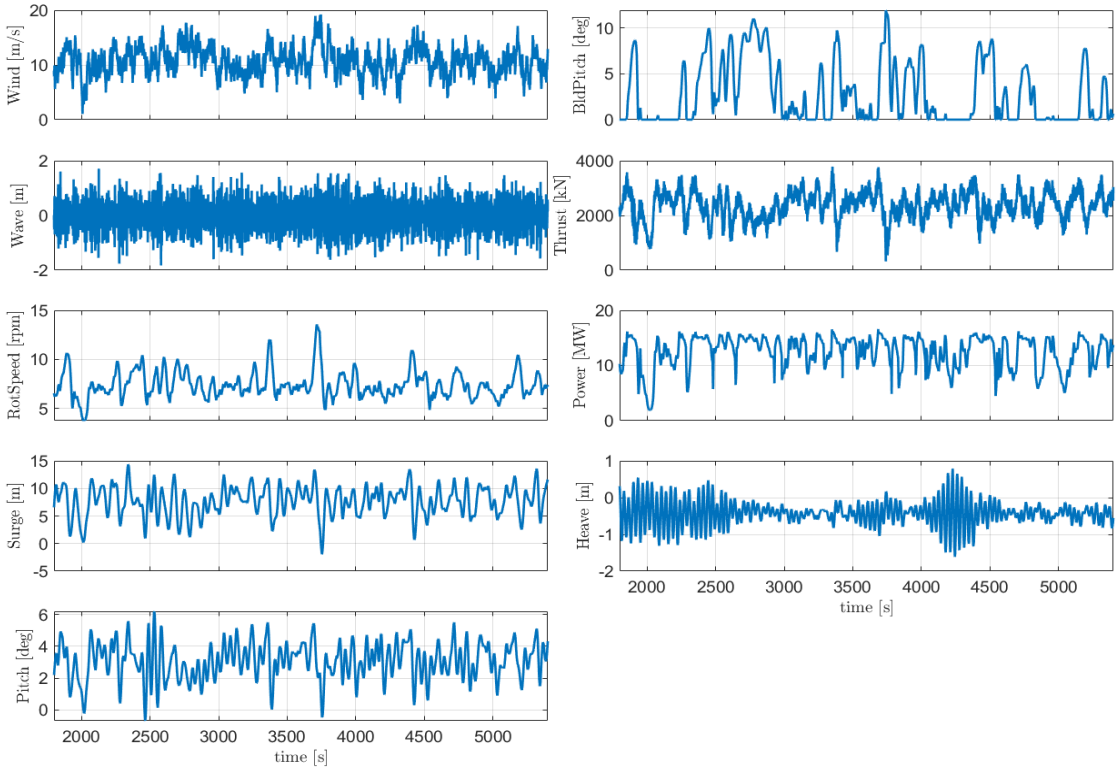

Figure 5-16: Timeseries response of WindCrete floater for DLC 1.3 at 10m/s

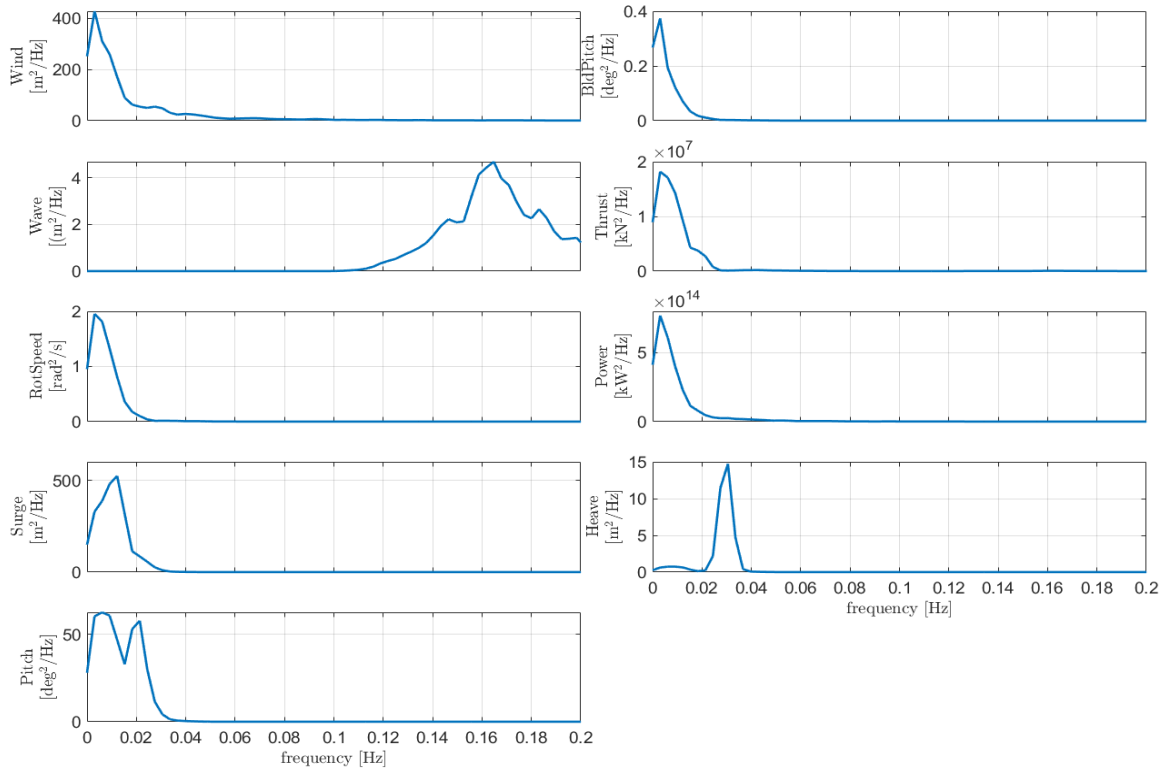

Figure 5-17: Power spectrum density response of WindCrete floater for DLC 1.3 at 10m/s

The following table shows the nacelle accelerations in all degrees of freedom. The nacelle translational accelerations are all within the ranges specified in [16].. The larger accelerations are found for the 20 m/s wind speed. At this wind speed the sway motion is larger than expected and further work is needed to understand the reason behind the sway response, and its higher nacelle acceleration.

Table 5-12: WindCrete's maximum nacelle accelerations in translation and rotation

	Nacc. acc in x-axis [m/s^2]	Nacc. acc in y-axis [m/s^2]	Nacc. acc in z-axis [m/s^2]	Nacc. rot. acc around x-axis [deg/s^2]	Nacc. rot. acc around y-axis [deg/s^2]	Nacc. rot. acc around z-axis [deg/s^2]
8 m/s	1.099	0.261	0.246	0.381	1.941	0.517
10.5 m/s	1.812	0.289	0.429	0.709	3.253	0.568
16 m/s	1.933	0.390	0.421	0.649	3.223	0.627
20 m/s	2.122	0.871	0.587	1.031	4.376	0.720
25 m/s	1.558	0.635	0.409	0.945	3.359	0.926

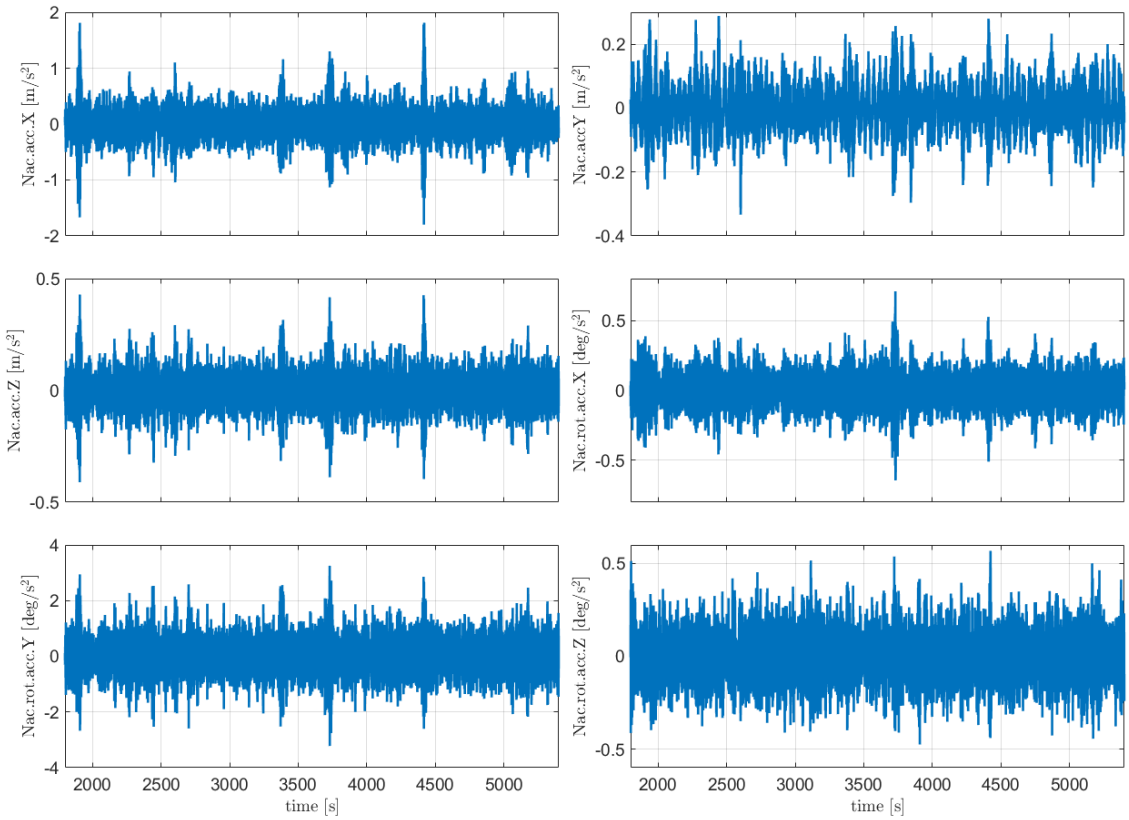

Figure 5-18: Timeseries response of nacelle acceleration of WindCrete floater for DLC 1.3 at 10.5m/s

5.6.6 Normal turbulence wind and extreme stochastic waves (DLC 1.6)

The next simulation carried out is DLC 1.6 [17], with a normal turbulence wind field for wind speeds (8, 10.5, 16, 20, 25) m/s and extreme stochastic wave of (Hs=5.11m, and Tp=9s). The first 1800s were excluded from the PSD analysis, to make sure there are no transient conditions. The second order wave forces are taken into consideration, by taking the difference QTF into account. The Figures shown here are only at windspeed 10.5m/s. The rest of the simulations can be seen in the Appendix.

In general, the turbine performs as expected. However, some motion ranges slightly violate the ranges in [16] and further tuning for the controller is required to keep the motion ranges within the limitations. These motions are shown underlined in the following table.

In this case also the pitch and surge motions are dominated by the wind loads and the wave loads are not very significant, as shown in Figure 5-20.

Table 5-13: WindCrete's motion ranges

	Yaw maximum [deg]	Yaw average [deg]	Pitch maximum [deg]	Pitch average [deg]	Roll maximum [deg]	Roll average [deg]
8 m/s	1.514	0.209	4.272	2.279	0.666	0.163
10.5 m/s	2.656	0.489	5.548	3.468	1.320	0.267

16 m/s	3.000	0.366	3.708	1.813	1.491	0.317
20 m/s	4.652	0.586	3.731	1.475	2.673	0.396
25 m/s	5.462	0.714	3.970	1.384	3.026	0.5145

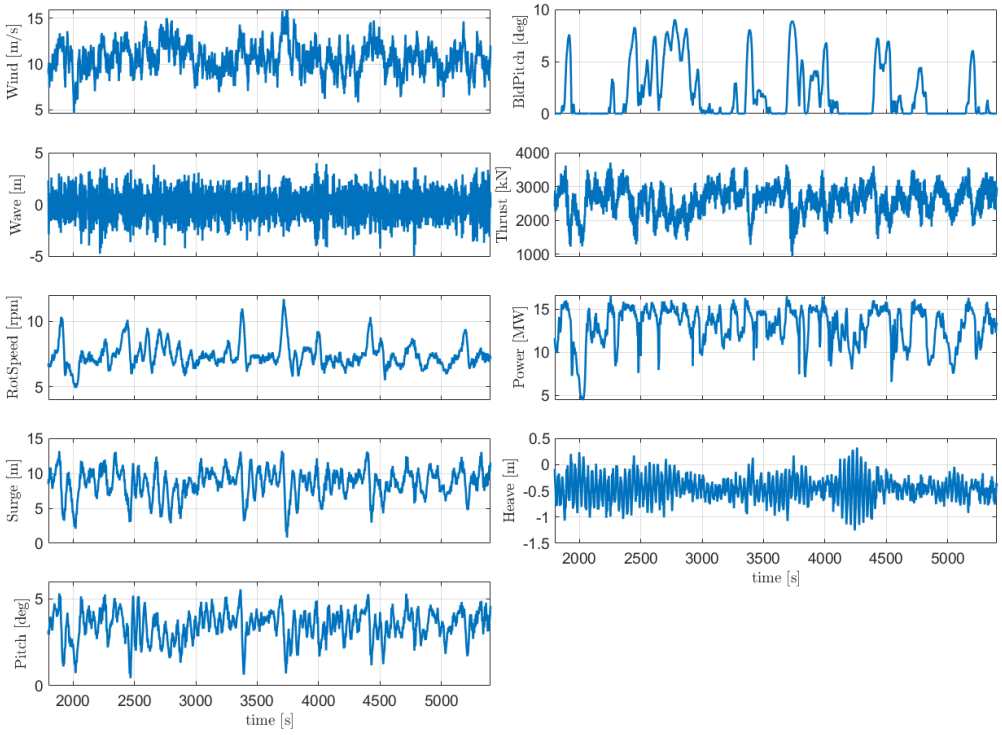

Figure 5-19: Timeseries response of WindCrete floater for DLC 1.6 at 10.5 m/s

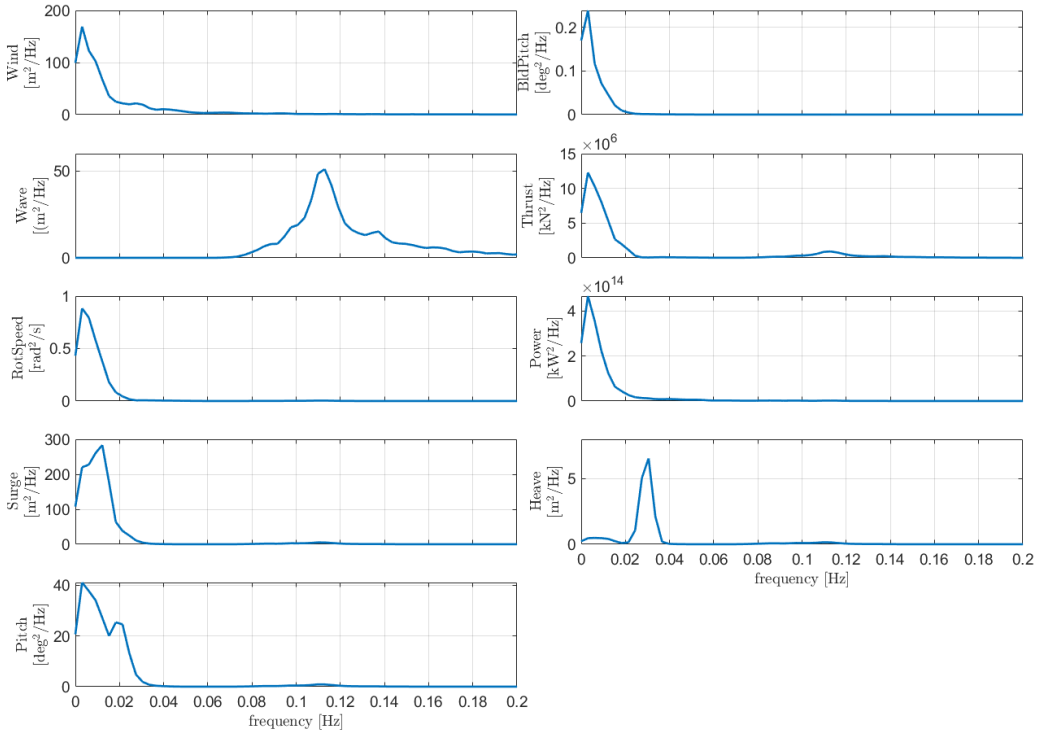

Figure 5-20: Power spectrum density of WindCrete floater for DLC 1.6 at 10.5m/s

The following table shows the nacelle acceleration in all simulated wind speeds. The accelerations are with the ranges defined in Table 4-2.

Table 5-14: WindCrete's maximum nacelle accelerations in translation and rotation

	Nacc. acc in x-axis [m/s^2]	Nacc. acc in y-axis [m/s^2]	Nacc. acc in z-axis [m/s^2]	Nacc. rot. acc around x-axis [deg/s^2]	Nacc. rot. acc around y-axis [deg/s^2]	Nacc. rot. acc around z-axis [deg/s^2]
8 m/s	1.514	0.161	0.276	0.230	1.220	0.304
10.5 m/s	1.945	0.232	0.390	0.404	2.022	0.362
16 m/s	1.882	0.229	0.374	0.361	2.054	0.448
20 m/s	1.797	0.382	0.355	0.642	2.481	0.588
25 m/s	1.807	0.562	0.375	0.672	2.560	0.802

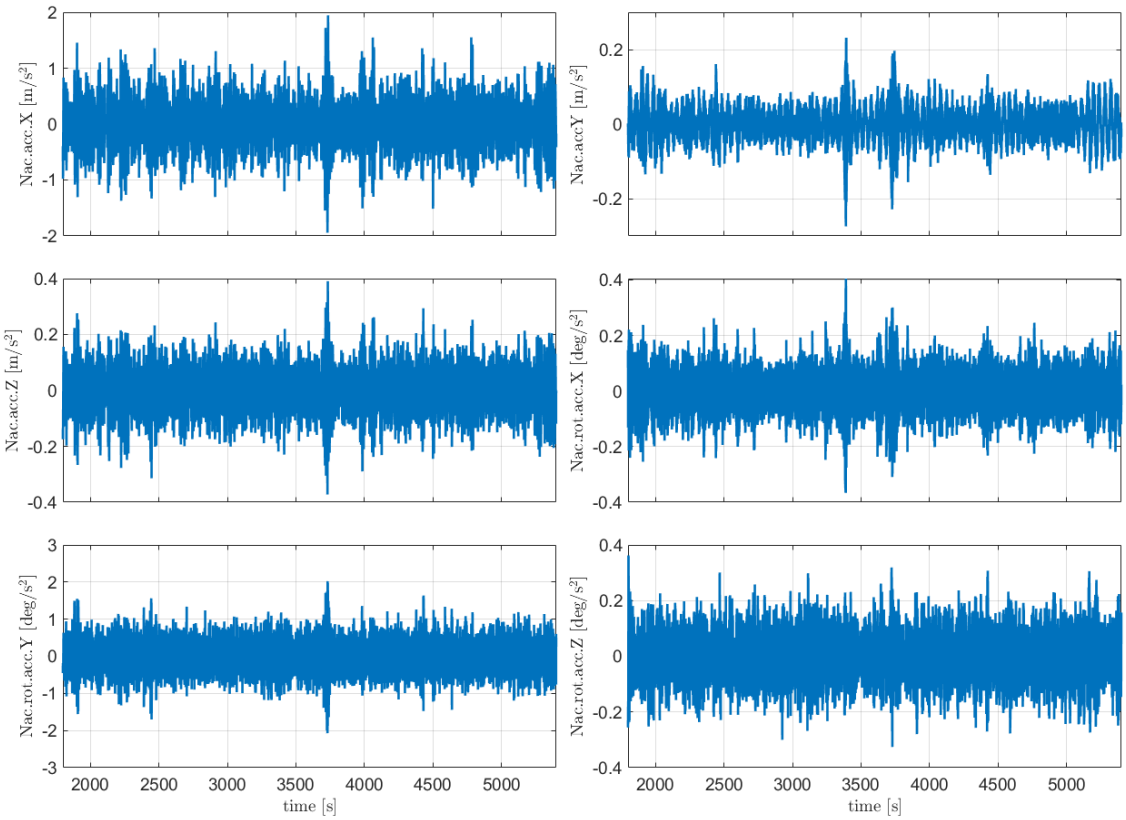

Figure 5-21: Timeseries response of nacelle acceleration of WindCrete floater for DLC 1.6 at 10.5 m/s

5.6.7 Power production with grid loss (DLC 2.1)

The power production with grid loss was simulated following [17]. A normal turbulence wind field with wind speed of 20m/s was used. A 600s simulation is used and the grid loss happens at 500s. A brake is applied to the generator shaft linearly. The braking torques starts at zero and ramps linearly to reach the rated turbine torque in 0.6s.

As the generator is turned off, due to grid loss, the rotation speed of the rotor increases. The rotor speed is controlled by the applied braking torque which brings the turbine to stop. The maximum pitch is 3.2 degrees, which is within the limits specified in [16] for emergency stop. Therefore, the turbine act as expected for this DLC.

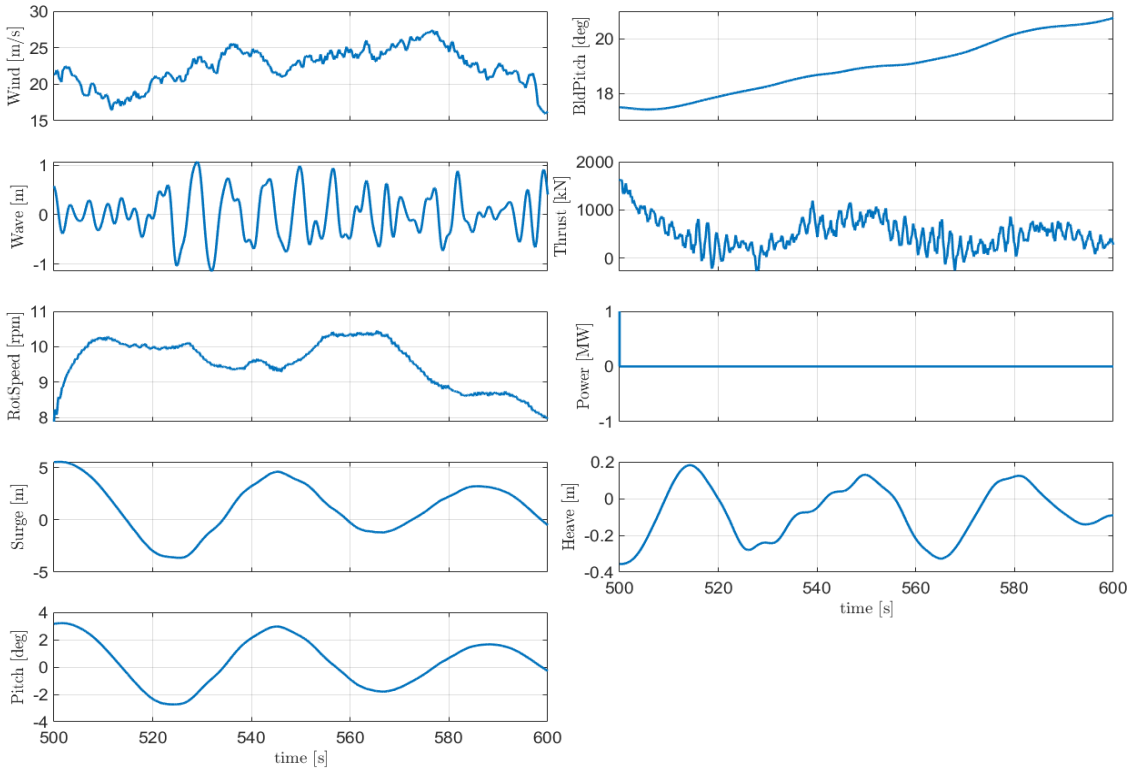

Figure 5-22: Timeseries response of WindCrete floater for DLC 2.1

Table 5-15: WindCrete's maximum nacelle accelerations in translation and rotation

Nacc. acc in x-axis [m/s^2]	Nacc. acc in y-axis [m/s^2]	Nacc. acc in z-axis [m/s^2]	Nacc. rot. acc around x-axis [deg/s^2]	Nacc. rot. acc around y-axis [deg/s^2]	Nacc. rot. acc around z-axis [deg/s^2]
1.024	0.598	0.268	2.467	2.315	0.425

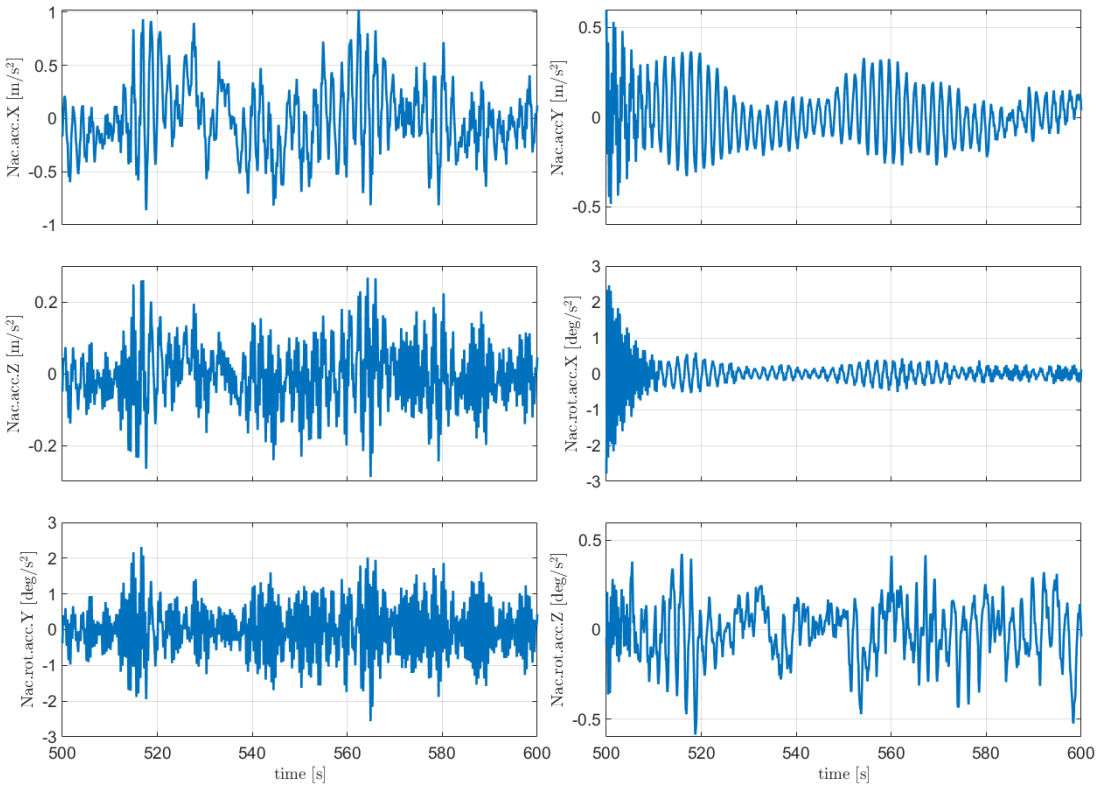

Figure 5-23: Timeseries response of nacelle acceleration of WindCrete floater for DLC 2.1

5.6.8 Parked turbine in 50-years extreme wind and waves (DLC 6.1)

A parked turbine with the feathering blades is simulated for 50-years extreme wind and waves. The values for extreme wind and waves used in the simulations were taken from [16] for the Gran Canaria site. The 50-years extreme winds value is 41.2m/s. The value for 50 years extreme waves is Hs=5.1m and Tp=9s. The duration of the simulation is 5400s, where the first 1800s were neglected to ensure we are out of the transient period.

The Table 5-16 shows the WindCrete's motion range under the DLC 6.1. In this simulation all the values are within the limits presented in Table 4-2 except for the pitch maximum rotation that exceeds the limit by 1.3 deg.

Table 5-16: WindCrete's motion ranges (underlined values have higher values than the limits introduced in Table 4-2)

Yaw maximum [deg]	Yaw average [deg]	Pitch maximum [deg]	Pitch average [deg]	Roll maximum [deg]	Roll average [deg]
1.852	0.274	8.308	4.904	1.571	0.117

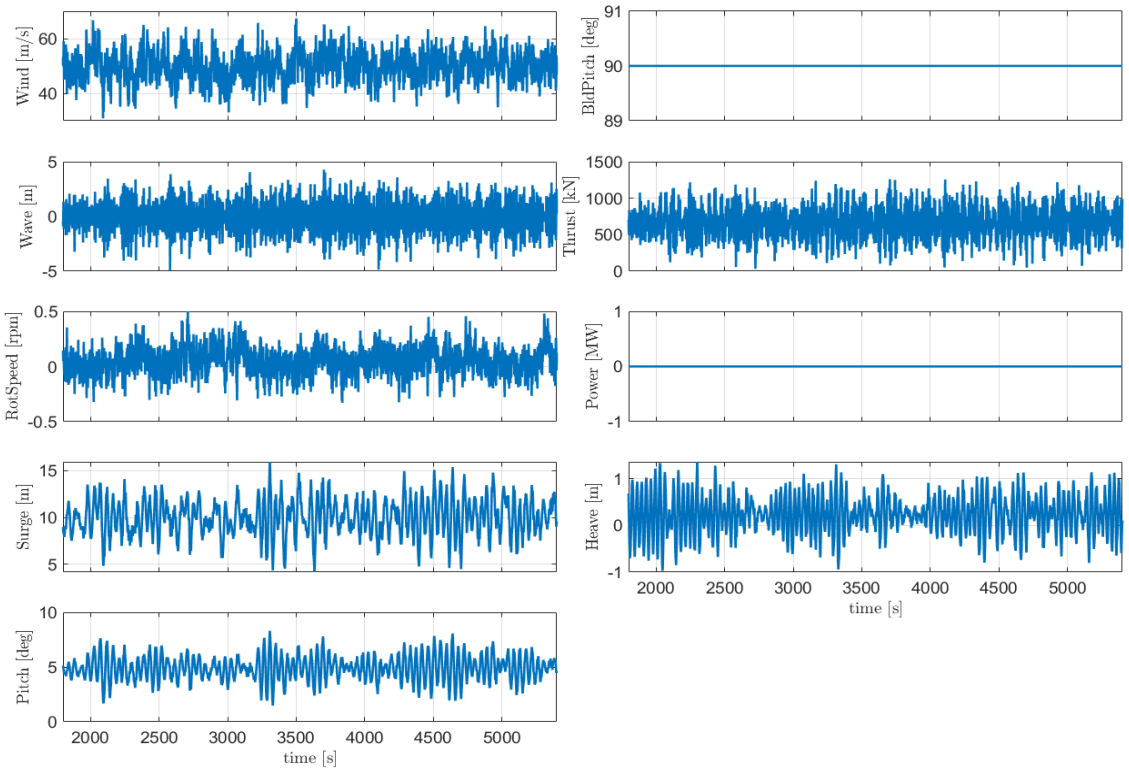

Figure 5-24: Timeseries response of WindCrete floater for DLC 6.1

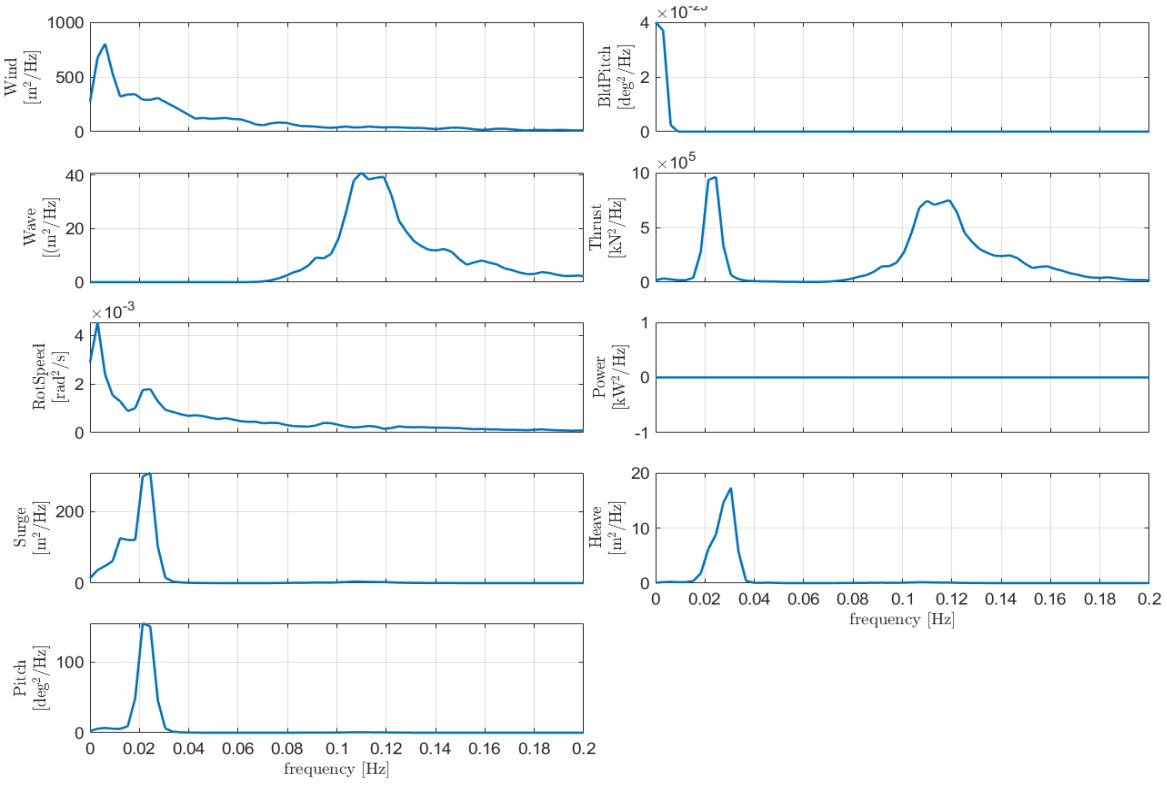

Figure 5-25: Power spectrum density of WindCrete floater for DLC 6.1

In Figure 5-25 we noticed that the wave spectrum is not visible in the PSD of platform motions. The motions are mostly excited at their natural frequencies by wind and by the low-frequency second order waves, but not by the linear wave spectrum. We ran a simulation with the 50-years sea state (Hs=5.1m and Tp=9s) in the absence of wind, with a simulation duration of 14000s to make sure we don't have any transient effects. In Figure 5-26 the wave spectrum appears in the PSD of surge and pitch motions. The main peak in surge, pitch, sway and roll happens exactly at the pitch natural frequency, which is 0.024 Hz. The main peak in both the heave and yaw motions happens exactly at the heave and yaw natural frequencies, respectively. Since there is no wind in the simulation, the resonance is caused by second-order hydrodynamic loads.

The resonant responses are very sensitive to the amount of damping, which is very uncertain at the moment due to the absence of physical tests to compare to. However, it is clear that the effect of the second order forcing on the platform is very relevant, especially compared to the response to linear wave loads. As previously observed, the response of the system to linear wave loads is relatively small, likely due to the large inertia of the system and the relatively larger aerodynamic and second-order hydrodynamic loads.

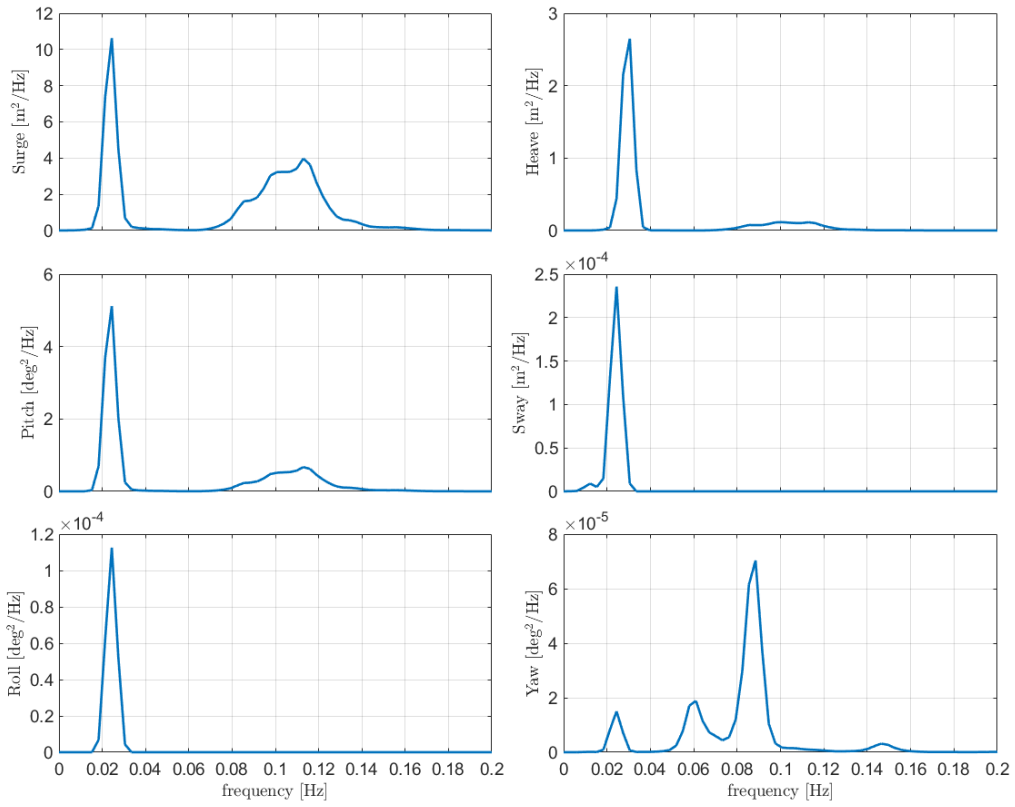

Figure 5-26: Power spectrum density of WindCrete floater for 50 years extreme waves in absence of wind

Table 5-17: WindCrete's maximum nacelle accelerations in translation and rotation

Nacc. acc in x-axis [m/s^2]	Nacc. acc in y-axis [m/s^2]	Nacc. acc in z-axis [m/s^2]	Nacc. rot. acc around x-axis [deg/s^2]	Nacc. rot. acc around y-axis [deg/s^2]	Nacc. rot. acc around z-axis [deg/s^2]
1.428	0.407	0.228	0.653	0.640	0.285

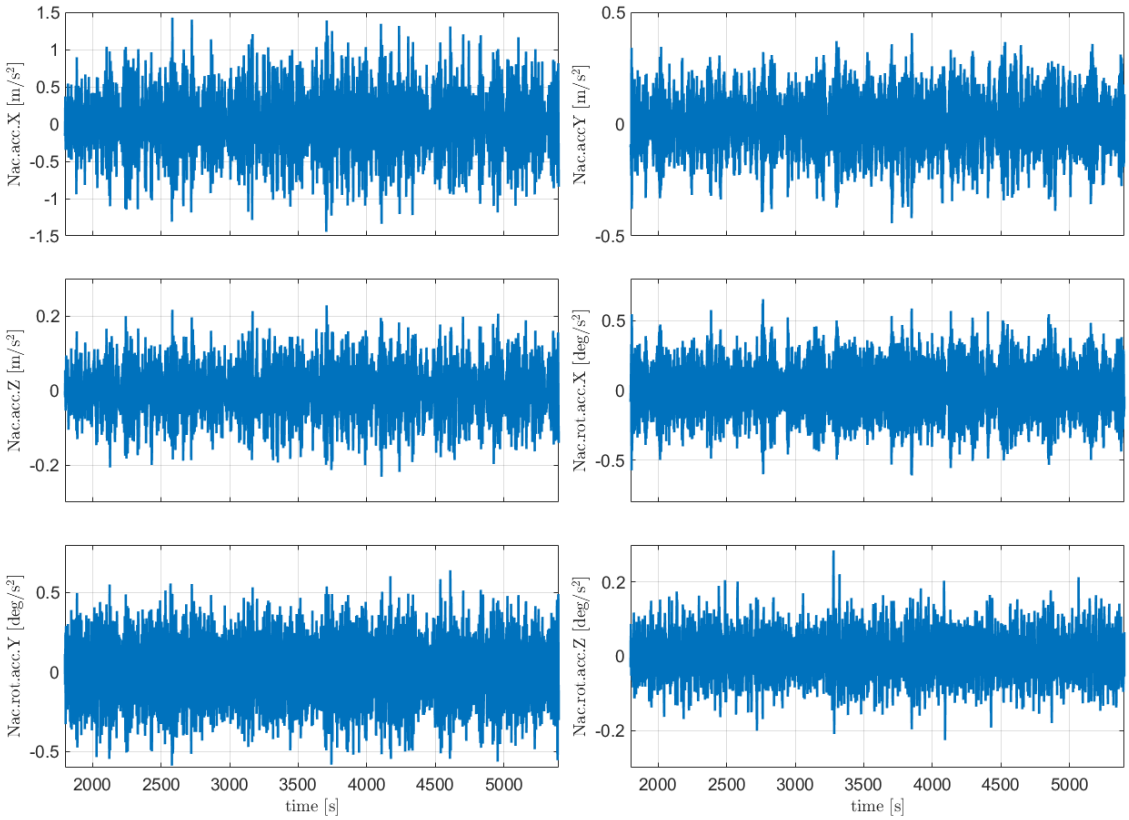

Figure 5-27: Timeseries response of nacelle acceleration of WindCrete floater for DLC 6.1

6 ActiveFloat floater

6.1 Platform design

ActiveFloat floater has been developed by COBRA and is currently being designed by COBRA and ESTEYCO. The platform is a semi-submersible concrete floater with three external vertical columns placed at 120 degrees. The external columns are connected to a central shaft that holds the connection with the tower that ends in the turbine. The three vertical columns are connected to the central shaft through three pontoons. The vertical columns provide the buoyancy and stability to the system while the pontoons are structural members as the central shaft from where the turbine loads are transferred and also add heave damping. The platform external columns have the same height as the central cone where the access platform is located. The platform is made of reinforced concrete, except for the tower that is made of structural steel.

The platform is transported un-ballasted in order to reduce draught requirements of navigation channels or shipyards where the fabrication takes place. The platform is designed to have a transportation draft between 11 and 13 meters whereas the operational draft is 26.50 meters.

Circular heave plates are provided at the bottom of each external column, in order to increase damping.

The column diameter is kept equal towards to the pontoons beam. The pontoons have a rectangular cross-section member with a central bulkhead that split the span of the pontoon decks.

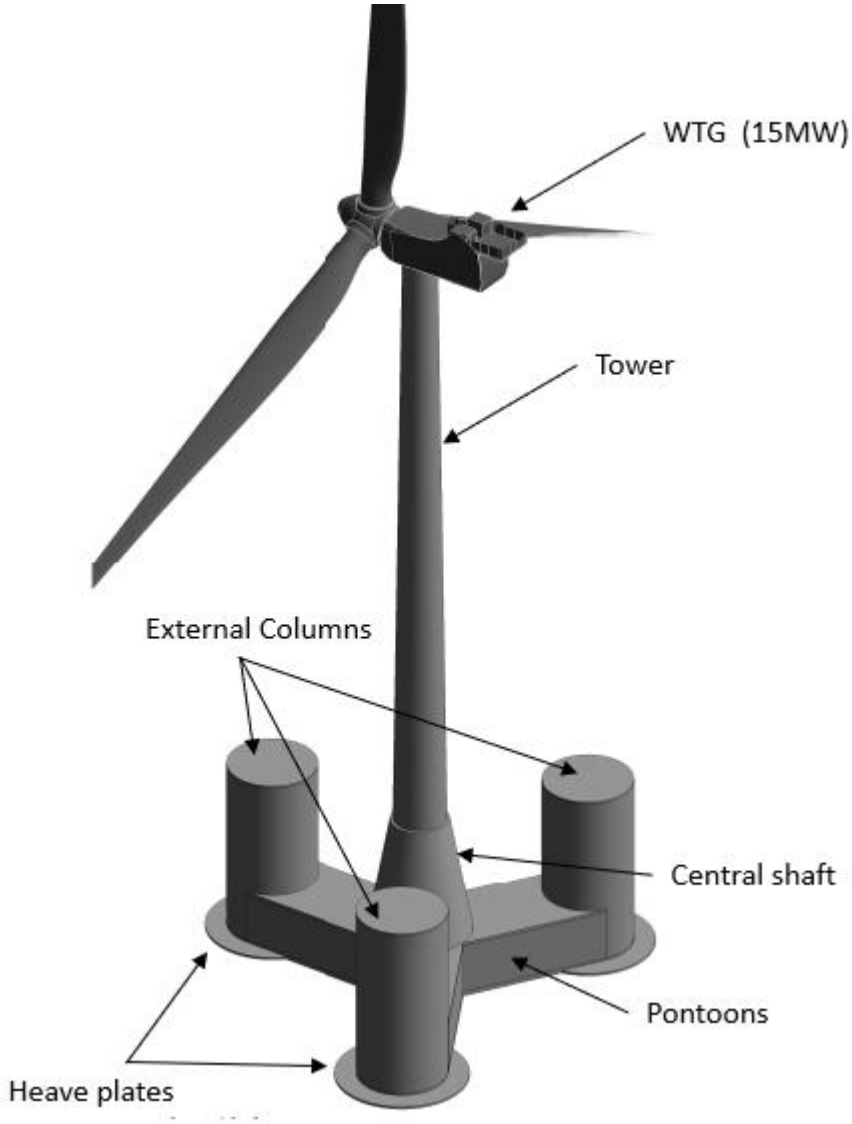

Figure 6-1 - Activefloat Platform. Overview

The main dimensions are indicated in the following table.

Table 6-1 - Activefloat Platform. Main dimensions

Main dimensions	
Hub height (m above sea level)	135.00
Columns Diameter (m)	17.00
Columns separation (center to tower center) (m)	34.00
Columns height (m)	35.50
Central cone base diameter (m)	19.60
Central cone top diameter (m)	11.00
Tower base diameter (m)	10.00
Tower top diameter (m)	6.50
Tower length (m)	120.50

Pontoons height (m)	11.50
Heave plate cantilever (m)	4.00
Overall beam (m)	83.90

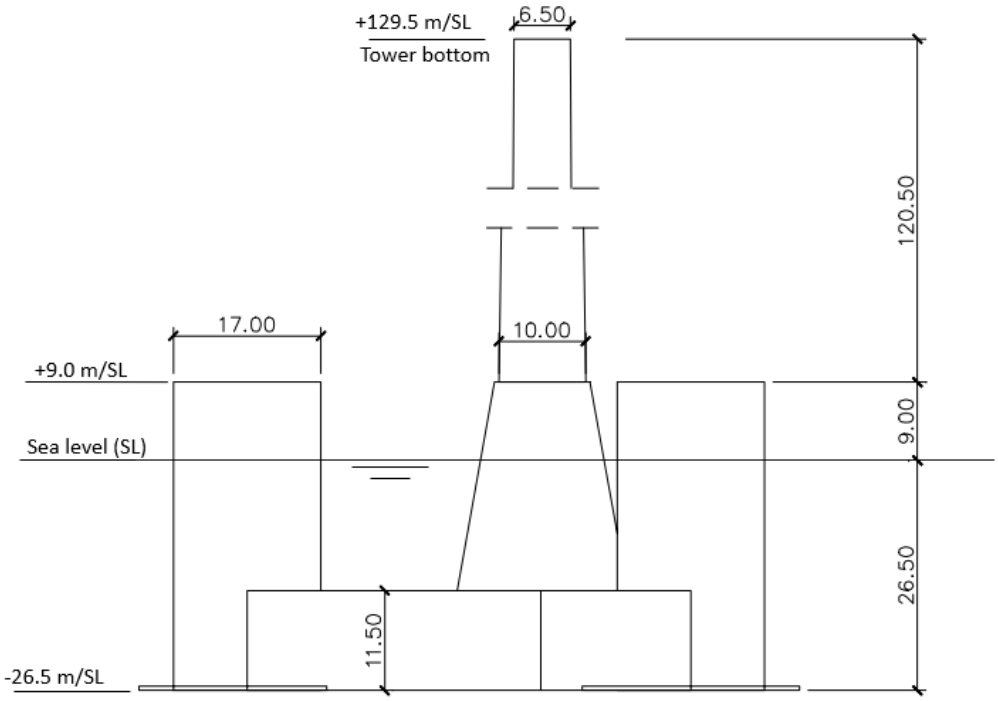

Figure 6-2 - Activefloat Platform. Operation phase. Elevation (Units: meters)

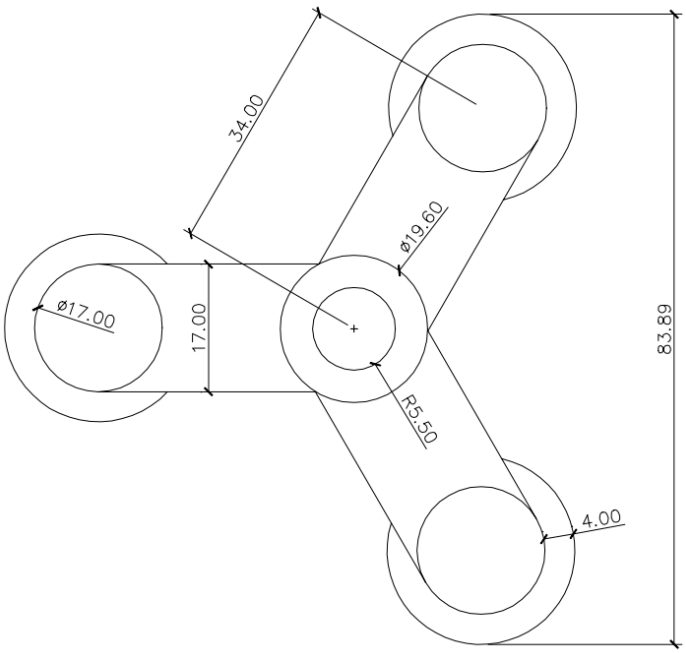

Figure 6-3 - Activefloat Platform. Plan View (Units: meters)

The hub height of the floating system is adjusted to be at 135 m above sea level according to the following constraints:

- Access platform to be out of the reach of the 50-years wave crest accounting with
- Minimum air gap of 20% of Hs or 1.50 meters, whichever is larger.
- Hub height to be 6 meters plus the semi-rotor diameter. The 6 meters allowance is for an operating crane located at the access platform.

The naval key parameters are shown in the following table.

Table 6-2 - Activefloat Platform. Naval key parameters

Naval parameters	
Displacement (m^3)	36431.22
Active Ballast weight (t)	6360.00
Operation Draught (m)	26.50
KG (m)	15.41
KB (m)	10.67
GM (m)	6.41
GMc (m)	6.14

The floater inertias (concrete platform and ballast, without tower nor RNA) are indicated in the following table.

Table 6-3 - Activefloat Platform. Floater inertias

Platform inertias	
Ixx (t.m2)	1.57E+07
Iyy (t.m2)	1.57E+07
Izz (t.m2)	2.58E+07
rxx (m)	21.14
ryy (m)	21.14
rzz (m)	27.1

6.1.1 Ballast system

The structure is designed so that the pontoons are fully ballasted during turbine operation. However, the central shaft is left empty in order to store machinery in a dry environment, such as the active ballast system.

The pontoons fully ballasted are structurally efficient since differential pressure is very limited to the pre-service phases. The lower slab of the central shaft in the other hand, requires a heavy structure since it has to resist permanently a differential pressure (26.5 meters in the site B configuration).

The columns are ballasted partially. The platform design tries to ensure that columns have enough ballast in order to be able to compensate the pitch produced by the mean thrust with the so called “Active ballast system”.

The coordinate system considered is indicated in the following figure:

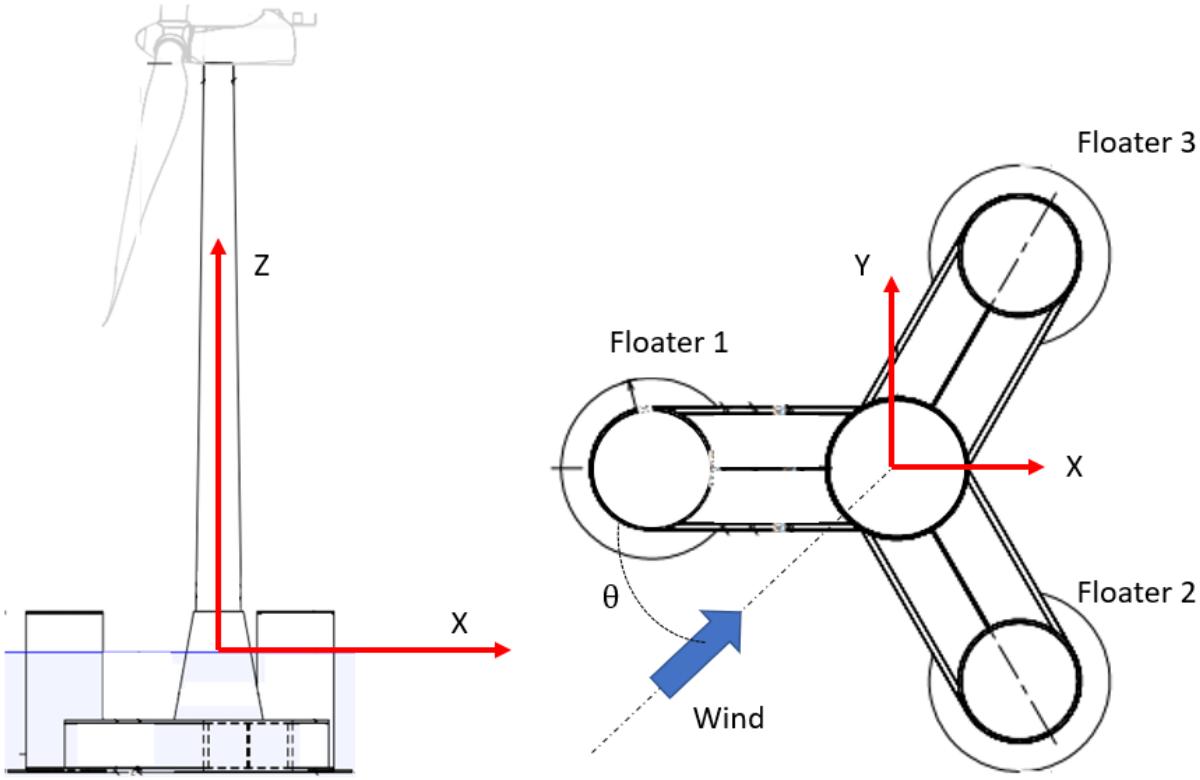

Figure 6-4 - Activefloat Platform. Coordinate system

The origin is located at the sea level at the axis of the tower. The X coordinate is aligned with the mid plane of the platform and pointing to the floater 2 and 3. The Y axis is aligned orthogonal to the mid plane of the platform pointing according to the right-hand rule that makes the Z axis upwards.

The base weight control of the platform in operation condition in still water, is shown in the following table. Note that the ballast water is divided in two, the ballast inside the pontoons (permanent ballast), that does not change after the installation of the platform, and the ballast in tanks or external columns. The ballast in the columns may be varied through the active ballast system in order to trim the platform as demanded by the external conditions.

Table 6-4 - Activefloat Platform. Weight control

Weight Control				
ITEM	**Weight (t)**	**X (m)**	**Y (m)**	**Z (m)**
RNA	1016.5	-7.023	0.000	133.840
TOWER	1088.5	0.000	0.000	56.919
Internals	100.0	0.000	0.000	56.919
FLOATER	34387.2	0.000	0.000	-17.529
TOTAL	**36592.2**	**-0.195**	**0.000**	**-10.906**

Note that the above has accounted for the mooring hang off. In order to keep the design draft of 26.5 meters, 750 tonnes of ballast water are removed from the tanks.

6.1.2 Active ballast system

The active ballast system consists in a pump arrangement that allows to transfer water from column to column, providing a corrective moment that reduces the mean pitch potentially to zero.

This section is aimed to define the ballast plan for the different wind speeds to be run in the coupled simulations, i.e. 8, 10.5, 16, 20, 25 m/s.

The thrust assigned to each wind speed is, preliminary, the mean thrust of the steady state wind.

Table 6-5 - Activefloat Platform. Active Ballast system (X,Y,Z are the coordinates of the centre of gravity for the Floater+Ballast)

DLC	Wind speed (m/s)	Floater + Ballast			
		M (t)	X (m)	Y (m)	Z (m)
1.3	8	34387.2	-0.379	0	-17.59
	10.5	34387.2	-0.522	0	-17.59
	16	34387.2	-0.259	0	-17.59
	20	34387.2	-0.196	0	-17.59
	25	34387.2	-0.181	0	-17.59
1.6 / 2.1	8	34387.2	-0.365	0	-17.59
	10.5	34387.2	-0.594	0	-17.59
	16	34387.2	-0.272	0	-17.59
	20	34387.2	-0.207	0	-17.59
	25	34387.2	-0.188	0	-17.59
6.1	vref	34387.2	0	0	-17.59

6.2 Tower model

The tower definition is as indicated in the following table. The tower starts at the top of the central concrete cone of the platform, at 9.0 meters above sea level. The above tower top and bottom diameters are kept from the turbine report in order to ensure the geometry compatibility.

Table 6-6 - *Activefloat Platform. Tower definition*

Height Fraction	Outer Diameter [m]	Thickness [mm]	Area [m2]	CoG [m]	Mass [t]
0.00	10	59	1.843	-	-
0.10	9.65	59	1.778	6.05	175
0.20	9.30	49	1.424	18.15	173.1
0.30	8.95	44.5	1.245	30.25	138.2
0.40	8.60	42	1.129	42.35	117.7
0.50	8.25	42	1.083	54.45	105.6
0.60	7.90	38	0.939	66.55	101.4
0.70	7.55	27.95	0.660	78.65	90.1
0.80	7.20	28.5	0.642	90.75	65.2
0.90	6.85	31	0.664	102.85	62.4

1.00	6.5	31	0.630	114.95	59.8
			Total	**47.9**	**1088.5**

6.3 Hydrodynamic model

The hydrodynamic model is initially produced in ANSYS AQWA. The model consisted in a boundary element model with a mesh of 2 meters size. The model is calibrated against previous tank tests of similar platforms and the linear additional damping, as well as the Morison drag coefficients, used in the model, are adjusted.

After the ANSYS AQWA output is created (LIS and QTF files) it is exported to the WAMIT output format, which is the format of hydrodynamic files required by FAST and used for the coupled simulations.

6.3.1 First order hydrodynamics

Next figures show the linear forces per unit wave amplitude for the Activefloat.

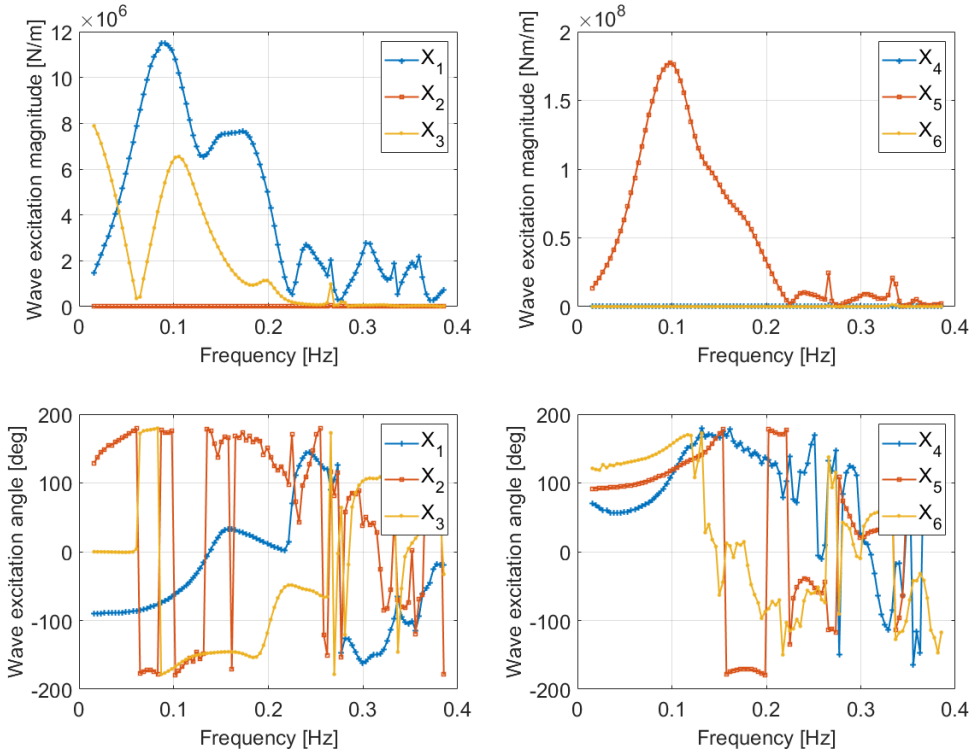

Figure 6-5 - Activefloat first order wave excitation forces and moments (0º wave heading direction)

6.3.2 Radiation hydrodynamics

Next graphs present the radiation characterization of the Activefloat. Firstly, the added mass matrix for infinite frequency is presented. After the added mass evolution versus the frequency is shown. Note that units for the matrix are consistent with the graphs below.

Table 6-7 - *Activefloat Platform. Added mass matrix (infinite freq.)*

	X	Y	Z	RX	RY	RZ

X	1.77E+07	4.57E+02	1.61E+03	1.01E+05	-9.54E+07	-6.74E+04
Y	-1.16E+03	1.77E+07	2.39E+03	9.57E+07	-2.71E+04	2.74E+04
Z	1.90E+03	-2.07E+03	3.32E+07	-4.05E+05	5.46E+05	2.05E+05
RX	-1.51E+05	1.03E+08	-3.06E+05	1.00E+10	6.99E+06	-3.57E+06
RY	-1.03E+08	-5.26E+04	4.53E+05	4.51E+06	1.00E+10	-5.00E+05
RZ	-4.80E+04	-5.51E+03	1.24E+04	4.64E+06	2.85E+06	1.57E+10

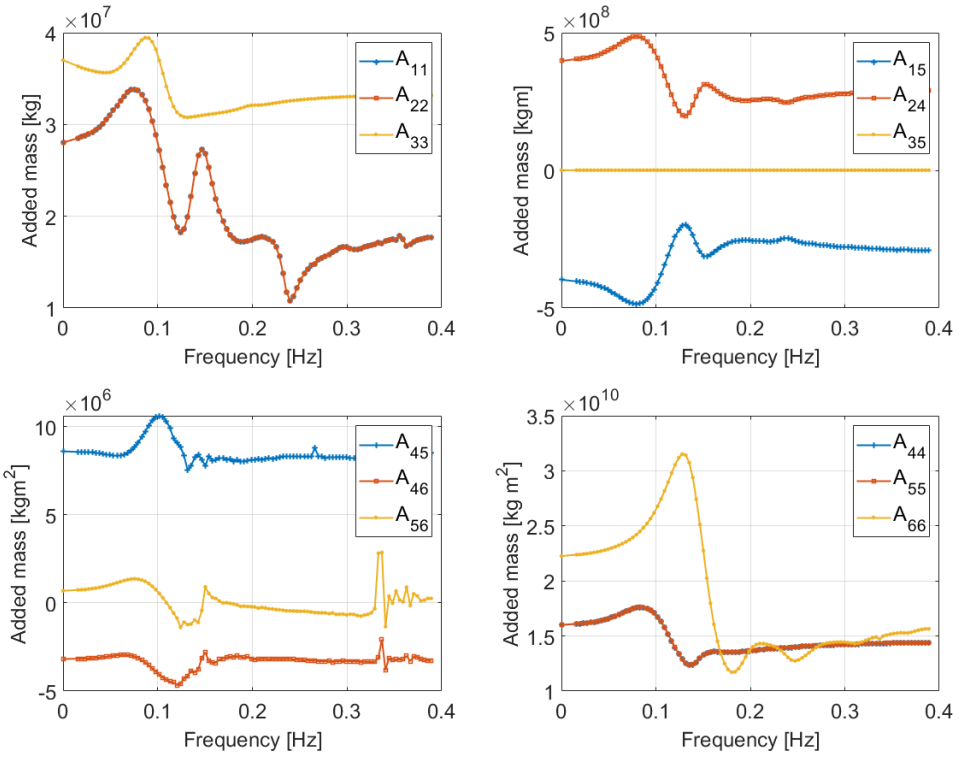

Figure 6-6 – Activefloat hydrodynamic added mass

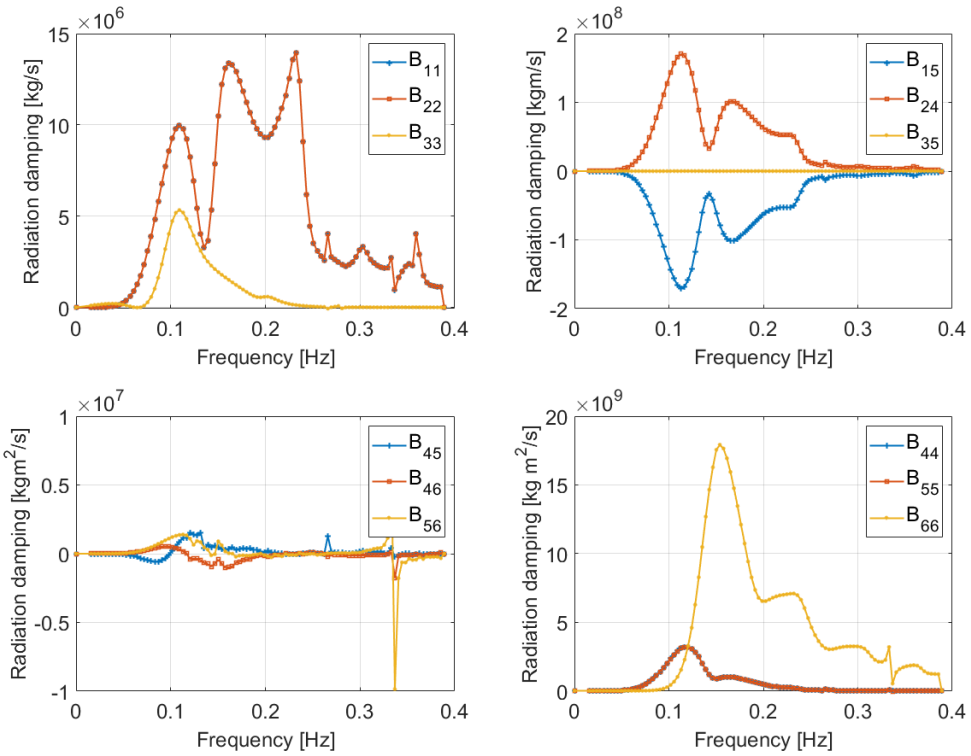

Figure 6-7: Activefloat hydrodynamic potential damping

6.3.3 Viscous forces

The viscous effects were modeled in Hydrodyn through the Morison equation. The floater was defined by seven members; four members represented the four vertical columns and three members for the horizontal pontoons (see Figure 6-8). Activefloat is considered brand new hence no marine growth was taken into account in the viscous model. However, the marine growth effects must be taken into account in the design process [22].

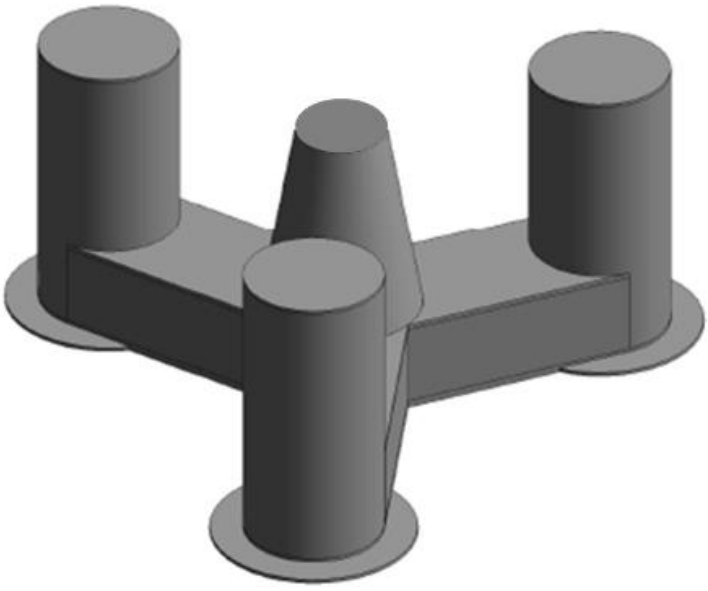

Figure 6-8: Activefloat geometry

The Morison drag coefficients used are defined differently for the central vertical column, the outer vertical columns and the horizontal pontoon and heave plates. The methodology used here is similar to the methodology used in [22] for the OO-Star Semi floater.

Central vertical column:

- One member was used to model the central tapered vertical column. The member has a top diameter of 11m, and a lower diameter of 19.62. The member ends at the top of the star shaped pontoons.
- The transverse viscous drag for this vertical column was derived following [23], where the drag coefficient is a function of the non-dimensional roughness (k/D). The non-dimensional roughness is the ratio of the surface roughness (k) and the diameter (D). In this report the non-dimensional roughness of concrete is taken as 3mm.
  Following equation (X) in [23]. The top transverse drag coefficient is 0.737 and the lower transverse drag coefficient is 0.687.

Outer vertical column:

- Three members represent the three outer vertical columns each with a constant diameter of 17m. The three members at the bottom of the star shaped pontoons.
- Similar to the central vertical column, the transverse viscous drag for this vertical column was derived following [23] , where the drag coefficient is a function of the non-dimensional roughness (k/D). Following equation (X) in [23]. The value of the transverse drag coefficients over the three vertical cylinders is 0.699.

Horizontal pontoons (star-shaped):

The remaining three members represent the three legs of the star-shaped base of Activefloat. The main challenge, is that Hydrodyn is only able to model cylindrical shaped members using Morison elements. In order to overcome this obstacle, the methodology used in [22] was followed, and explained through the coming section. First, the drag coefficients of the real physical system are obtained from literature. Afterwards, the drag coefficients for the modelled areas in Hydrodyn are calculated; such that the final drag forces acting on the floater are equal for the real physical model and Hydrodyn implementation.

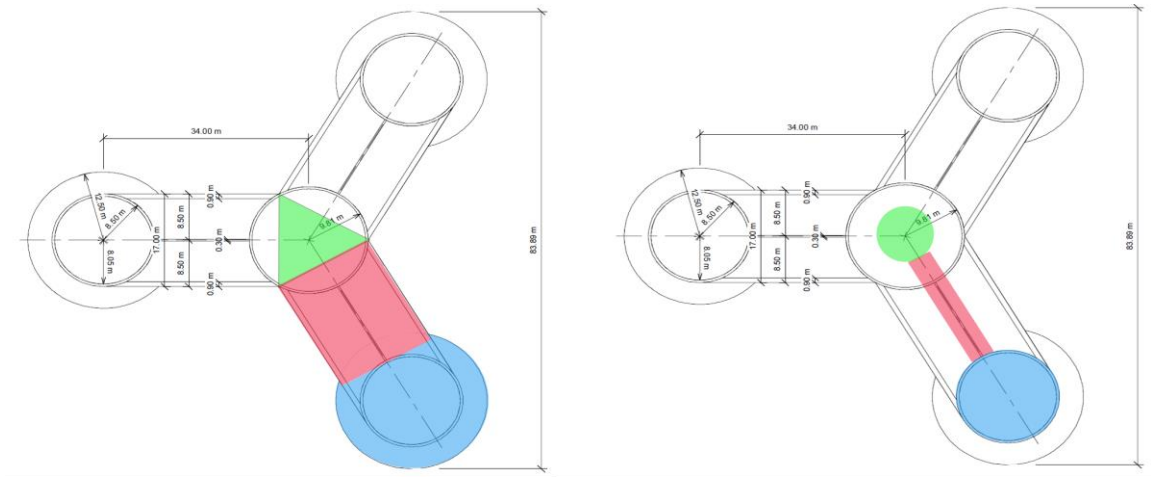

Figure 6-9: The left hand side represents the physical floater model and the right-hand side represents the Hydrodyn model of the floater

Figure 6-9 shows the real physical model on the left side and the Hydrodyn model on the right side. For simplicity, each leg of the star-shaped base is divided into three smaller parts. The green triangle represents the inner heave plate, the red rectangle represents the pontoons, and the blue truncated circle represents the outer heave plates.

On the right side of Figure 6-9, is the Hydrodyn model. Where the green circle is the cross-section area of the member representing the center vertical column, the red rectangle represents the cross-section area of the cylindrical members of the pontoons, finally the blue circle represents the cross-sectional area of the outer vertical cylinder's member.

For simplicity, we will compare each of these three colored cross-section areas on their own showing values of both the real physical model and the Hydrodyn model.

Center heave plate (green)

In the real physical model, the center heave plate is a triangle of area A_{1ph}=125.14 m^2.

In the Hydrodyn model, the cross-sectional area of the inner column is A_{1mo}=226.98m^2 , and the axial drag coefficient C_{D1mo} needs to be calculated in equation (1).

Pontoon (red)

In the physical model, the pontoons have a height h_1= 11.5m, and a width h_2= 17m. The transverse and axial drag coefficient of this shape is C_D=2.05 [22], due to the flow separation at sharp corners.

In the Hydrodyn model, the pontoons are modelled as cylinders with diameter h_1= 11.5m. This way the transverse drag is properly modelled. The cylinders start from a radial distance r_1=4.91m, and end at a radial distance r_2=25.5m, from the center of the platform.

Outer heave plate (blue)

In the physical model, the outer heave plates are with truncated cross-sectional area of A_{3ph}= 451.94m^2. From literature [24], the axial drag coefficient of such a shape is equal to C_{D3ph}=10.

In the Hydrodyn model, the outer heave plate cross-section area is A_{3mo}= 302.33m^2, and the drag coefficient C_{D3mo} is calculated in equations (1,2).

$$\int_{r_1}^{r_2} \frac{1}{2}\rho C_D h_2 \dot{z}|\dot{z}|dr + \frac{1}{2}\rho C_{D3ph} A_{3ph}\dot{z}|\dot{z}| + \frac{1}{2}\frac{1}{3}\rho C_D A_{1ph}\dot{z}|\dot{z}| = \int_{r_1}^{r_2} \frac{1}{2}\rho C_D h_1 \dot{z}|\dot{z}|dr + \frac{1}{4}\rho C_{D3mo} A_{3mo}\dot{z}|\dot{z}| + \frac{1}{4}\frac{1}{3}\rho C_{D1mo} A_{1mo}\dot{z}|\dot{z}| \quad (1)$$

$$\int_{r_1}^{r_2} \frac{1}{2}\rho C_D h_2 \dot{\theta}|\dot{\theta}|r^3 dr + \frac{1}{2}\rho C_{D3ph} A_{3ph}\dot{\theta}|\dot{\theta}|R^3 = \int_{r_1}^{r_2} \frac{1}{2}\rho C_D h_1 \dot{\theta}|\dot{\theta}|r^3 dr + \frac{1}{4}\rho C_{D3mo} A_{3mo}\dot{\theta}|\dot{\theta}|R^3 \quad (2)$$

Following equations 9 and 10 from [22], equation 1 represents the drag forces in still water in the axial z direction. The left-hand side of the equation represents the drag forces on the real physical model, where the first term represents the drag on the pontoon, second term is the drag on the outer heave plate, and the third term represents the drag on the center heave plate. The third term for the central heave plate is divided by three as this area is included in all three star-shaped legs of the floater.

On the right-hand side, the first term represents the drag on the pontoon cylinders. The second term represents the drag on the outer heave plate, and the third term represents the drag on the central heave plate. The second and third terms are divided by two because Hydrodyn assumes two joints per heave plate. The third term for the central heave plate is divided by three because, similar to the left-hand side, it is repeated in all three star-shaped legs of the platform.

Equation 2 represents the drag moment around the y axis (pitch degree of freedom). The moment due to the central heave plate is neglected for simplicity. This is a valid assumption due to the small arm of moment for the central heave plate. The left-hand side of equation 2 represents the real physical moment. The first term in the left-hand side represents the moment due to the pontoons. The second term represents the moment on the outer heave plates with R=34m.

The right-hand side of equation 2 represents the pitch drag moment in the Hydrodyn model. The drag forces on the pontoon cylinders. The second term represents the drag moment on the outer heave plate. The second term is divided by two, similar to equation 1, because Hydrodyn assumes two joints per heave plate.

Equations 1 and 2 are solved simultaneously to calculate the axial coefficients C_{D1mo} and C_{D3mo} for the Hydrodyn model.

The parameters of the physical model and the Hydrodyn model are summarized in the following table.

Table 6-8: Parameters of the physical model and the Hydrodyn model

Property	Physical value	Model value	Colour in Figure 6-2
Pontoon leg height (h_1)	11.5m	11.5m	Red
Pontoon leg width (h_2)	17m	11.5m	Red

Transverse drag coefficient of for pontoon (C_D)	C_D=2.05	C_D=2.05	Red
Outer heave plate area	A_{3ph}=451.94m^2	A_{3mo}= 302.33m^2	Blue
Outer heave plate coefficient	C_{D3ph}=10	C_{D3mo}=40.09	Blue
Central heave plate area	A_{1ph}=125.14 m^2	A_{1mo}=226.98m^2	Green
Central heave plate coefficient	C_D=2.05	C_{D1mo}=5.7	Green

6.3.4 Second order forces

The second order forces are related to the waves' nonlinear effects and in some cases, it is important to take them into account. These loads are quadratic with the wave amplitude and they are related to the effect of a pair of waves with several frequencies. An AQWA diffraction analysis can calculate the two contributions to this type of loads, diff – frequencies and sum – frequencies terms.

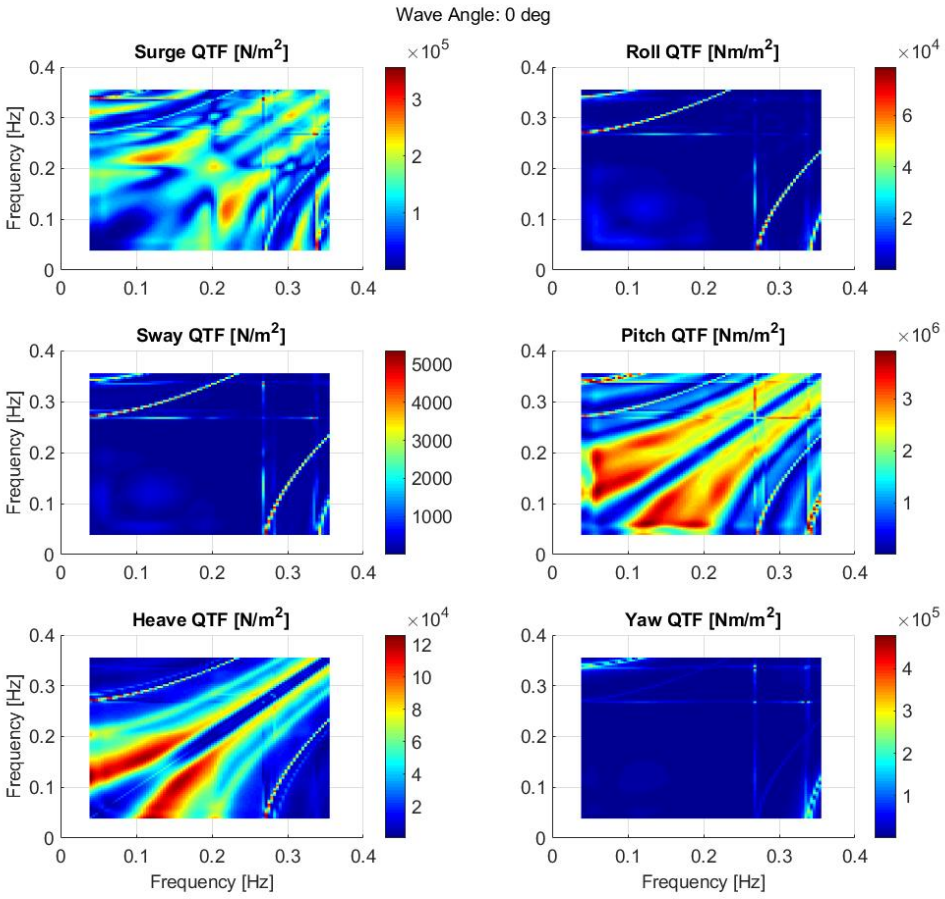

Figure 6-10: Difference Quadratic Transfer Function (QTF) for wave direction = 0

6.4 Mooring line model

The mooring system attached to the Activefloat is a three catenary mooring line system. The design was done such that at maximum rotor thrust, the maximum surge is below 15m, and no vertical forces are applied on the anchor. Moordyn coupled to FAST was used to the calculation of the mooring lines dynamics. The lines are modelled as chain lines, with diameter 0.16m, and axial stiffness of 2.3 GN. The mass per unit length of the line is equal to 561.2 kg/m. The total unstretched lines length is 614m and divided into 80 calculation segments.

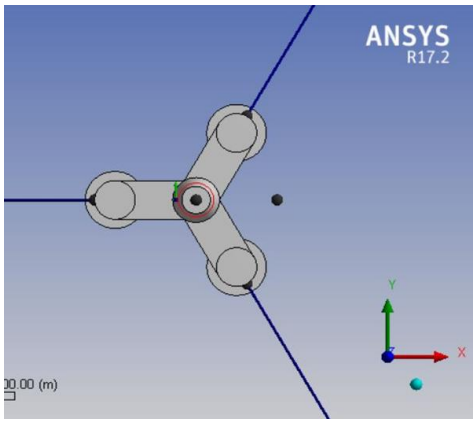

Figure 6-11: Mooring fairlead connection to Activefloat

Table 6-9: Mooring lines configuration

Line #	Anchor coordinates [m]			Fairlead coordinates[m]		
	X	Y	Z	X	Y	Z
1	-600.0	0.0	-200	-42.5	0.0	-15.0
2	300	-519.6152	-200	21.25	-36.806	-15.0
3	300	519.6152	-200	21.25	36.806	-15.0

6.5 Controller adaptation

The controller adaptation for the ActiveFloat platform follows essentially the same steps as in the case of WindCrete platform. However, we used the same retuned controller WindCrete and achieved an acceptable result. Therefore, at this step a sperate tuning of the controller for this platform is not carried out. The controller parameters will be further optimized for Activefloat at a later stage of the project.

6.6 System Identification

Simulations shown in Table 4-3 are done to identify the system properties. We will show the outputs of these simulations in the following sections for the Activefoat floater.

6.6.1 Static Equilibrium

First, we ran a static equilibrium simulation to identify the offsets in heave pitch and surge in the absence of wind and waves. The goal is to make sure that the system is balanced and the global mass and net buoyancy match each other.

The offsets especially in pitch and surge are because the CG of the tower top mass has an offset from the tower axis.

Table 6-10: Offsets of the platform in the 6 DOFs

Surge [m]	Sway [m]	Heave [m]	Roll [deg]	Pitch [deg]	Yaw [deg]
0.052	0.0	0.025	0.0	-1.799	0.0

6.6.2 Free Decays

We then ran decay tests for surge, heave, pitch and yaw DOFs. The natural frequencies of these DOFs are calculated and are listed in Table 6-11. For every DOF an initial displacement was introduced, and the system was left to oscillate freely in the absence of wind and waves. The mooring lines were attached to the system during all decay simulations.

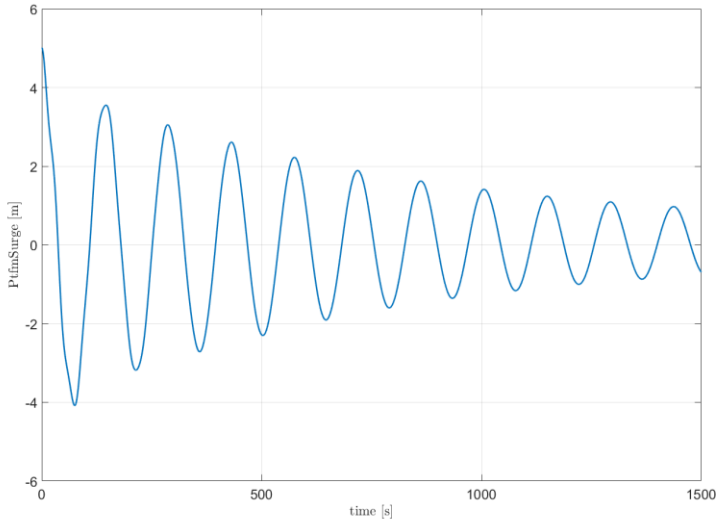

Figure 6-12: Surge decay of Activefloat floater

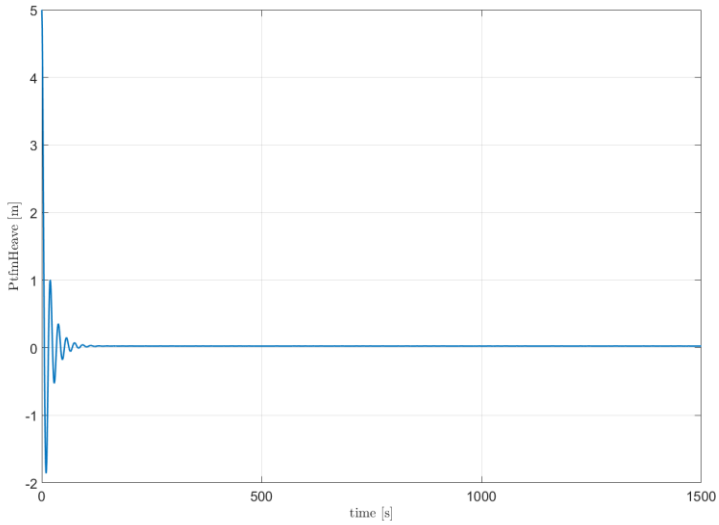

Figure 6-13: Heave decay of Activefloat floater

Table 6-11: Activefloat's natural frequencies in surge, heave, pitch and yaw

	Surge [Hz] / [s]	Heave [Hz] / [s]	Pitch [Hz] / [s]	Yaw [Hz] / [s]
Frequency [Hz]	0.0061	0.05493	0.0305	0.01221
Period [s]	163.9	18.2	32.7	81.9

Moreover, we also did tower decay test for in both side to side and fore-aft DOFs for the floating moored configuration. The goal is to check that the tower's natural frequencies lie outside the 1P and 3P frequencies. From [1], the 1P frequency range of [0.0833 to 0.1260] Hz and a 3P range of [0.25 to 0.378] Hz are used. The tower side to side and fore-aft natural frequencies are shown in the table below. The tower's frequencies are outside the 1P and 3P frequencies range.

Table 6-12: Activefloat's tower natural frequencies

Tower side to side [Hz]	Tower fore-aft [Hz]
0.4395	0.4395

6.6.3 Step Wind

We used step wind field of steady wind velocities, in the absence of waves to check the controller's performance. The wind field started at 3m/s and increased, with 1m/s step, till 25m/s then back to 3m/s also with 1m/s step. The duration of the step is 200s for every wind speed. During this simulation the active ballast system was not active because the mass properties of the system cannot be changed during a simulation.

Figure 6-14 shows that the controller is performing properly for different degrees of freedom.

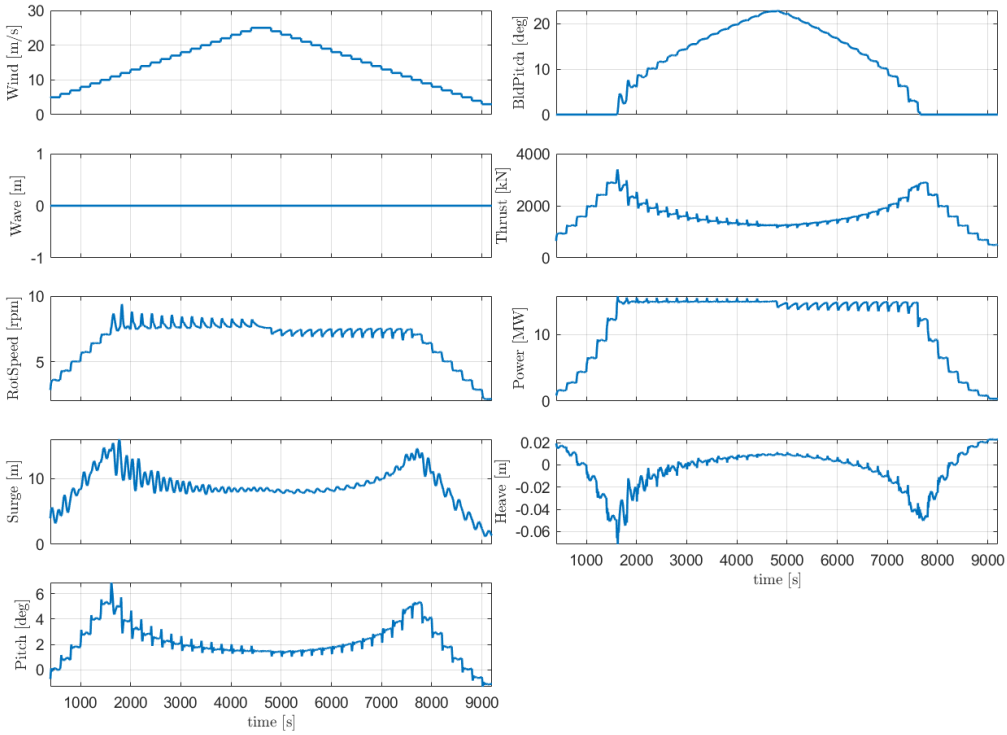

Figure 6-14: Timeseries response of Activefloat floater

6.6.4 Regular waves

The next and last step for the Activefloat system identification is regular wave simulation. In the absence of wind, we simulated the floating wind turbine with the regular waves of significant height (Hs) = 2m and peak period (Tp) of 6s. These wave characteristics were taken from the Gran Canaria site characteristics in [16].

The time series for the floating response is shown in Figure 6-15. The turbine response is stable for all degrees of freedom. The thrust force shown in the figure is the force along the shaft of the turbine (including inertia effects), because of this the thrust is not equal to zero. As observed for the WindCrete floater, the response to regular waves is small, due to the large inertia of the system and the relatively small wave amplitude used.

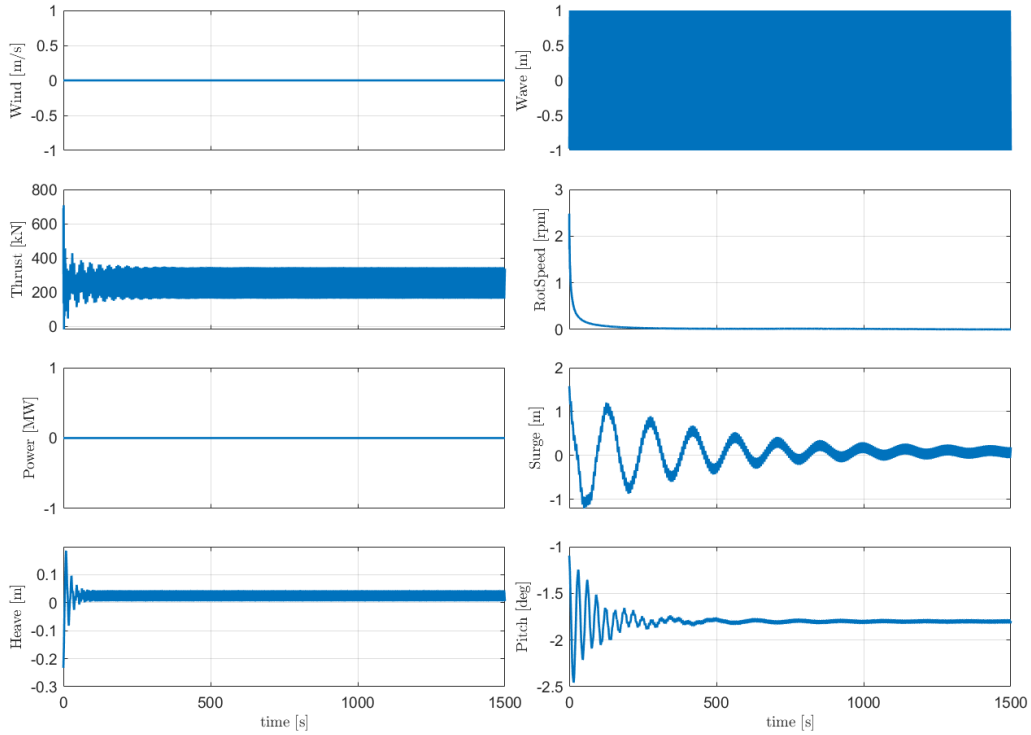

Figure 6-15: Timeseries response of Activefloat floater for regular waves

6.6.5 Extreme turbulence wind and stochastic waves (DLC 1.3)

The next simulation carried out is DLC 1.3 [IEC standard], were an extreme turbulent wind field for wind speeds (8, 10.5, 16, 20, 25) m/s and stochastic wave of (Hs=2m, and Tp=6s). The first 1800s were excluded from the PSD analysis, to make sure there are no transient conditions. The second order wave forces are taken into consideration, by taking the difference QTF into account. We decided to use only the difference QTF as it is the most relevant for our system due to the low natural frequencies of the floater. The Figures shown here are only at windspeed 10.5m/s. The rest of the simulations can be seen in the Appendix.

The system is performing as expected with some results out of the validity ranges set in [17]. This is considered acceptable given that the results in the following table are absolute maximums and even so, the deviations are small. Also, it shall be noted that the current model is an early design than requires refinement.

Table 6-13: Activefloat's motion ranges

	Yaw maximum [deg]	Yaw average [deg]	Pitch maximum [deg]	Pitch average [deg]	Roll maximum [deg]	Roll average [deg]
8 m/s	5.358	0.403	5.160	0.049	0.942	0.374
10.5 m/s	8.273	1.059	-5.459	0.017	1.341	0.525
16 m/s	7.951	1.155	3.660	0.031	1.752	0.687
20 m/s	14.130	1.756	3.508	0.029	2.440	0.837

25 m/s	13.850	2.226	-2.867	0.022	3.228	1.042

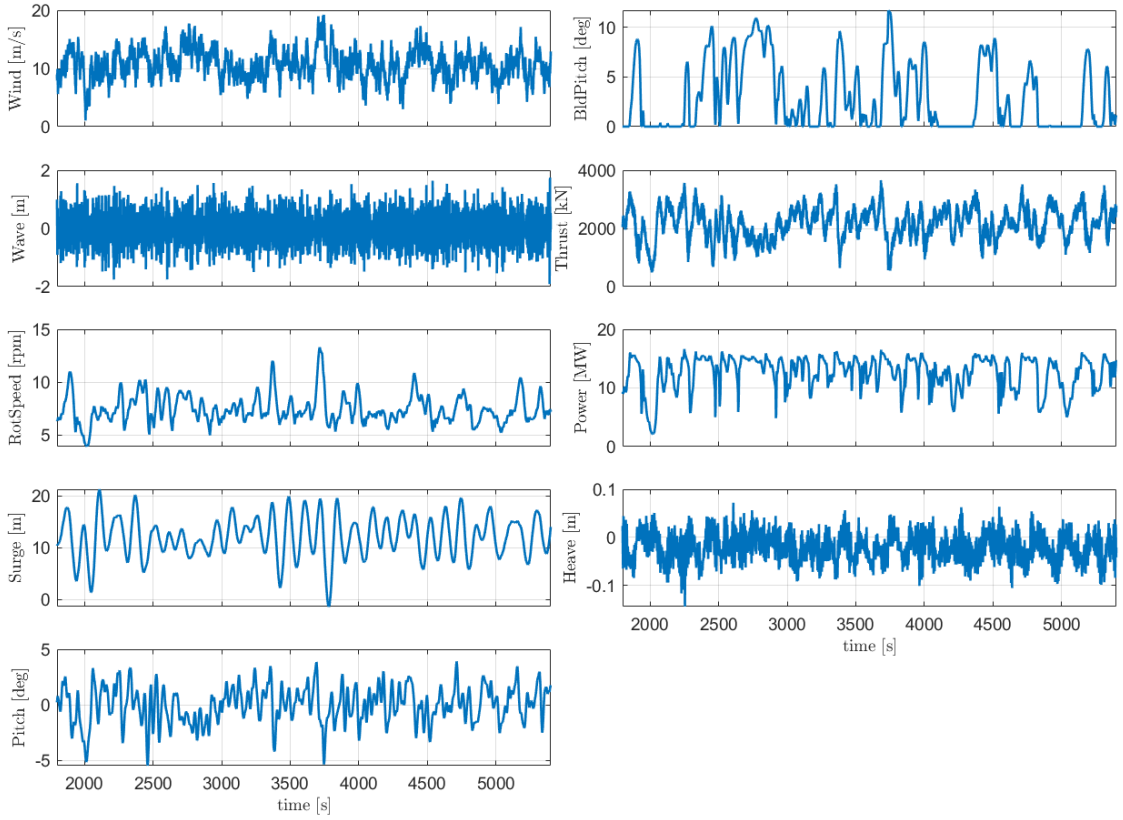

Figure 6-16: Timeseries response of Activefloat floater for DLC 1.3 wind speed 10.5 m/s

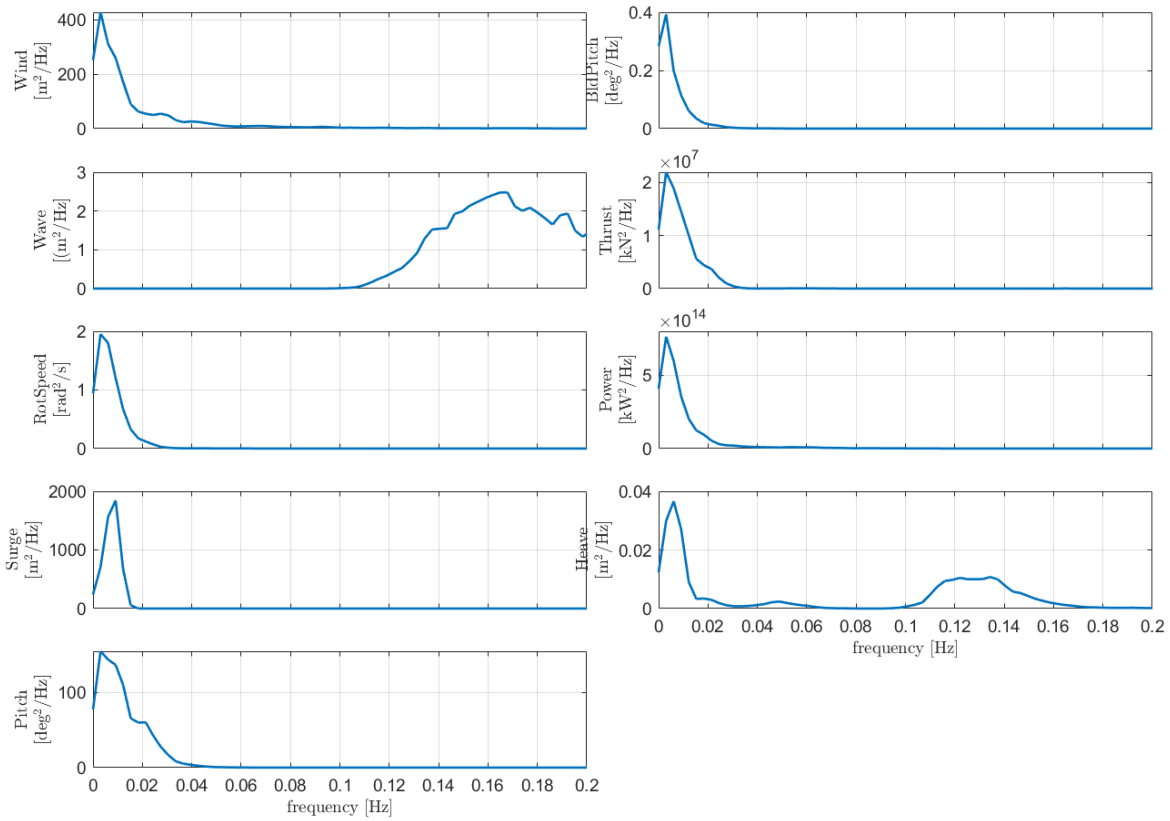

Figure 6-17: Power spectrum density of Activefloat floater for DLC 1.3 at wind speed 10.5 m/s

Table 6-14: Activefloat's maximum nacelle accelerations in translation and rotation

	Nacc. acc in x-axis [m/s^2]	Nacc. acc in y-axis [m/s^2]	Nacc. acc in z-axis [m/s^2]	Nacc. rot. acc around x-axis [deg/s^2]	Nacc. rot. acc around y-axis [deg/s^2]	Nacc. rot. acc around z-axis [deg/s^2]
8 m/s	0.918	0.338	0.264	0.892	2.879	0.121
10.5 m/s	1.826	0.486	0.593	1.429	6.223	0.171
16 m/s	1.717	0.838	0.565	1.341	4.815	0.148
20 m/s	1.786	0.892	0.722	1.473	6.429	0.162
25 m/s	1.385	0.793	0.602	1.650	6.166	0.176

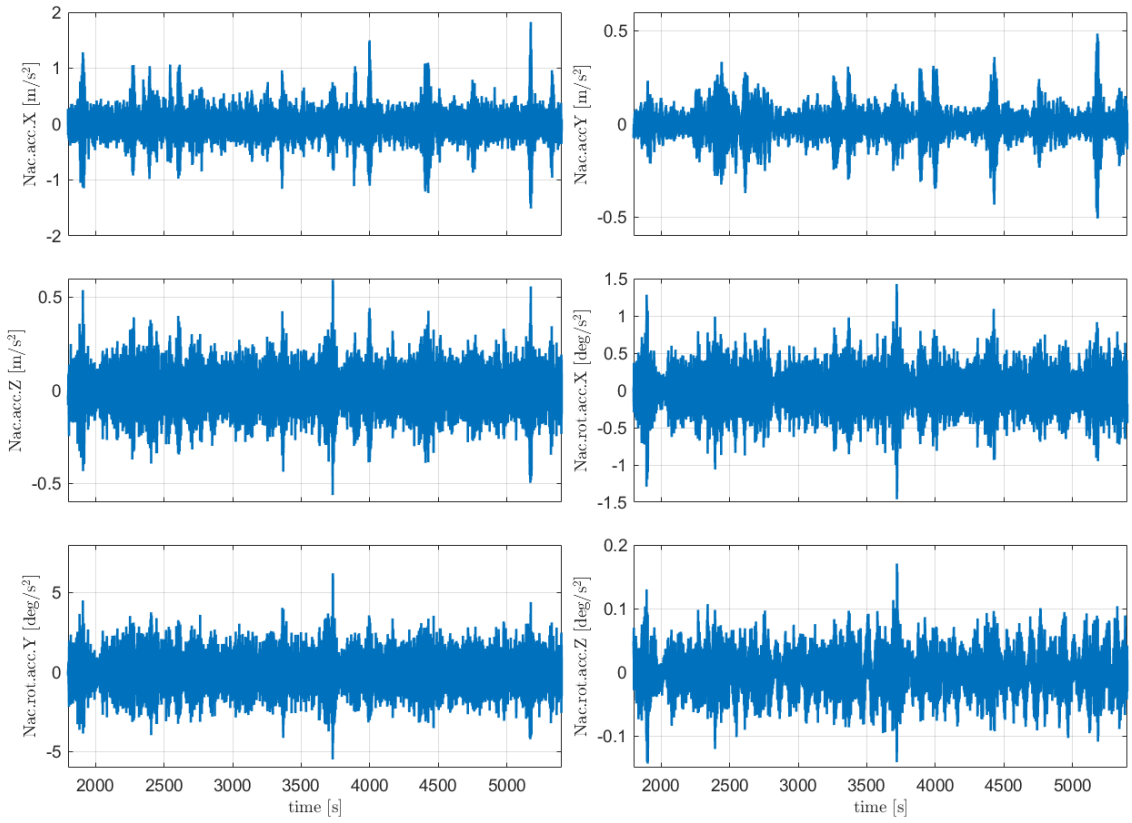

Figure 6-18: Timeseries response of nacelle acceleration of Activefloat floater for DLC 1.3 wind speed 10.5 m/s

As observed for the WindCrete, the floater response is dominated by wind loads in all the degrees of freedom. The wave spectrum is only visible in the PSD of heave. This is due to the relatively mild wave conditions at the site (even for a 50-year sea state) and the much larger turbine size.

In the time series of nacelle acceleration we can see that there are high repeated oscillations. We had a closer look at the PSD to understand the reasons behind these oscillations. We can see in Figure 6-19 that there are three peaks in the frequency spectrum, the first corresponds to the natural frequencies of the floater, excited by the wind and the low-frequency second order wave forces. The second is the wave peak frequency. Finally, the highest peak at 0.47 Hz corresponds to the tower natural frequency. Therefore, the peaks in the nacelle acceleration time series are due to tower vibrations.

We looked at the timeseries of the wind, blade pitch, thrust, and nacelle accelerations again to understand the reason of the tower excitation in Figure 6-20. When there is a sudden increase in the blade pitch, the thrust force decreases, and hence the horizontal force on the tower is suddenly reduced. This sudden drop of the horizontal applied force on the tower leads to tower oscillations, which causes the peaks in the nacelle accelerations. We believe that these impulsive forces can be decreased by tuning the blade pitch rate of the controller (making pitching slower), then the change in thrust will be also slower.

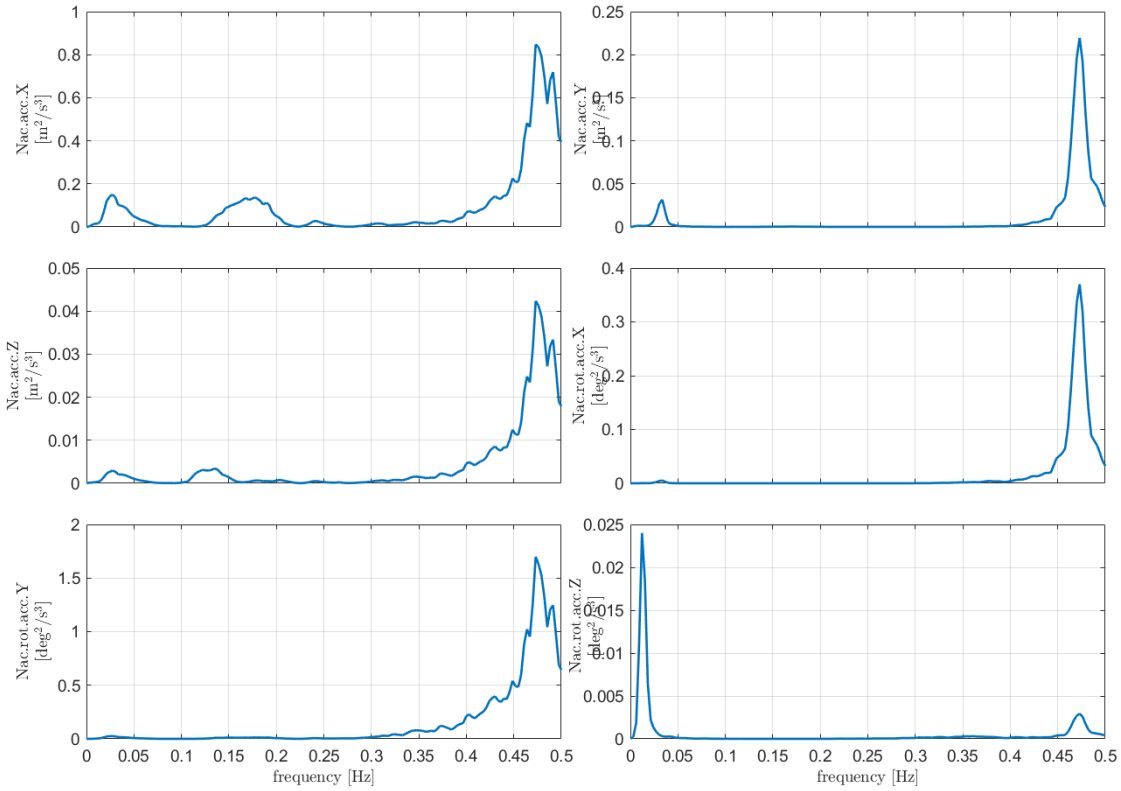

Figure 6-19: Frequency response of nacelle acceleration of Activefloat floater for DLC 1.3 wind speed 10.5 m/s

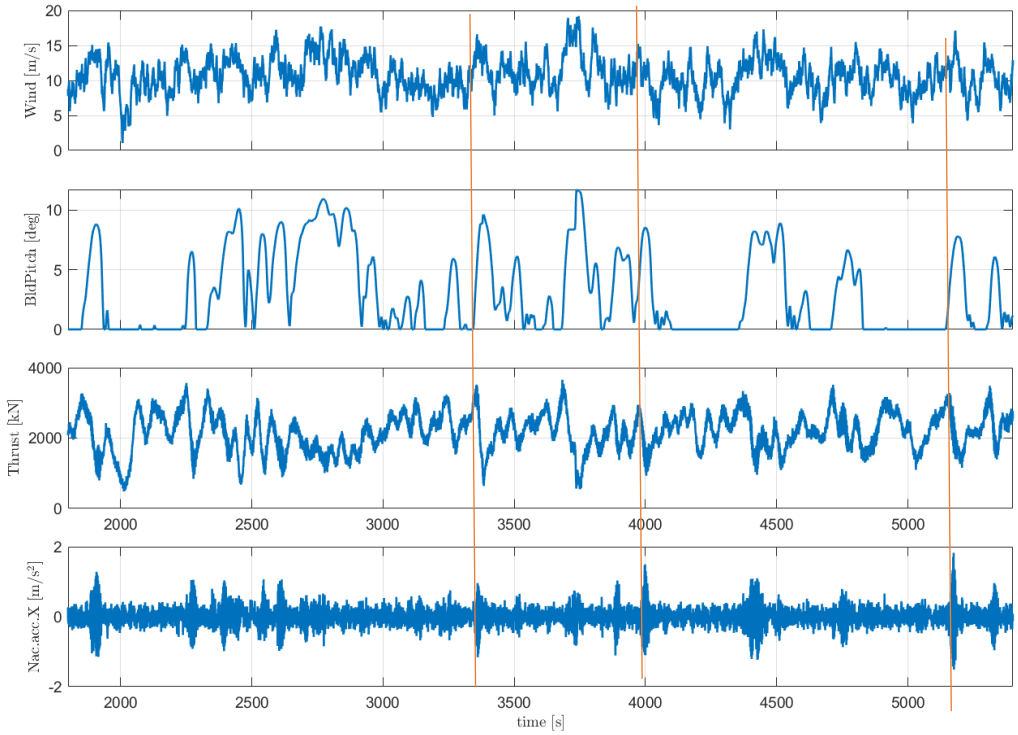

Figure 6-20: Timeseries of wind, blade pitch, thrust and nacelle acceleration of nacelle acceleration of Activefloat floater for DLC 1.3 wind speed 10.5 m/s

6.6.6 Normal turbulence wind and extreme stochastic waves (DLC 1.6)

The next simulation carried out is DLC 1.6 [IEC standard], with a normal turbulence wind field for wind speeds (8, 10.5, 16, 20, 25) m/s and extreme stochastic wave of (Hs=5.11m, and Tp=9s). The first 1800s were excluded from the PSD analysis, to make sure there are no transient conditions. The second order wave forces are taken into consideration, by taking the difference QTF into account. The Figures shown here are only at windspeed 10.5m/s. The rest of the simulations can be seen in the Appendix.

The system is performing as expected with some results out of the validity ranges set in [17]. This is considered acceptable given that the results in the following table are absolute maximums and even so, the deviations are small. Also, it shall be noted that the current model is an early design than requires refinement.

Table 6-15: Activefloat's motion ranges

	Yaw maximum [deg]	Yaw average [deg]	Pitch maximum [deg]	Pitch average [deg]	Roll maximum [deg]	Roll average [deg]
8 m/s	3.324	0.485	-2.709	0.043	0.657	0.365
10.5 m/s	5.446	1.072	-4.111	0.027	1.063	0.547
16 m/s	5.698	1.166	-2.545	0.024	1.426	0.700
20 m/s	10.319	1.719	-2.599	0.022	2.106	0.840
25 m/s	11.272	2.254	-2.441	0.019	2.720	1.047

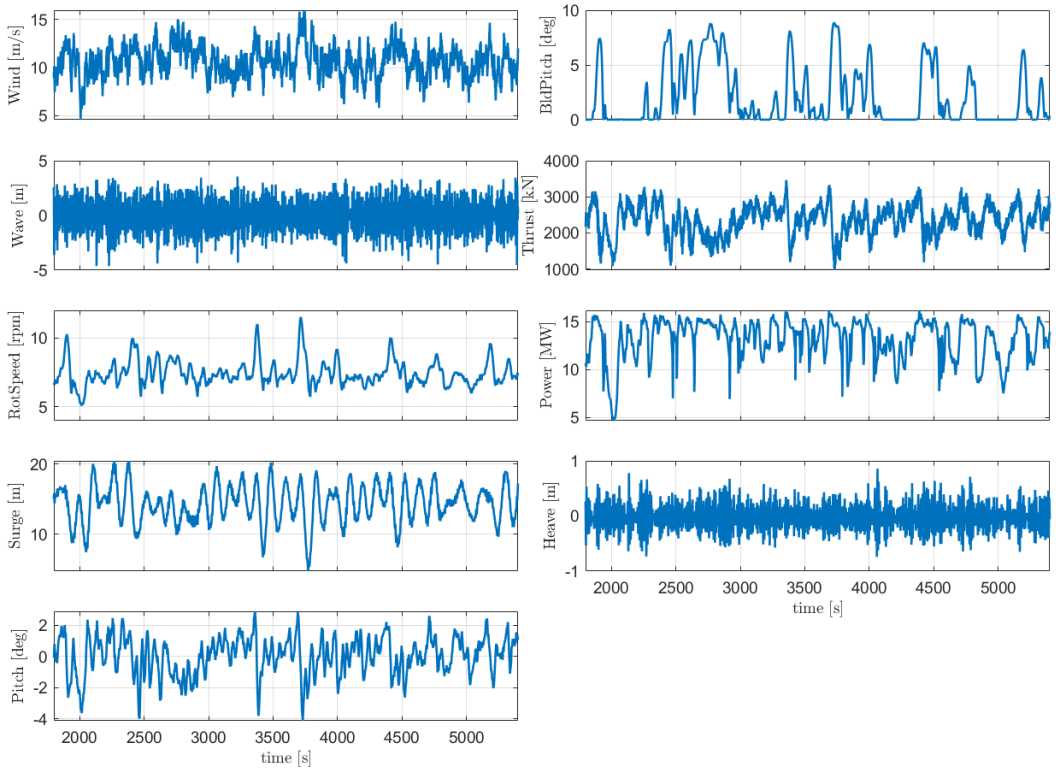

Figure 6-21: Timeseries response of Activefloat floater DLC 1.6 at wind speed 10.5 m/s

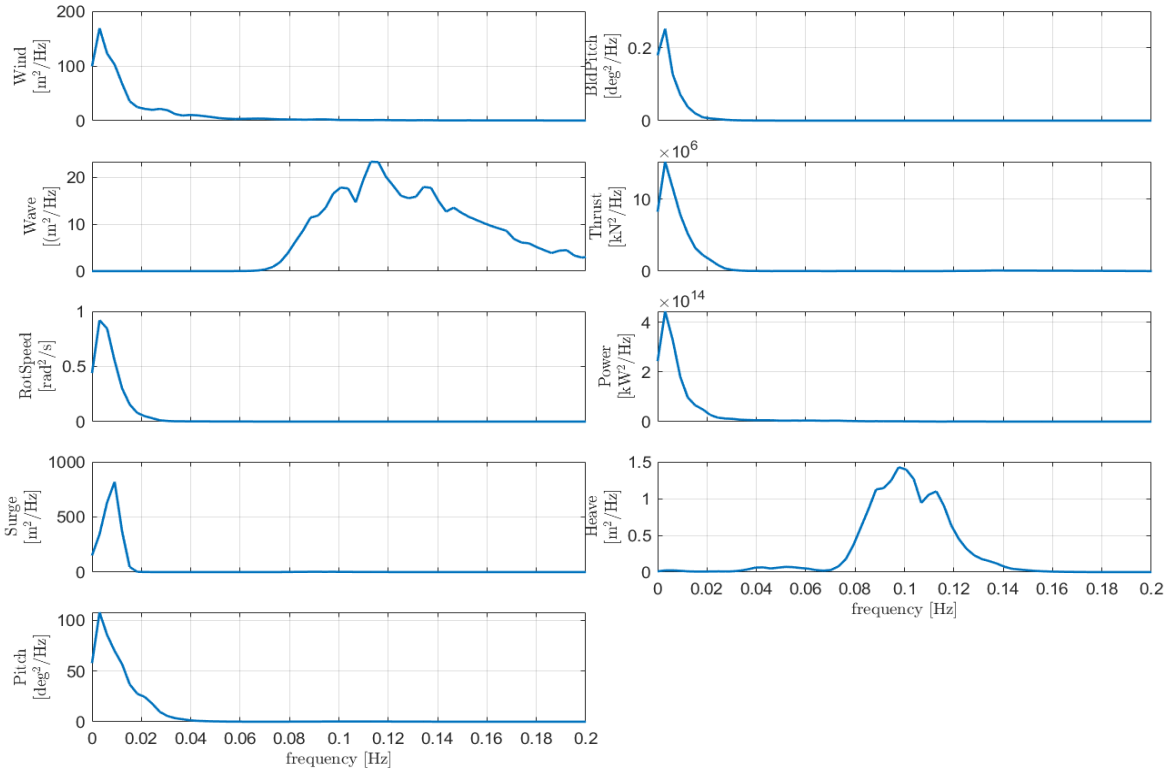

Figure 6-22: Power spectrum density of Activefloat floater for DLC 1.6 windspeed 10.5 m/s

Table 6-16: Activefloat's maximum nacelle accelerations in translation and rotation

	Nacc. acc in x-axis [m/s^2]	Nacc. acc in y-axis [m/s^2]	Nacc. acc in z-axis [m/s^2]	Nacc. rot. acc around x-axis [deg/s^2]	Nacc. rot. acc around y-axis [deg/s^2]	Nacc. rot. acc around z-axis [deg/s^2]
8 m/s	0.843	0.084	0.368	0.341	1.809	0.047
10.5 m/s	1.347	0.343	0.576	0.822	3.133	0.075
16 m/s	1.337	0.372	0.615	0.944	3.564	0.102
20 m/s	1.563	0.697	0.565	1.175	4.282	0.120
25 m/s	1.168	0.619	0.557	1.235	4.034	0.121

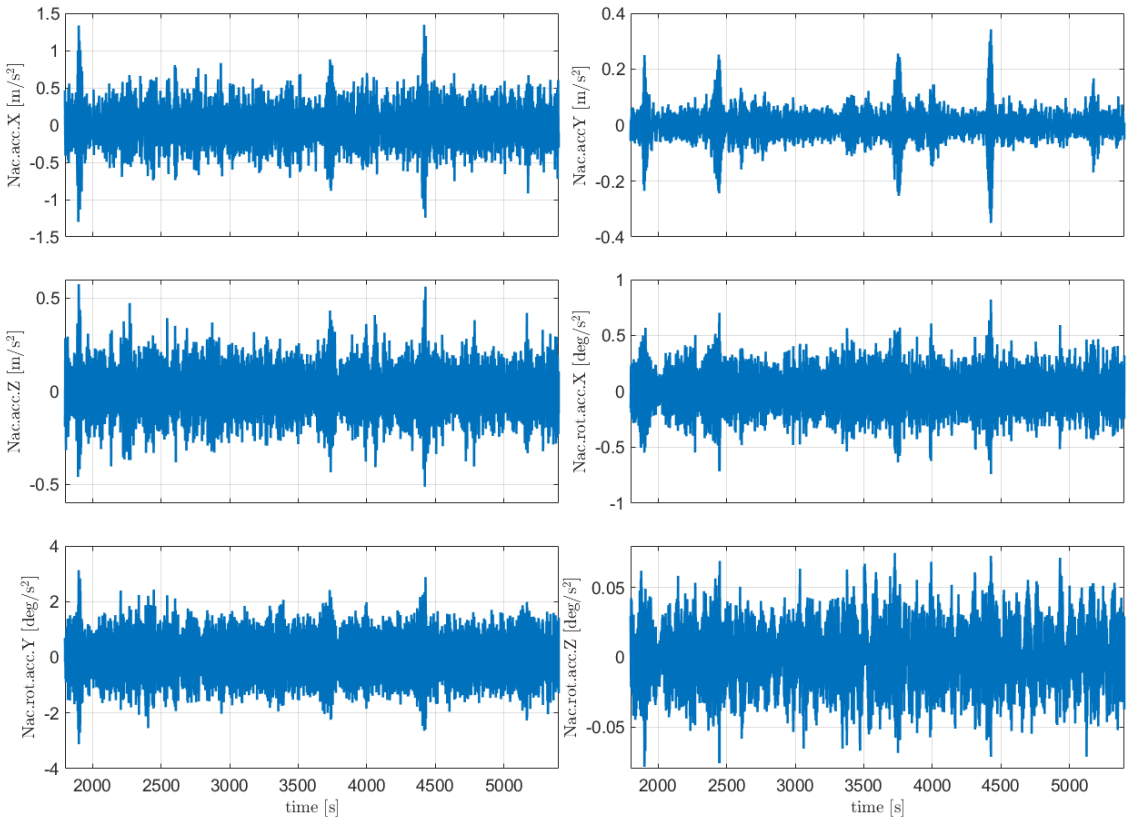

Figure 6-23: Timeseries response of nacelle acceleration of Activefloat floater DLC 1.6

6.6.7 Power production with grid loss (DLC 2.1)

The power production with grid loss was simulated following [IEC standard]. A normal turbulence wind field with wind speed of 20m/s was used. A 600s simulation is used and the grid loss happens at 500s. A brake is applied to the generator shaft linearly. The braking torques starts at zero and ramps linearly to reach the rated turbine torque in 0.6s.

The maximum pitch is -6.29 degrees.

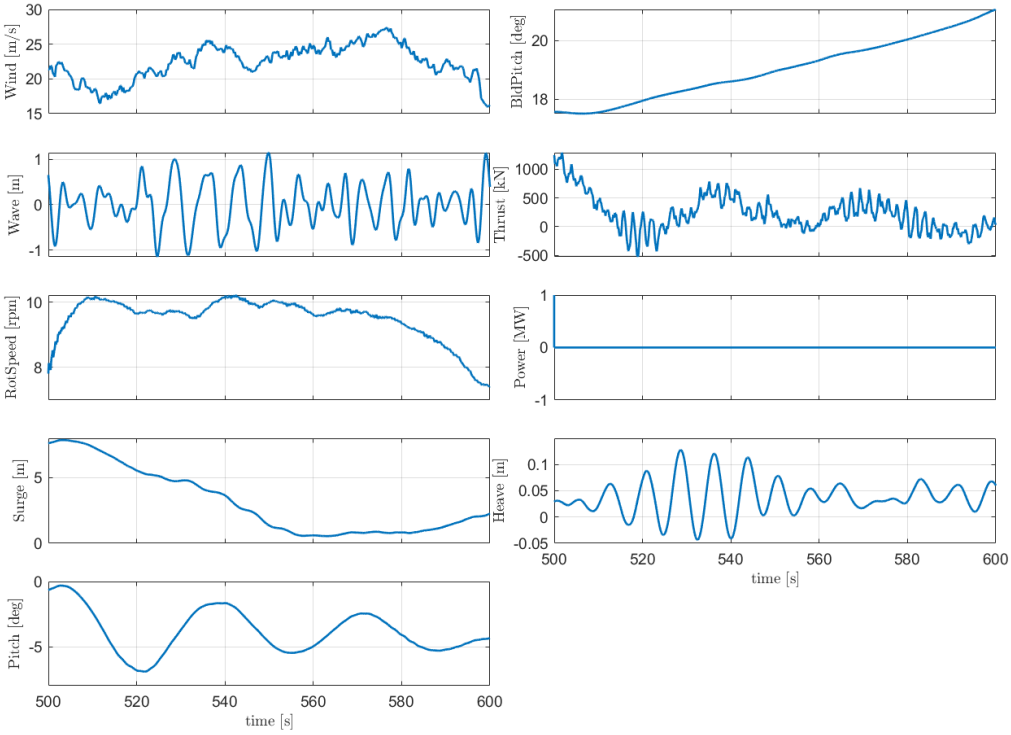

Figure 6-24: Timeseries response of Activefloat floater for DLC 2.1

Table 6-17: Activefloat's maximum nacelle accelerations in translation and rotation

Nacc. acc in x-axis [m/s^2]	Nacc. acc in y-axis [m/s^2]	Nacc. acc in z-axis [m/s^2]	Nacc. rot. acc around x-axis [deg/s^2]	Nacc. rot. acc around y-axis [deg/s^2]	Nacc. rot. acc around z-axis [deg/s^2]
1.107	0.660	0.419	10.060	3.450	1.025

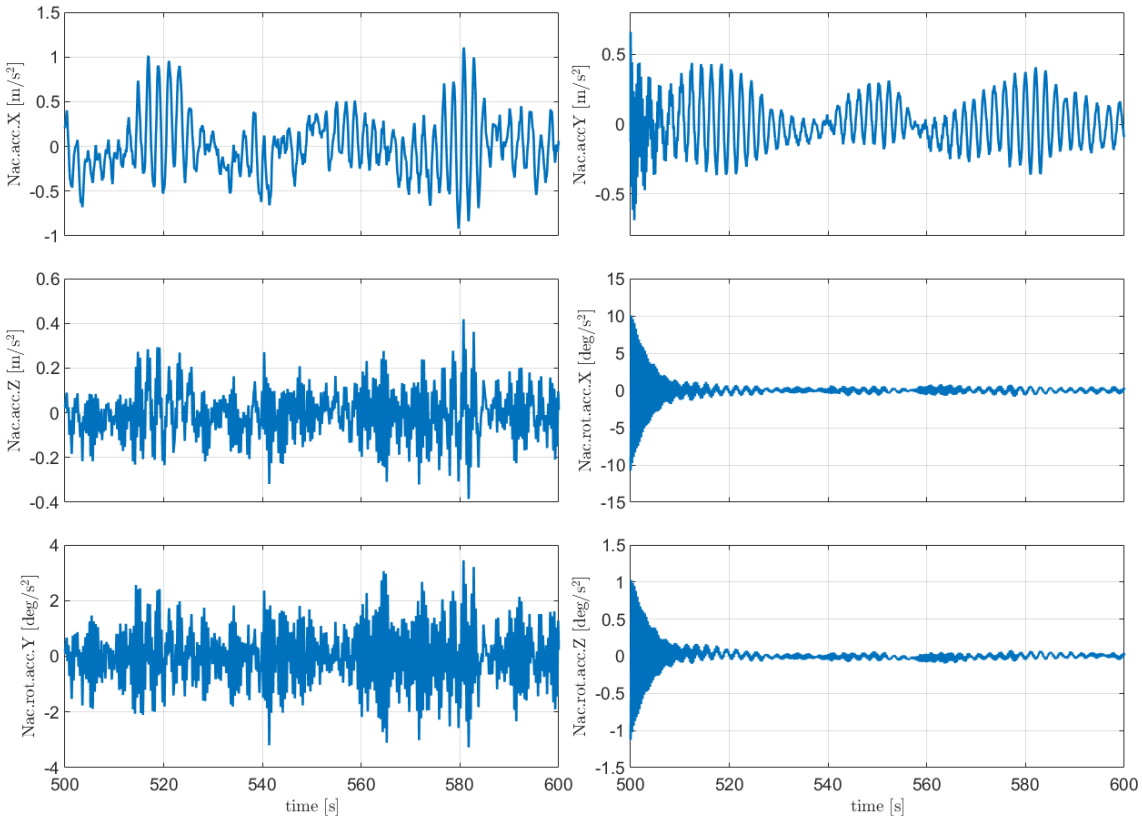

Figure 6-25: Timeseries response of nacelle acceleration Activefloat floater for DLC 2.1

6.6.8 Parked turbine in 50-years extreme wind and waves (DLC 6.1)

A parked turbine with the blades fully pitched out of the wind is simulated for 50-years extreme wind and waves. The values for extreme wind and waves used in the simulations were taken from [DL1.2 ref] for the Gran Canaria site. The 50-years extreme winds value is 41.2m/s. The value for 50 years extreme waves is Hs=5.1m and Tp=9s. The duration of the simulation is 5400s, where the first 1800s were neglected to ensure we are out of the transient period.

Table 6-18: Activefloat's motion ranges

Yaw maximum [deg]	Yaw average [deg]	Pitch maximum [deg]	Pitch average [deg]	Roll maximum [deg]	Roll average [deg]
2.747	0.199	3.697	0.875	1.888	0.176

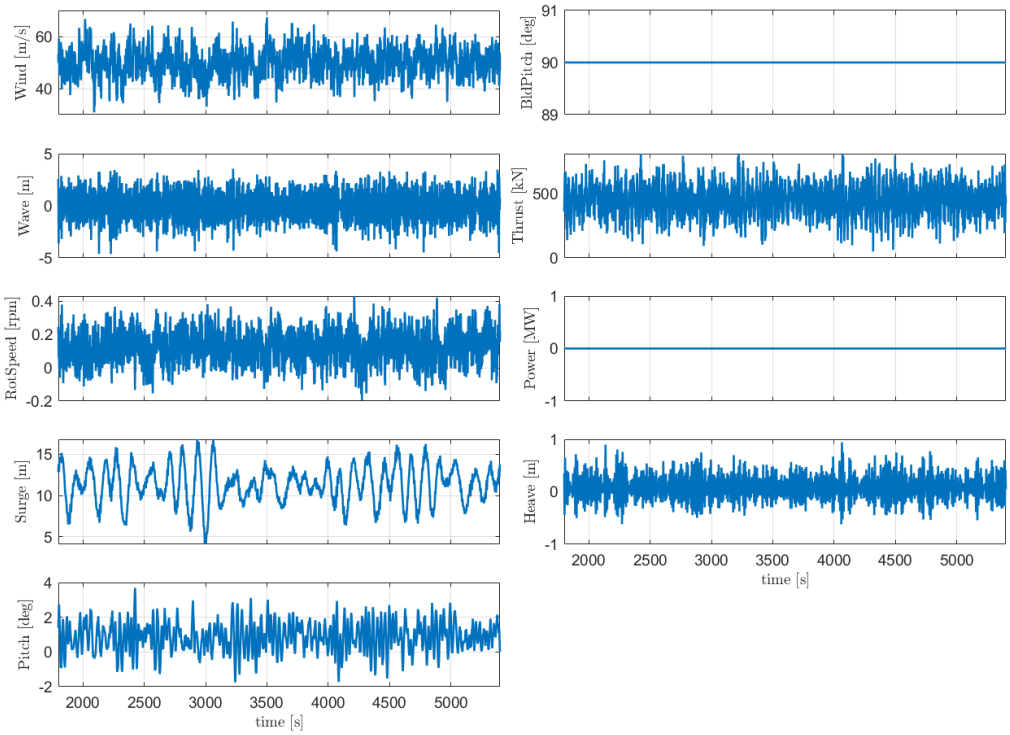

Figure 6-26: Timeseries response of Activefloat floater for DLC 6.1

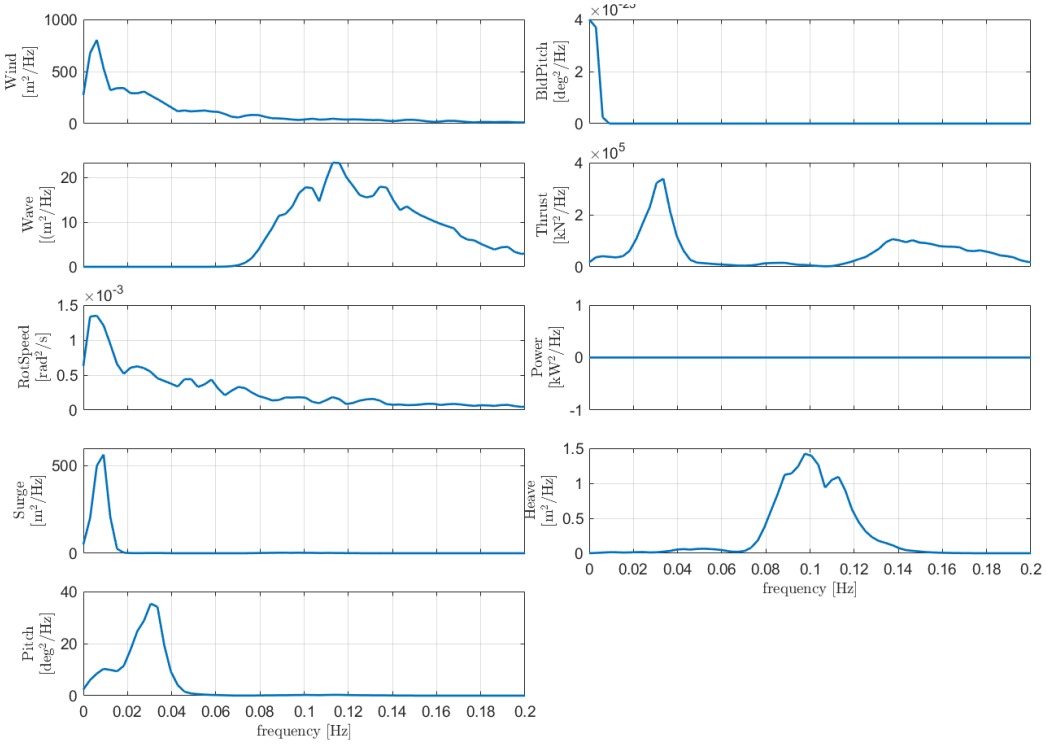

Figure 6-27: Power spectrum density of Activefloat floater for DLC 6.1

Table 6-19: Activefloat's maximum nacelle accelerations in translation and rotation

Nacc. acc in x-axis [m/s^2]	Nacc. acc in y-axis [m/s^2]	Nacc. acc in z-axis [m/s^2]	Nacc. rot. acc around x-axis [deg/s^2]	Nacc. rot. acc around y-axis [deg/s^2]	Nacc. rot. acc around z-axis [deg/s^2]
0.827	0.411	0.347	0.741	1.040	0.075

Looking at the PSD of the floater response, it is clear that the surge and pitch responses are resonant, dominated by wind and second-order hydrodynamic loads. The linear wave loads are only visible in the PSD of heave.

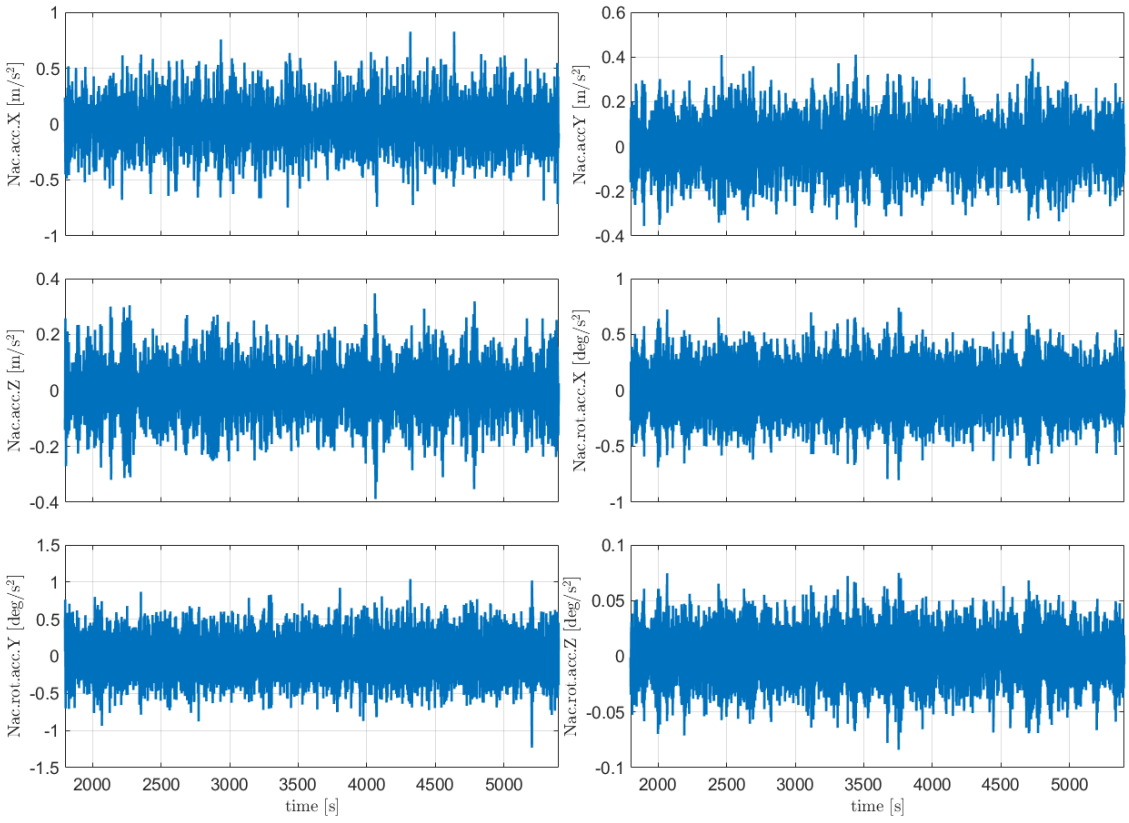

Figure 6-28: Timeseries response of Activefloat floater for DLC 6.1

7 Models accessibility

The OpenFAST models of both floaters are available for public use on the following link http://corewind.eu/. In case of publication in work using these models, proper referencing of this report should be included.

8 Conclusion

In this report we presented two floating OpenFAST models for a spar (WindCrete), and a semi-submersible (Activefloat). The turbine used in this report is the IEA Wind 15MW reference wind turbine. The aerodynamics of the turbine and the rotor nacelle assembly were not the main goal of the task, since the OpenFAST model presented by IEA Task 37 was used as a base model for the rotor-nacelle assembly. Our main goal is to introduce

both floaters and the changes needed in the numerical models to couple the floaters and the turbine, including the mooring system and the modified wind turbine control settings. The detailed structure of both models is explained, including hydrodynamics, mooring system, tower and modifications to the controller properties.

A preliminary verification of the models is done and the results are shown through the report. The simulated responses are as expected and generally within the design limitations introduced in Table 4-2. The load cases are chosen to calculate the static offsets, natural frequencies, and check the controller performance, as well as to check the dynamic response of the models in normal and severe environmental conditions.

The responses of both floaters are strongly dominated by wind forces. The linear wave loads generally don't have a significant impact on the response spectra. This is likely due to the larger size of the wind turbine, and to the relatively mild sea conditions at the chosen site. The effect of second-order wave forces in the response is significant, especially compared to linear wave loads. This emphasizes the importance of second order forces as shown in Figure 5-26. However, we note the strong dependency of the resonant responses on the amount of damping and the need to compare to physical test results in order to properly calibrate the damping in the model. Wave tank tests will be carried out later within the COREWIND project.

The models will be used for the further work in COREWIND project on mooring design, dynamic cable design, wind farm dynamics and planning. The models are currently available to the public as indicated in section 7.

9 References

[1] E. Gaertner, J. Rinker, L. Sethuraman, F. Zahle, B. Anderson, G. Barter, N. Abbas, F. Meng, P. Bortolotti, W. Skrzypinski, G. Scott, R. Feil, H. Bredmose, K. Dykes, M. Shields, C. Allen and A. Viselli, "Definition of the IEA Wind 15-Megawatt Offshore Reference Wind Turbine," 2020.

[2] H. Bredmose, J. Rinker, W. Skrzypinski, F. Zahle, F. Meng, K. Dykes, E. Gaertner, G. Barter, P. Bortolotti, L. Sethuraman and M. Shields, "COREWIND D1.1: Definition of the 15 MW Reference Wind Turbine," 2020.

[3] T. Larsen and T. Hanson, "A method to avoid negative damped low frequent tower vibrations for a floating, pitch controlled wind turbine," *Journal of Physics: Conference Series,* vol. 75, no. 1, 2007.

[4] NREL, *ROSCO. Version 1.0.0,* GitHub, 2020.

[5] T. Burton, D. Sharpe, N. Jenkins and E. Bossanyi, Wind energy: handbook, J. Wiley & Sons, 2001.

[6] J. Jonkman and M. Sprague, "NWTC Information Portal (OpenFAST)," [Online]. Available: https://nwtc.nrel.gov/OpenFAST.

[7] C. Lee and J. Newman, "WAMIT," 2016. [Online]. Available: http://www.wamit.com/.

[8] Ansys®, *AQWA,* Release 19.0.

[9] W. Cummins, "The impulse response functions and ship motions," *Schiffstechnik,* vol. 9, pp. 101-109, 1962.

[10] C. Lee, "WAMIT Theory Manual," Cambridge, Massachusetts, 1995.

[11] J. Jonkman, "Dynamics of offshore floating wind turbines - Model development and verification," *Wind Energy,* vol. 12, no. 5, pp. 459-492, 2009.

[12] J. Morison, J. Johnson and S. Schaaf, "The force exerted by surface waves on piles," *Journal of Petroleum Technology,* vol. 2, no. 05, pp. 149-154, 1950.

[13] F. Madsen, A. Pegalajar-Jurado, H. Bredmose, R. Faerron-Guzman, K. Müller and F. Lemmer, "LIFES50+ D4.6: Model validation against experiments and map of model accuracy across load cases," 2018.

[14] T. Duarte, A. Sarmento and J. Jonkman, "Effects of second-order hydrodynamic forces on floating offshore wind turbines," in *Proceedings of the 32nd ASME Wind Energy Symposium*, 2014.

[15] M. Hall, "MoorDyn," 2017. [Online]. Available: http://www.matt-hall.ca/moordyn.html.

[16] F. Vigara, L. Cerdán, R. Durán, S. Muñoz, M. Lynch, S. Doole, C. Molins, P. Trubat and R. Guanche, "COREWIND D1.2: Design Basis," 2019.

[17] The International Electrotechnical Commission (IEC), "IEC 61400-3, Wind turbines - Part 3: Design requirements for offshore wind turbines," 2009.

[18] IEC, "Wind energy generation systems - Part 3-2: Design requirements for floating offshore wind turbines," 2019-04-05.

[19] J. Journée and W. Massie, , Offshore hydromechanics, Delft University of Technology, 2001.

[20] A. Campos, C. Molins, X. Gironella, P. Trubat and D. Alarcón, "Experimental rao's analysis of a monolithic concrete spar structure for offshore floating wind turbines," in *Proceedings of the 34th International Conference on Ocean, Offshore and Arctic Engineering. OMAE 2015*, St. John's, NL, Canada, 2015.

[21] S. Hoerner, Fluid-dynamic drag, theoretical, experimental and statistical information, Bakersfield, CA: by the author, 1965.

[22] A. Pegalajar-Jurado, F. Madsen, M. Borg and H. Bredmose, "LIFES50+ D4.5: Qualification of innovative floating substructures for 10MW wind turbines and water depths greater than 50m," 2018.

[23] DNVGL, "Environmental conditions and environmental loads," 2017.

[24] L. Tao and D. Dray, "Hydrodynamic Performance of Solid and Porous Heave Plates," *Ocean Engineering,* vol. 35, pp. 1006-1014, July 2018.

10 Appendix

10.1 WindCrete

10.1.1 Extreme turbulence wind and stochastic waves (DLC 1.3)

- 8m/s

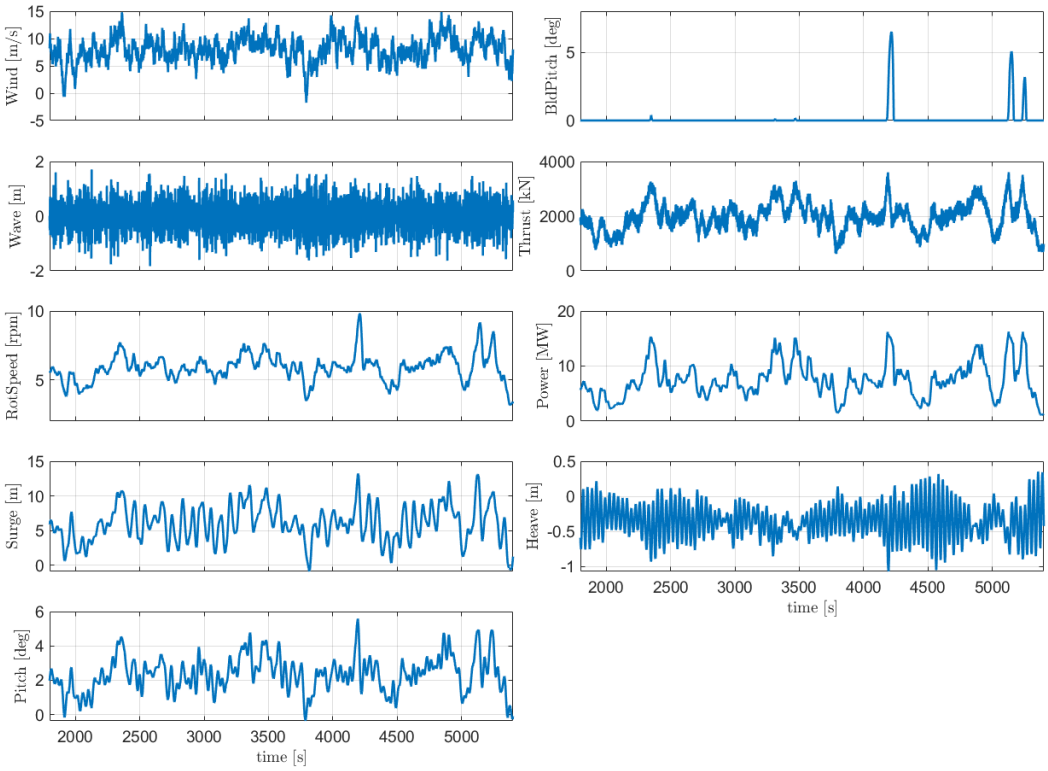

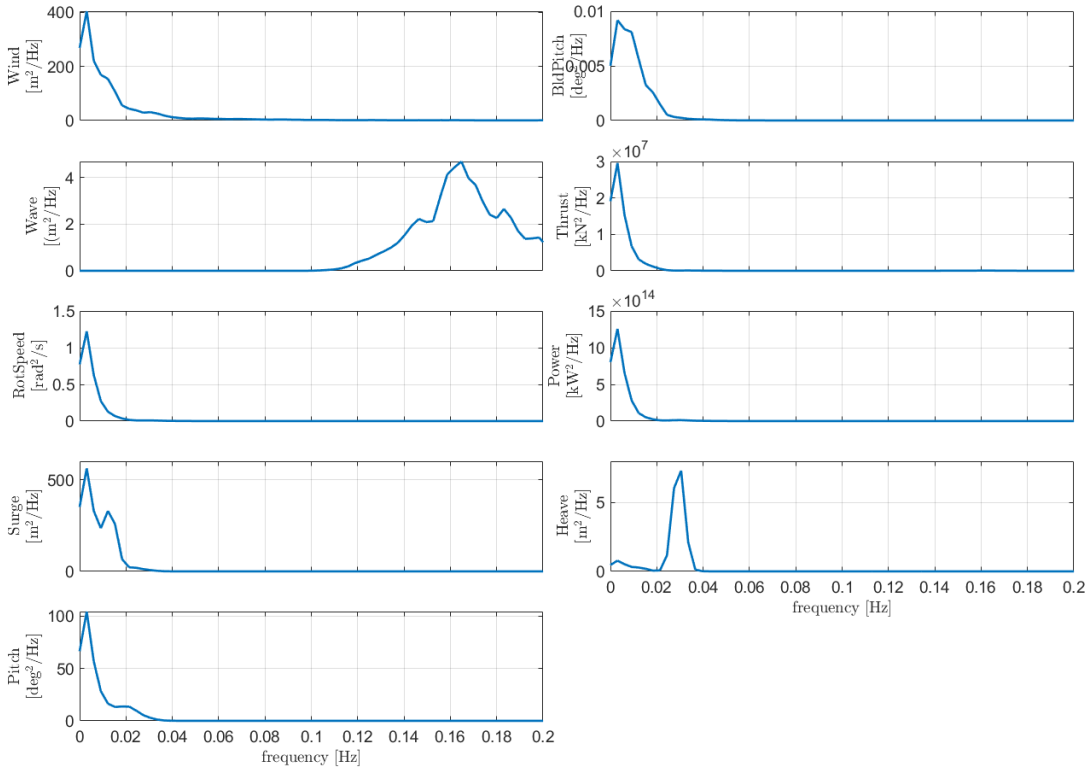
Wind [m²/Hz]
BldPitch [deg²/Hz]
Wave [(m²/Hz]
Thrust [kN²/Hz]
RotSpeed [rad²/s]
Power [kW²/Hz]
Surge [m²/Hz]
Heave [m²/Hz]
Pitch [deg²/Hz]
frequency [Hz]

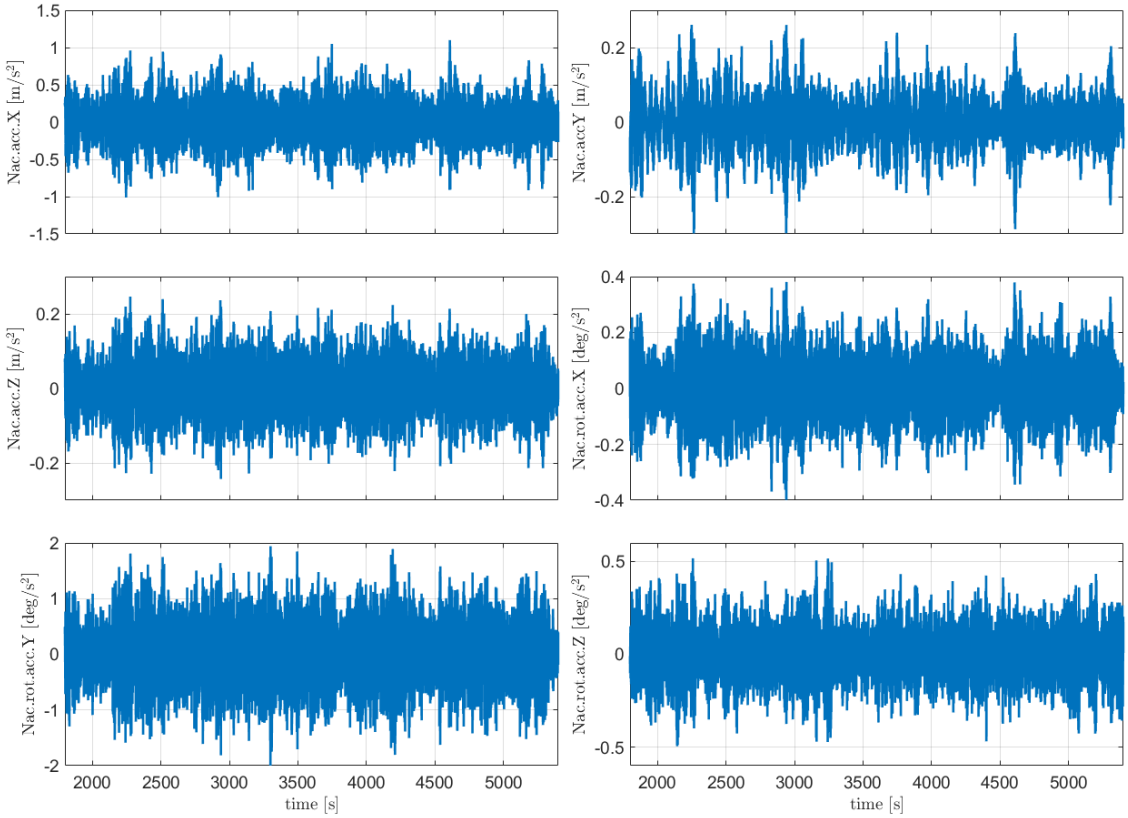
Nac.acc.X [m/s²]
Nac.acc.Y [m/s²]
Nac.acc.Z [m/s²]
Nac.rot.acc.X [deg/s²]
Nac.rot.acc.Y [deg/s²]
Nac.rot.acc.Z [deg/s²]
time [s]

- 16m/s

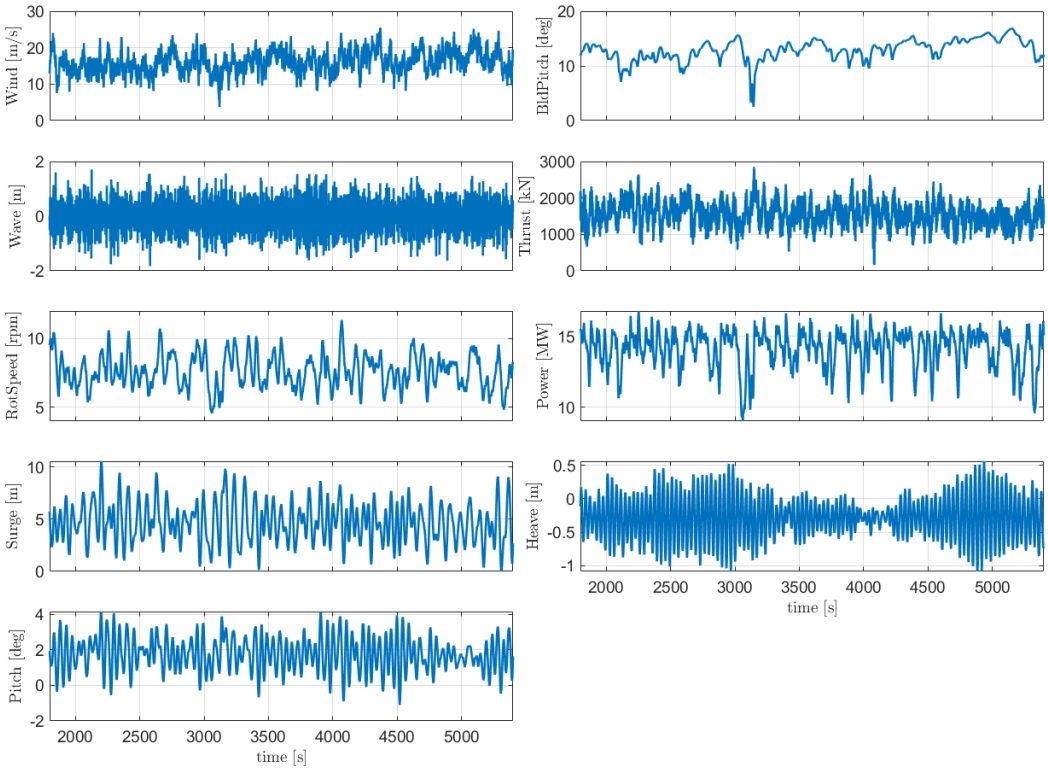
Wind [m/s]
BldPitch [deg]
Wave [m]
Thrust [kN]
RotSpeed [rpm]
Power [MW]
Surge [m]
Heave [m]
Pitch [deg]
time [s]

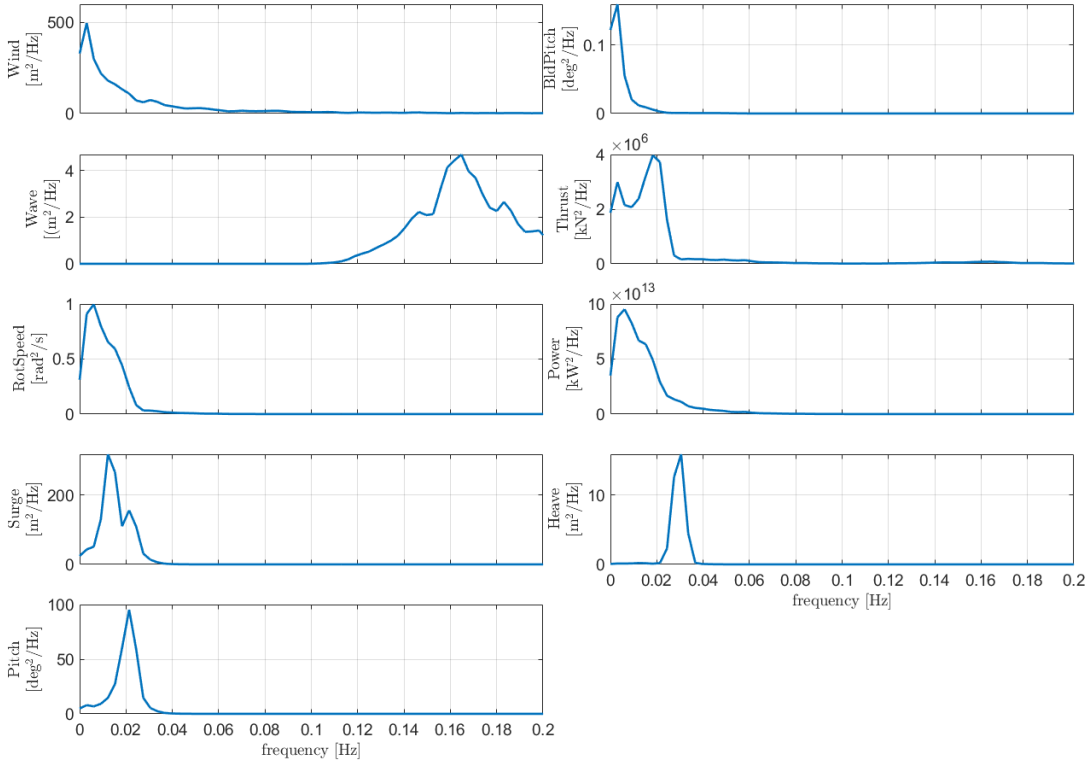
Wind [m²/Hz]
BldPitch [deg²/Hz]
Wave [(m²/Hz]
Thrust [kN²/Hz]
RotSpeed [rad²/s]
Power [kW²/Hz]
Surge [m²/Hz]
Heave [m²/Hz]
Pitch [deg²/Hz]
frequency [Hz]

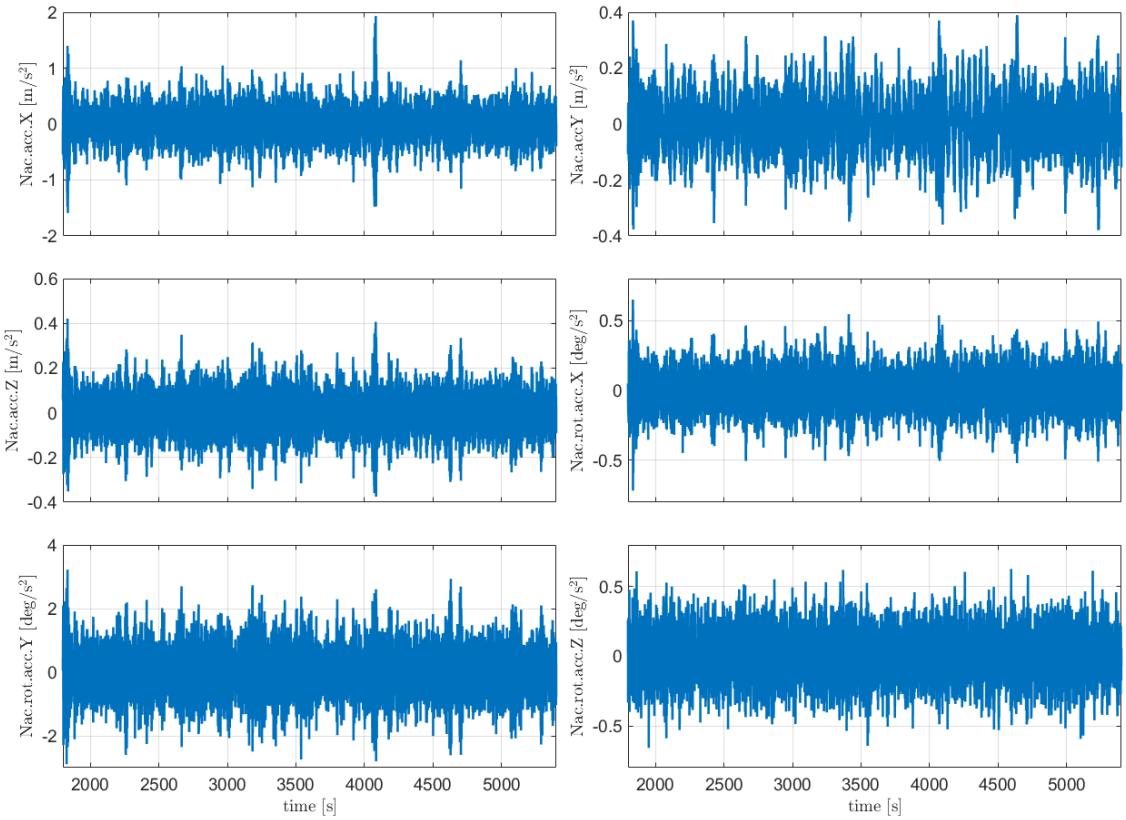
Nac.acc.X [m/s²]
Nac.accY [m/s²]
Nac.acc.Z [m/s²]
Nac.rot.acc.X [deg/s²]
Nac.rot.acc.Y [deg/s²]
Nac.rot.acc.Z [deg/s²]
time [s]
time [s]

- 20m/s

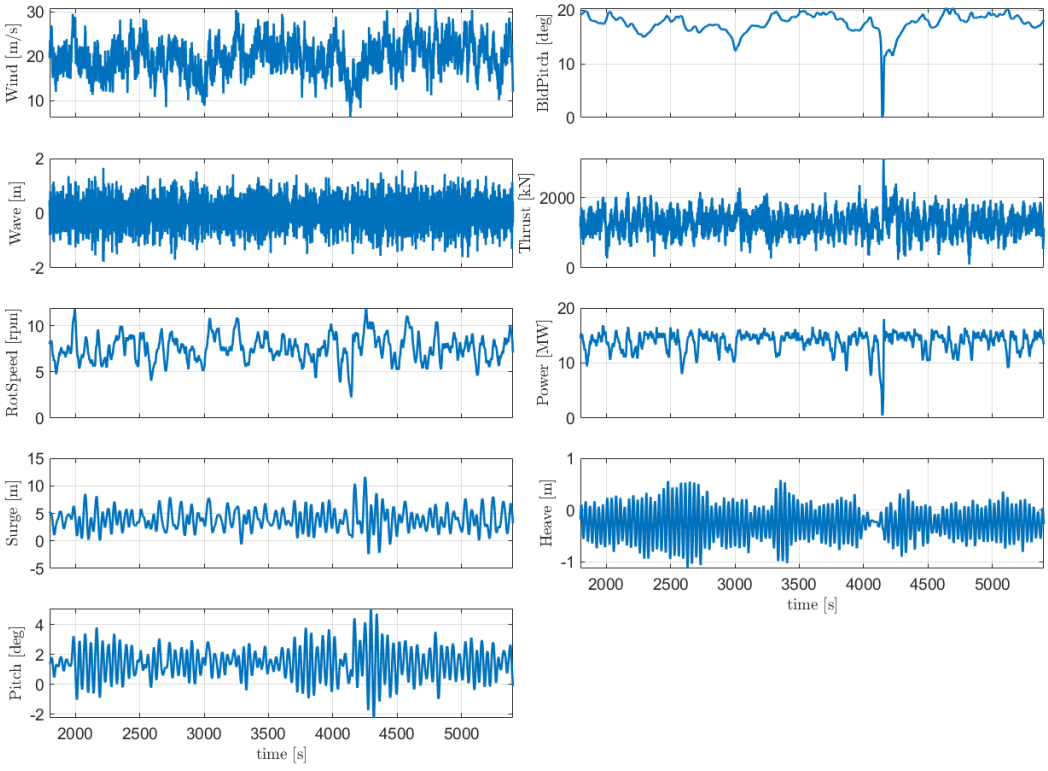
Wind [m/s]
BldPitch [deg]
Wave [m]
Thrust [kN]
RotSpeed [rpm]
Power [MW]
Surge [m]
Heave [m]
Pitch [deg]
time [s]
time [s]

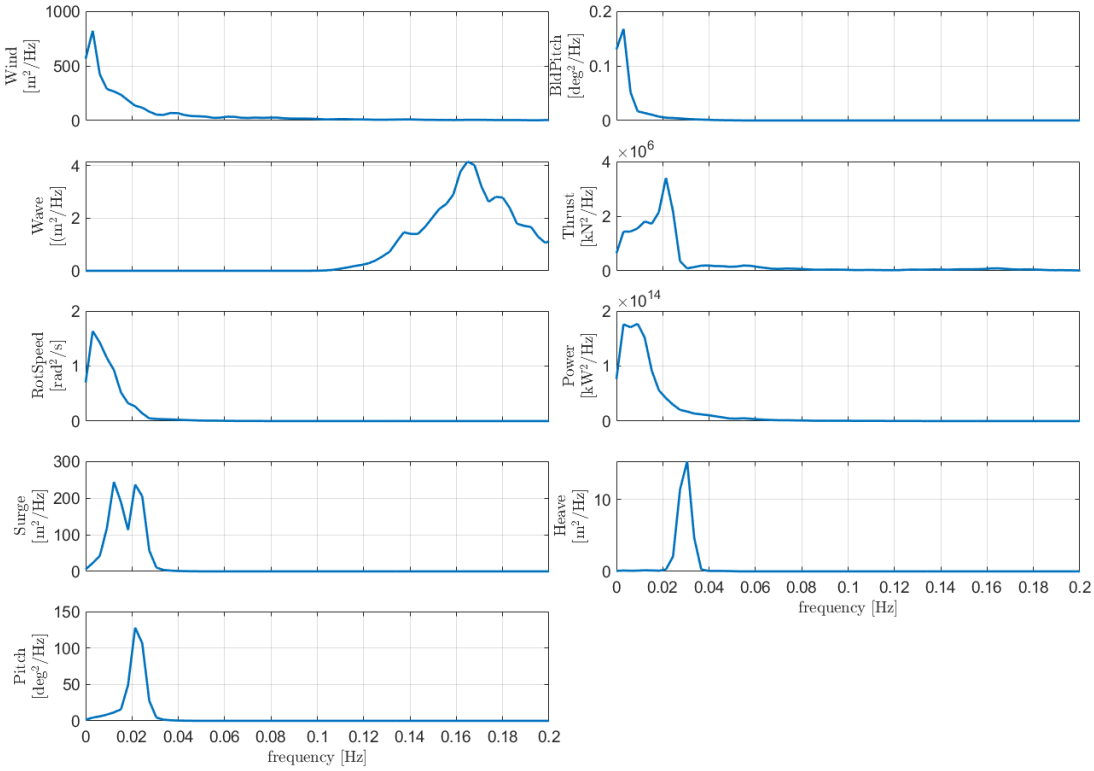
Wind [m²/Hz]
BldPitch [deg²/Hz]
Wave [(m²/Hz]
Thrust [kN²/Hz]
RotSpeed [rad²/s]
Power [kW²/Hz]
Surge [m²/Hz]
Heave [m²/Hz]
Pitch [deg²/Hz]
frequency [Hz]

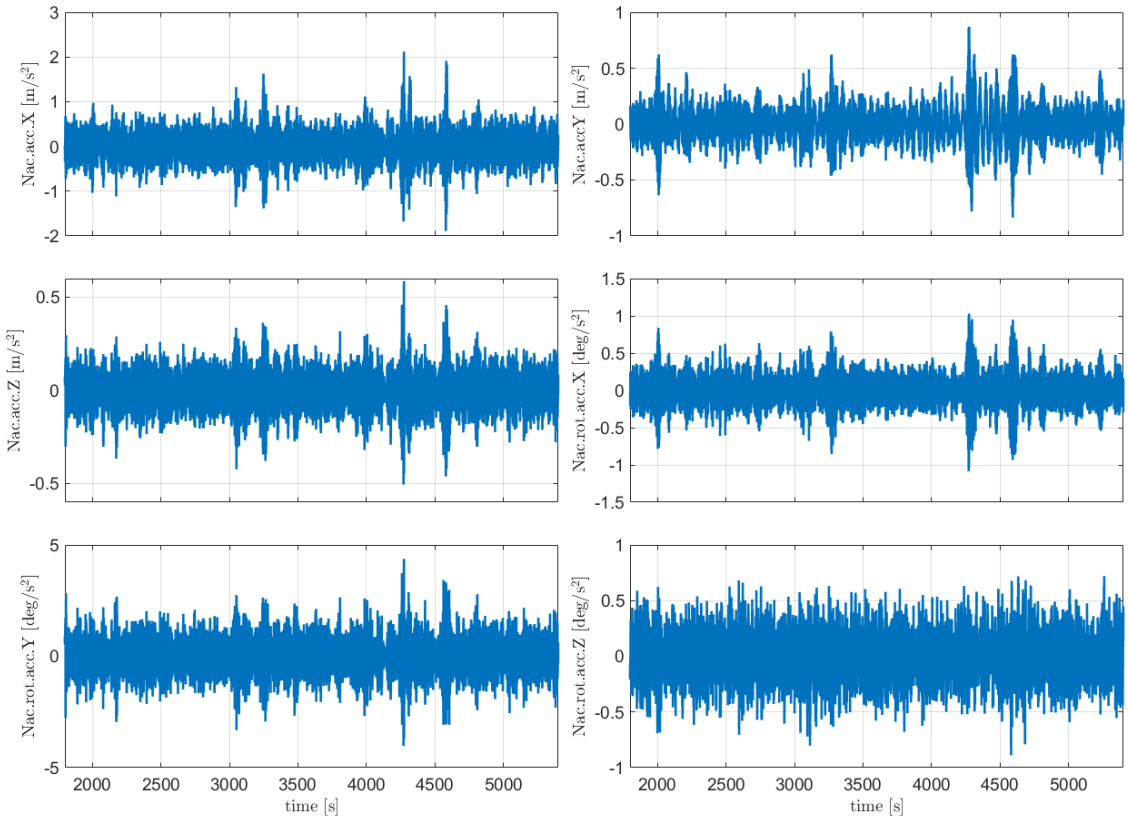
Nac.acc.X [m/s²]
Nac.acc.Y [m/s²]
Nac.acc.Z [m/s²]
Nac.rot.acc.X [deg/s²]
Nac.rot.acc.Y [deg/s²]
Nac.rot.acc.Z [deg/s²]
time [s]

- 25m/s

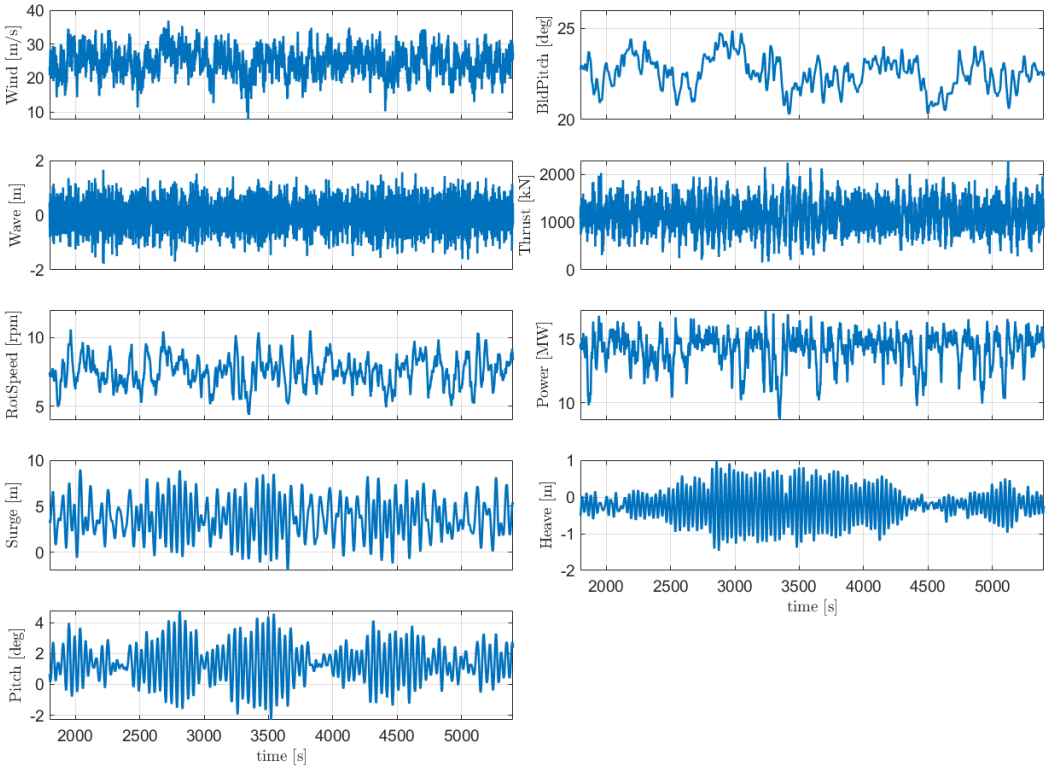
Wind [m/s]
BldPitch [deg]
Wave [m]
Thrust [kN]
RotSpeed [rpm]
Power [MW]
Surge [m]
Heave [m]
Pitch [deg]
time [s]

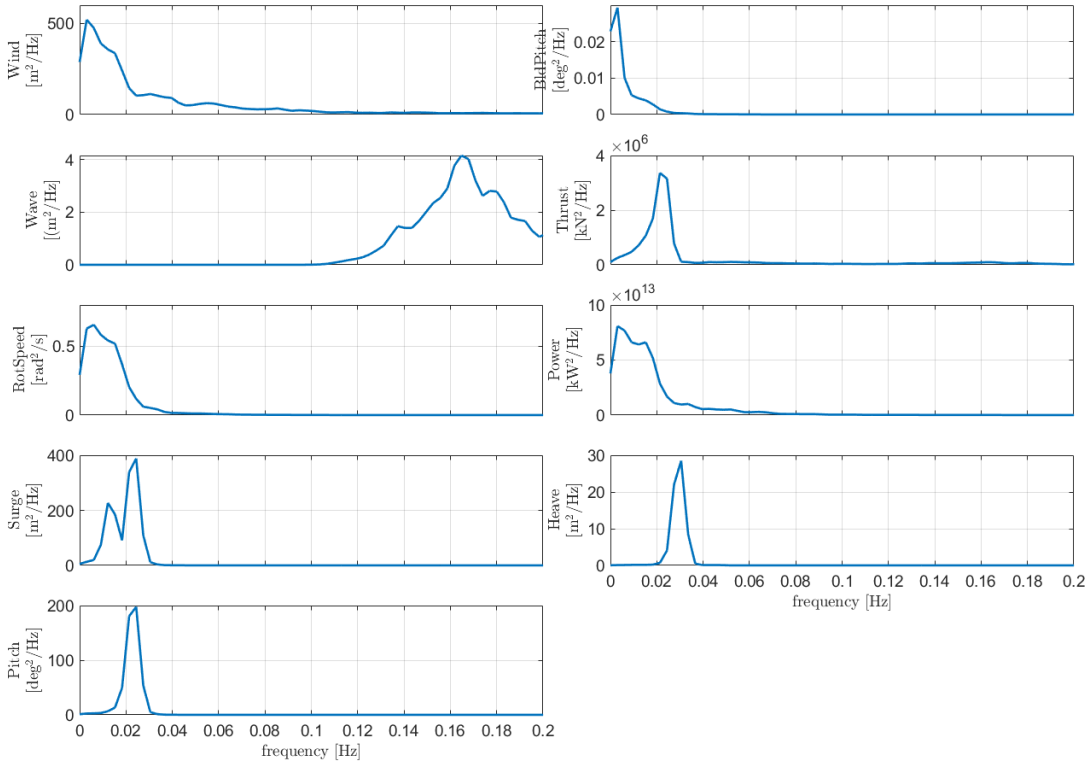
Wind [m²/Hz]
BldPitch [deg²/Hz]
Wave [(m²/Hz]
Thrust [kN²/Hz]
RotSpeed [rad²/s]
Power [kW²/Hz]
Surge [m²/Hz]
Heave [m²/Hz]
Pitch [deg²/Hz]
frequency [Hz]

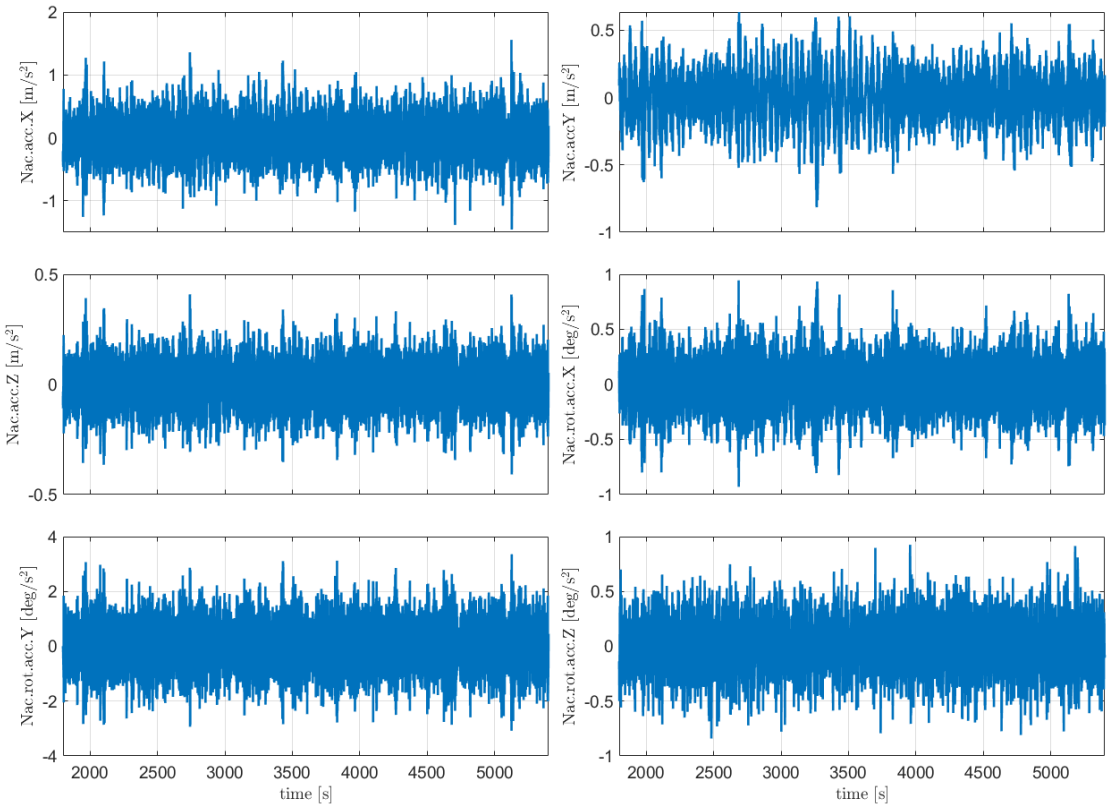

10.1.2 Normal turbulence wind and extreme stochastic waves (DLC 1.6)

- 8m/s

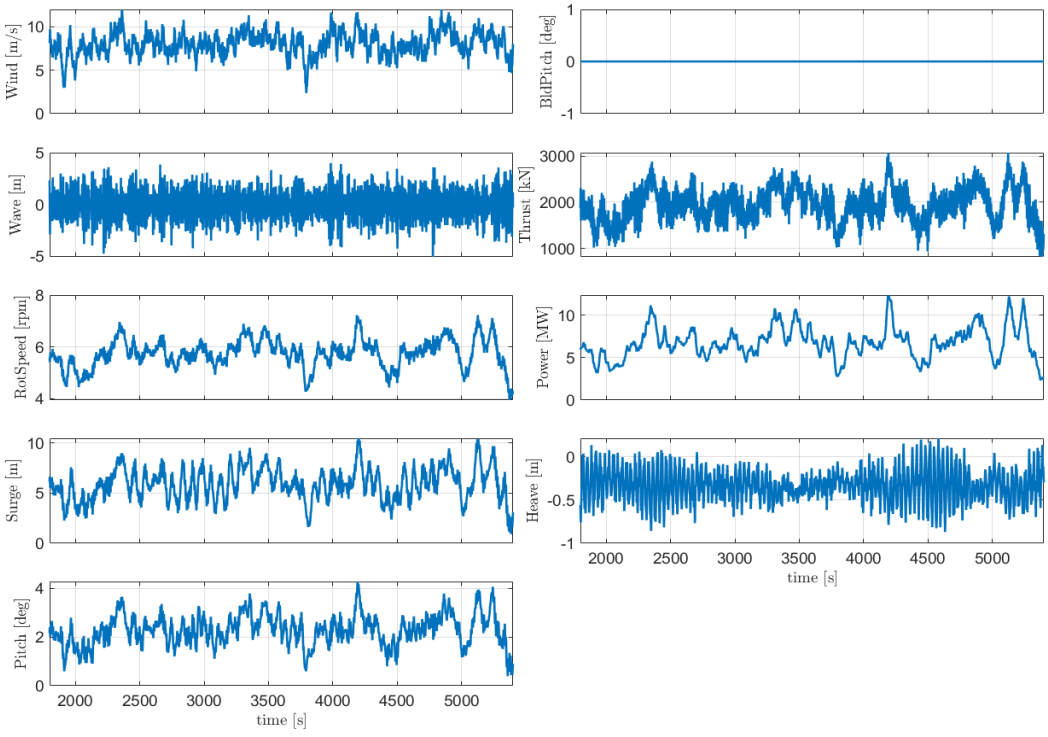

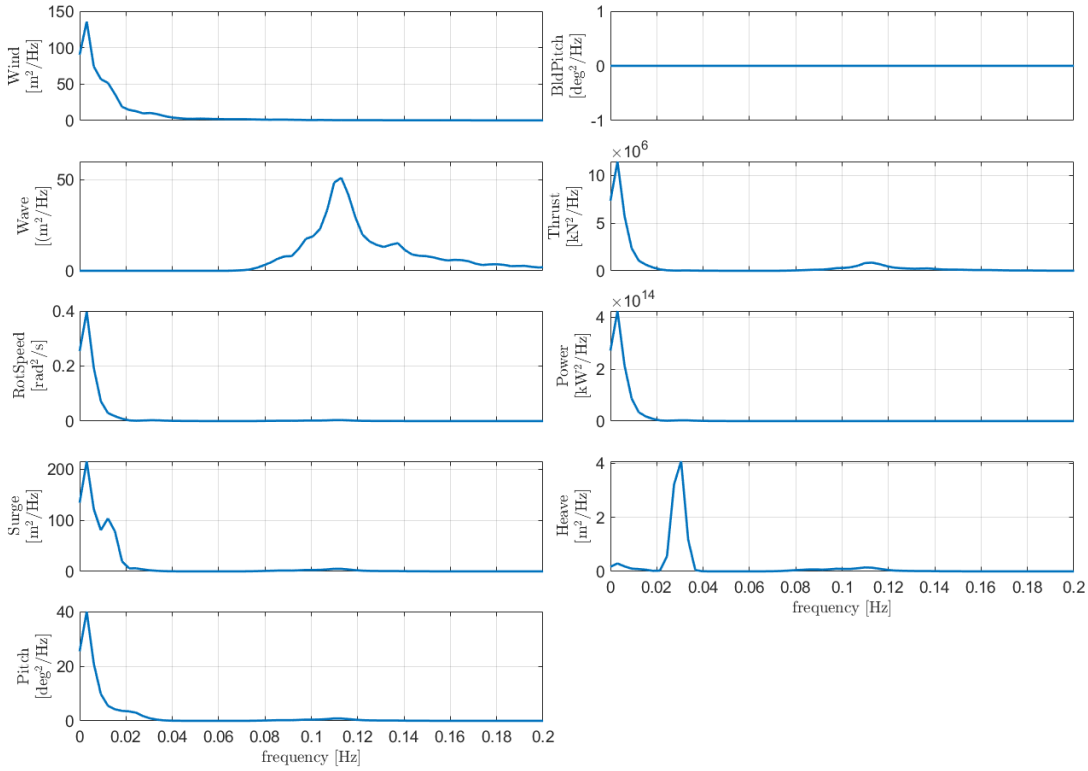
Wind [m²/Hz]
BldPitch [deg²/Hz]
Wave [(m²/Hz]
Thrust [kN²/Hz]
RotSpeed [rad²/s]
Power [kW²/Hz]
Surge [m²/Hz]
Heave [m²/Hz]
Pitch [deg²/Hz]
frequency [Hz]

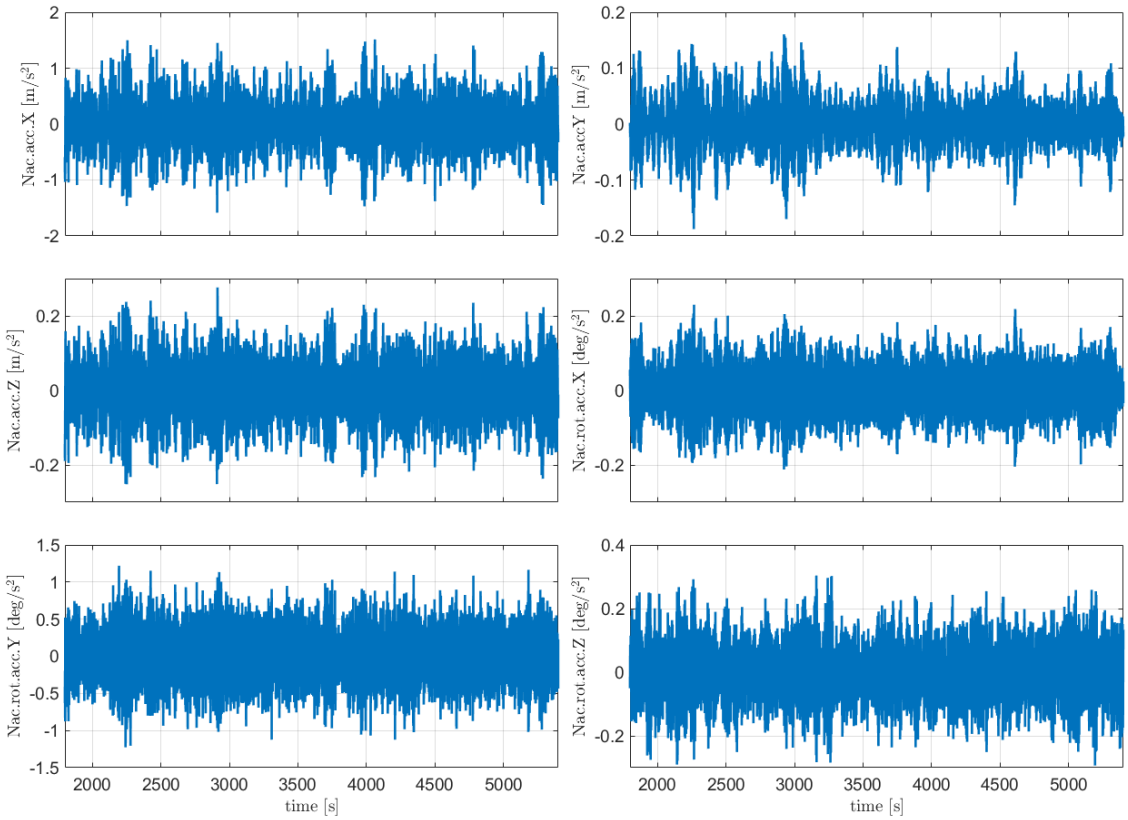
Nac.acc.X [m/s²]
Nac.accY [m/s²]
Nac.acc.Z [m/s²]
Nac.rot.acc.X [deg/s²]
Nac.rot.acc.Y [deg/s²]
Nac.rot.acc.Z [deg/s²]
time [s]

- 16m/s

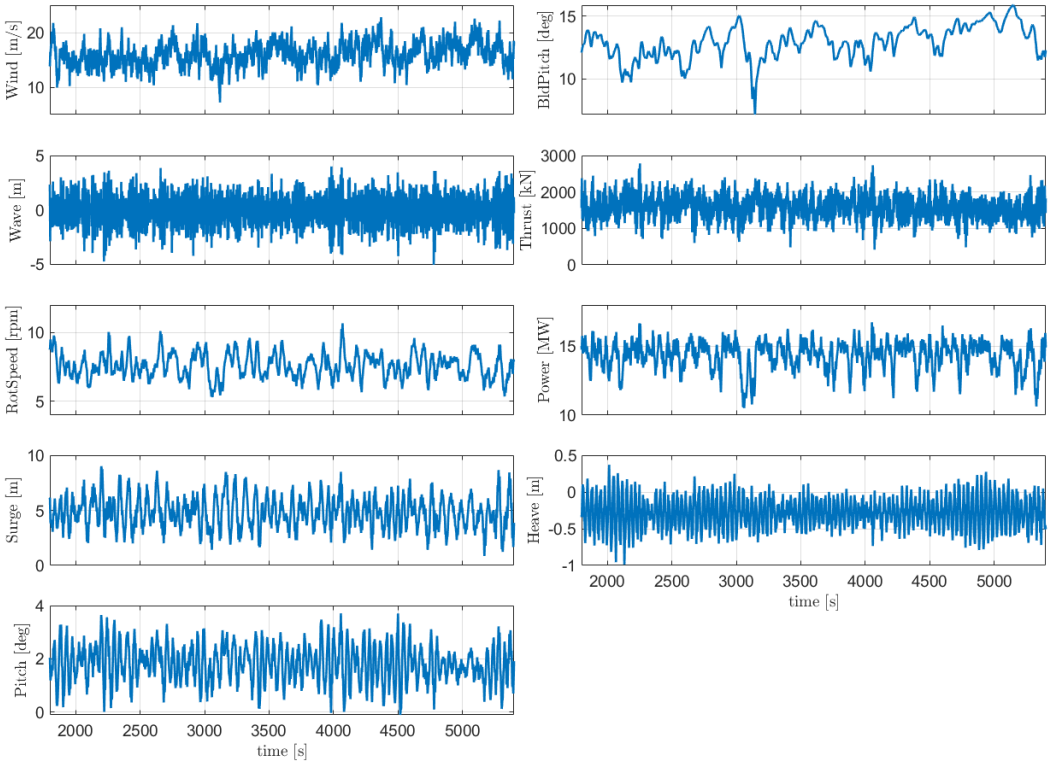
Wind [m/s]
BldPitch [deg]
Wave [m]
Thrust [kN]
RotSpeed [rpm]
Power [MW]
Surge [m]
Heave [m]
Pitch [deg]
time [s]

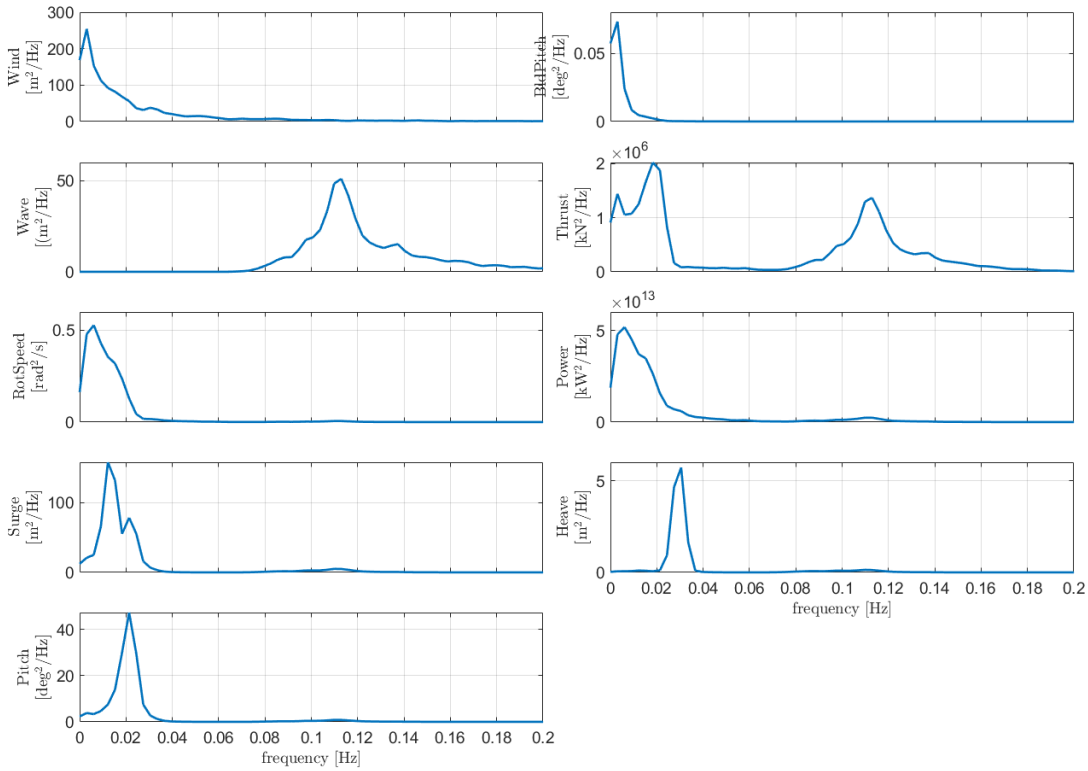
Wind [m²/Hz]
BldPitch [deg²/Hz]
Wave [(m²/Hz]
Thrust [kN²/Hz]
RotSpeed [rad²/s]
Power [kW²/Hz]
Surge [m²/Hz]
Heave [m²/Hz]
Pitch [deg²/Hz]
frequency [Hz]

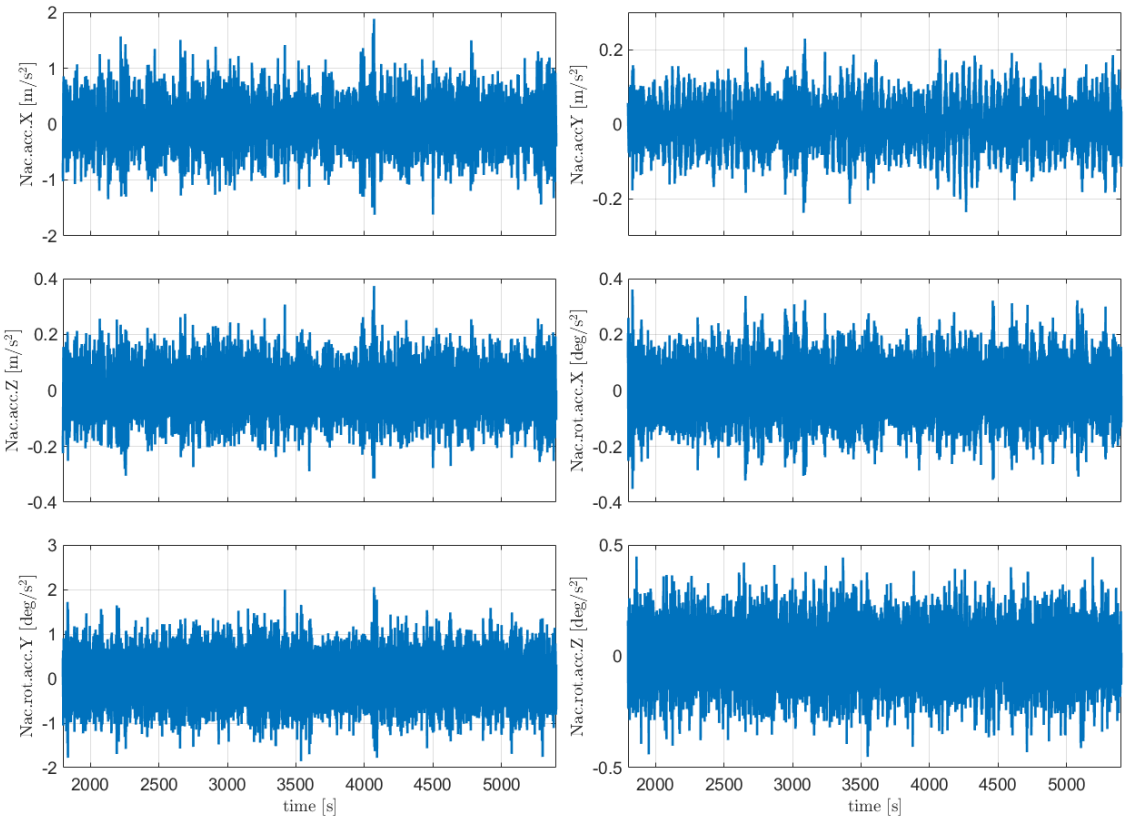
Nac.acc.X [m/s²]
Nac.accY [m/s²]
Nac.acc.Z [m/s²]
Nac.rot.acc.X [deg/s²]
Nac.rot.acc.Y [deg/s²]
Nac.rot.acc.Z [deg/s²]
time [s]
time [s]

- 20m/s

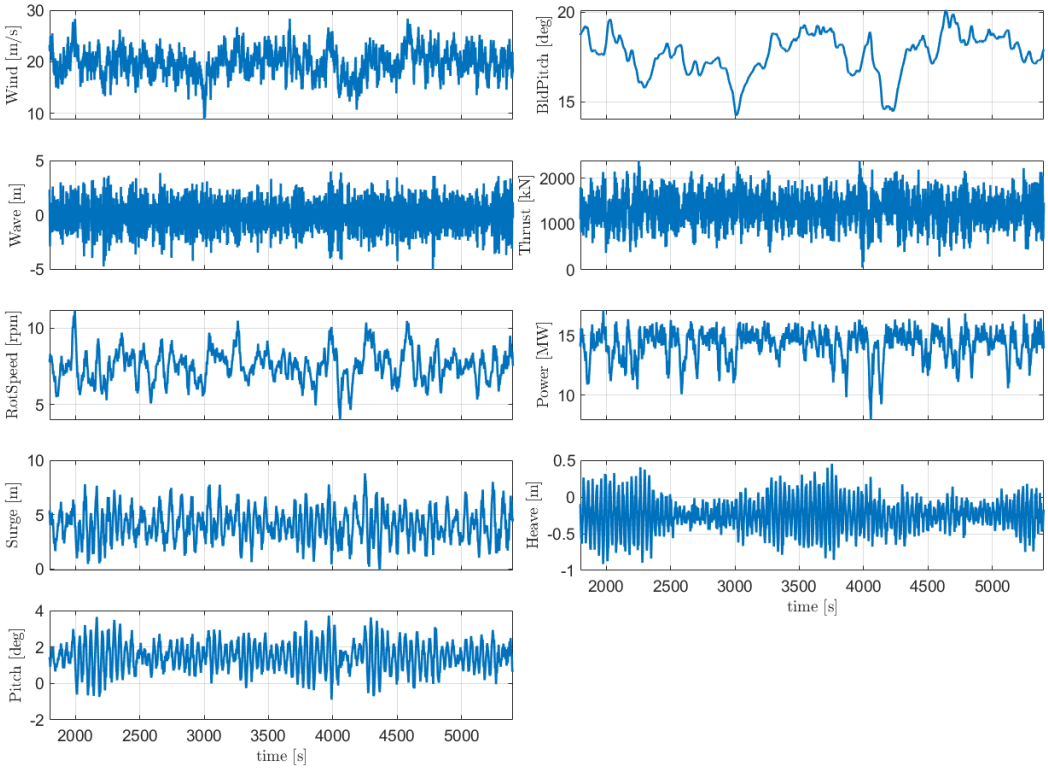
Wind [m/s]
BldPitch [deg]
Wave [m]
Thrust [kN]
RotSpeed [rpm]
Power [MW]
Surge [m]
Heave [m]
Pitch [deg]
time [s]
time [s]

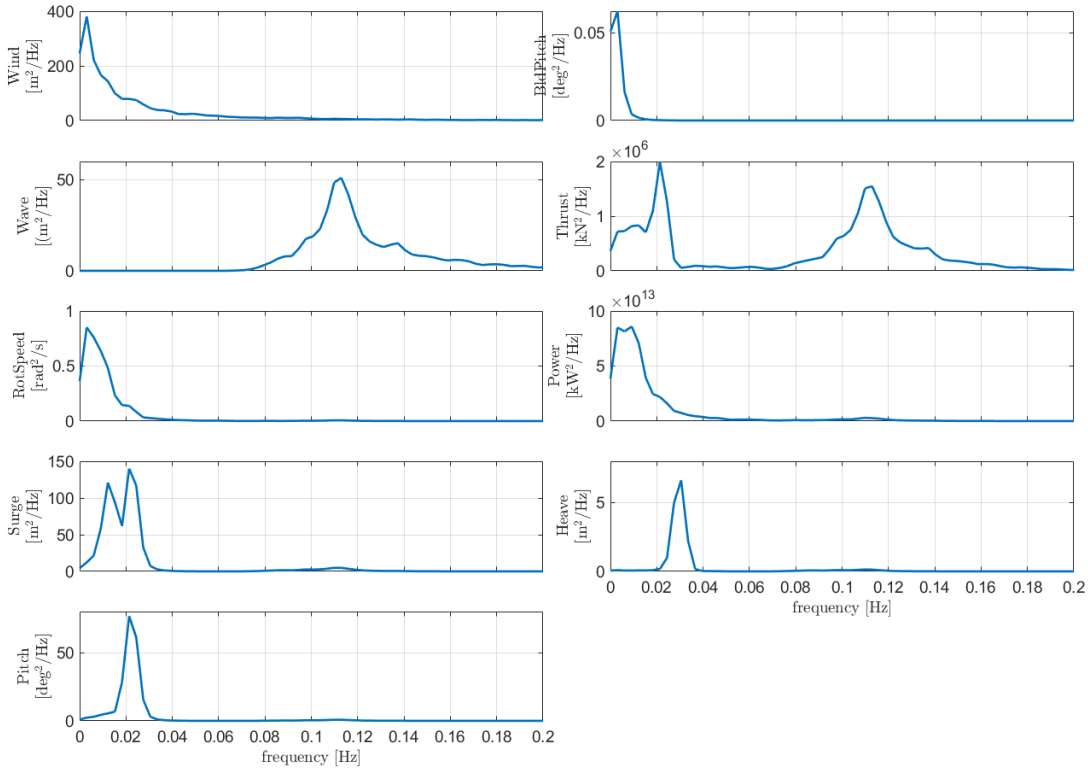
Wind [m²/Hz]
BldPitch [deg²/Hz]
Wave [(m²/Hz]
Thrust [kN²/Hz]
RotSpeed [rad²/s]
Power [kW²/Hz]
Surge [m²/Hz]
Heave [m²/Hz]
Pitch [deg²/Hz]
frequency [Hz]

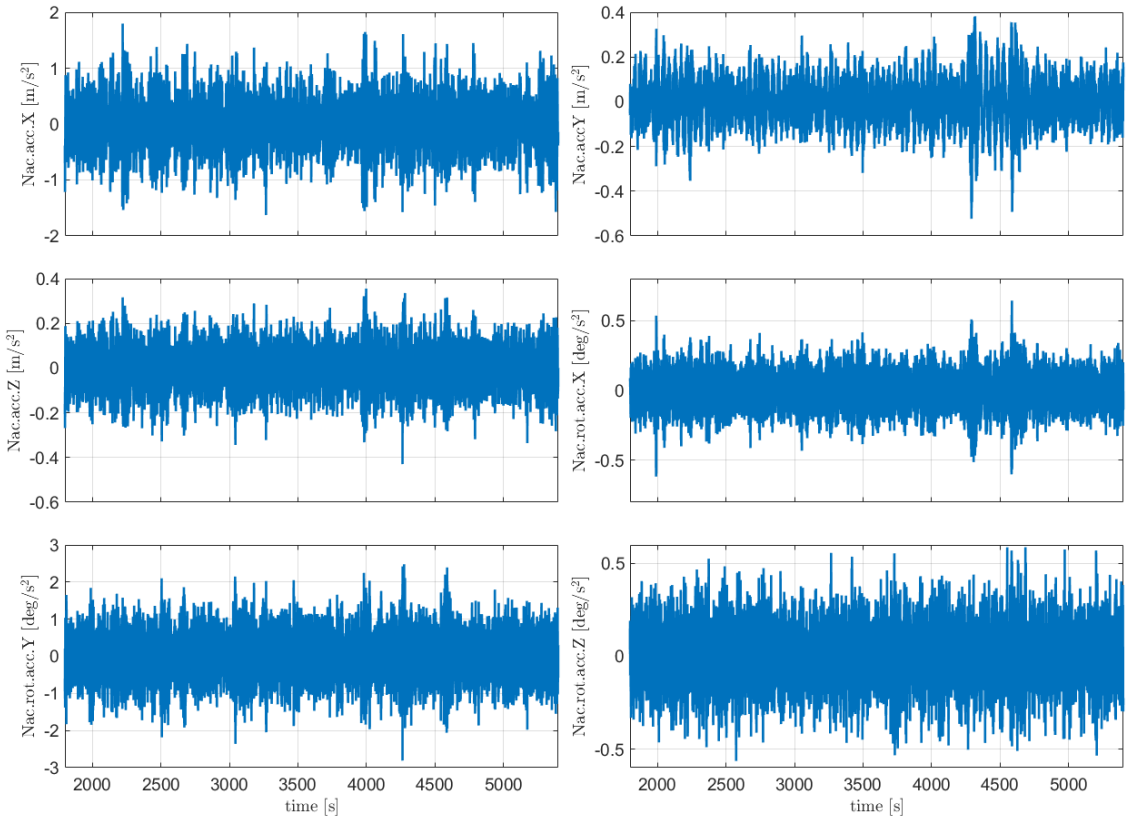
Nac.acc.X [m/s²]
Nac.acc.Y [m/s²]
Nac.acc.Z [m/s²]
Nac.rot.acc.X [deg/s²]
Nac.rot.acc.Y [deg/s²]
Nac.rot.acc.Z [deg/s²]
time [s]

- 25m/s

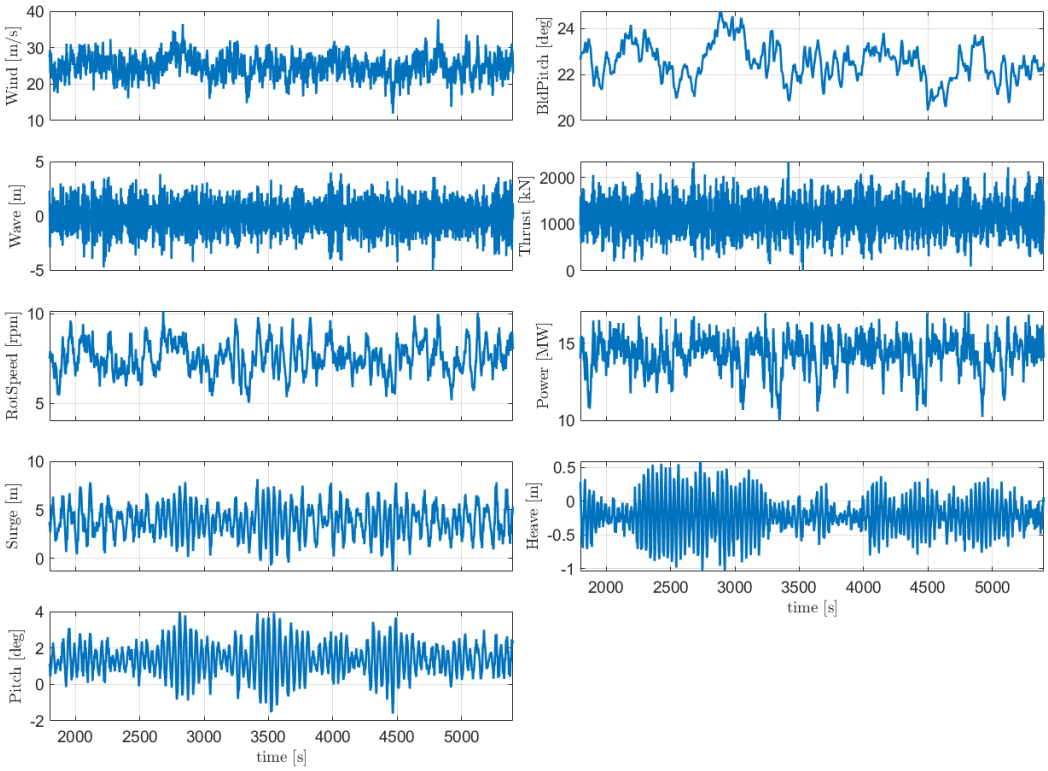
Wind [m/s]
BldPitch [deg]
Wave [m]
Thrust [kN]
RotSpeed [rpm]
Power [MW]
Surge [m]
Heave [m]
Pitch [deg]
time [s]

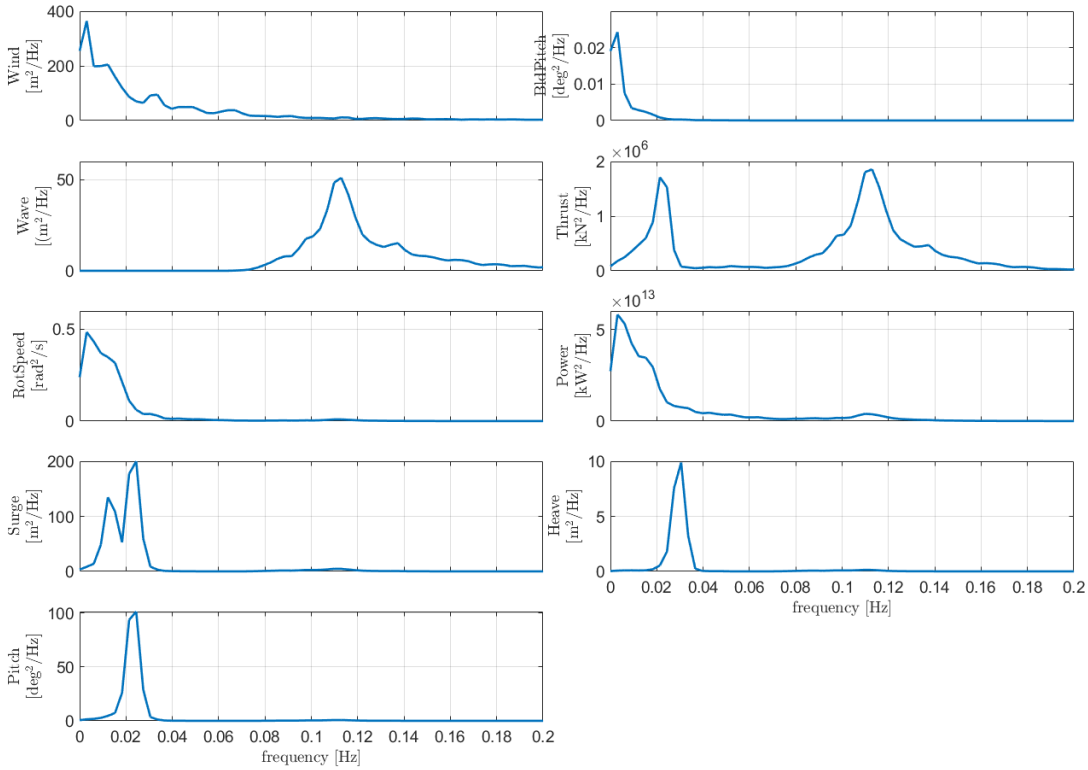
Wind [m²/Hz]
BldPitch [deg²/Hz]
Wave [(m²/Hz]
Thrust [kN²/Hz]
RotSpeed [rad²/s]
Power [kW²/Hz]
Surge [m²/Hz]
Heave [m²/Hz]
Pitch [deg²/Hz]
frequency [Hz]

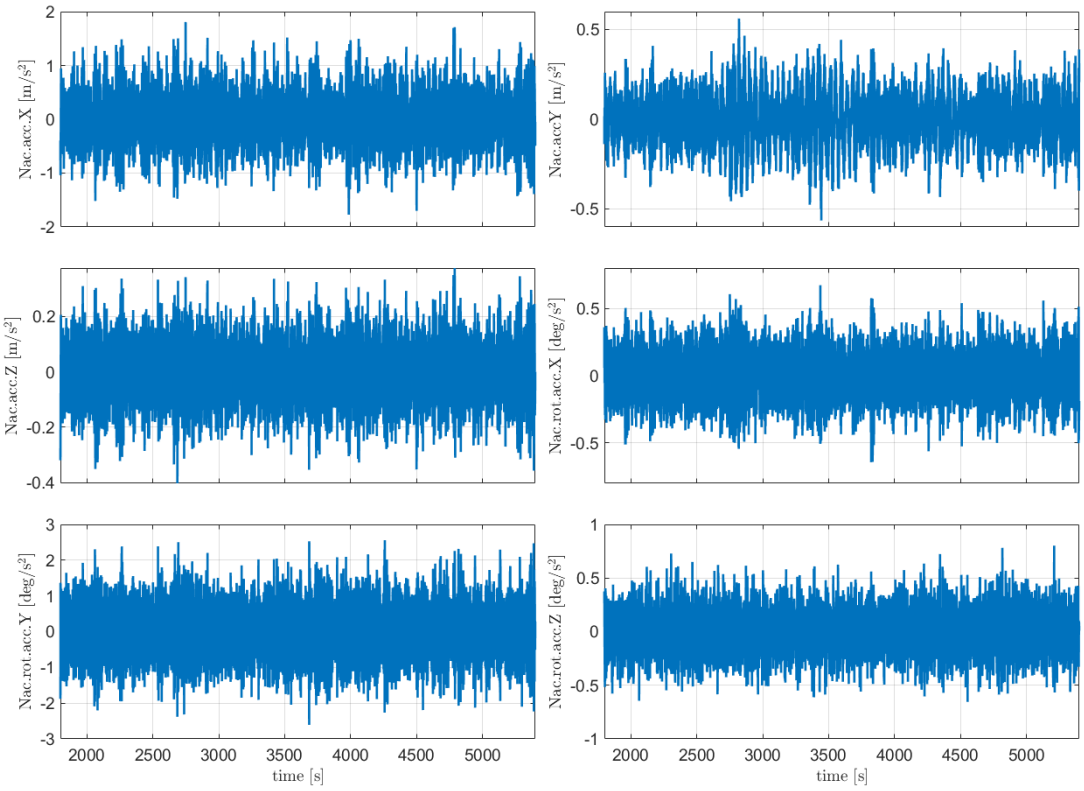

10.2 ActiveFloat

10.2.1 Extreme turbulence wind and stochastic waves (DLC 1.3)

- 8m/s

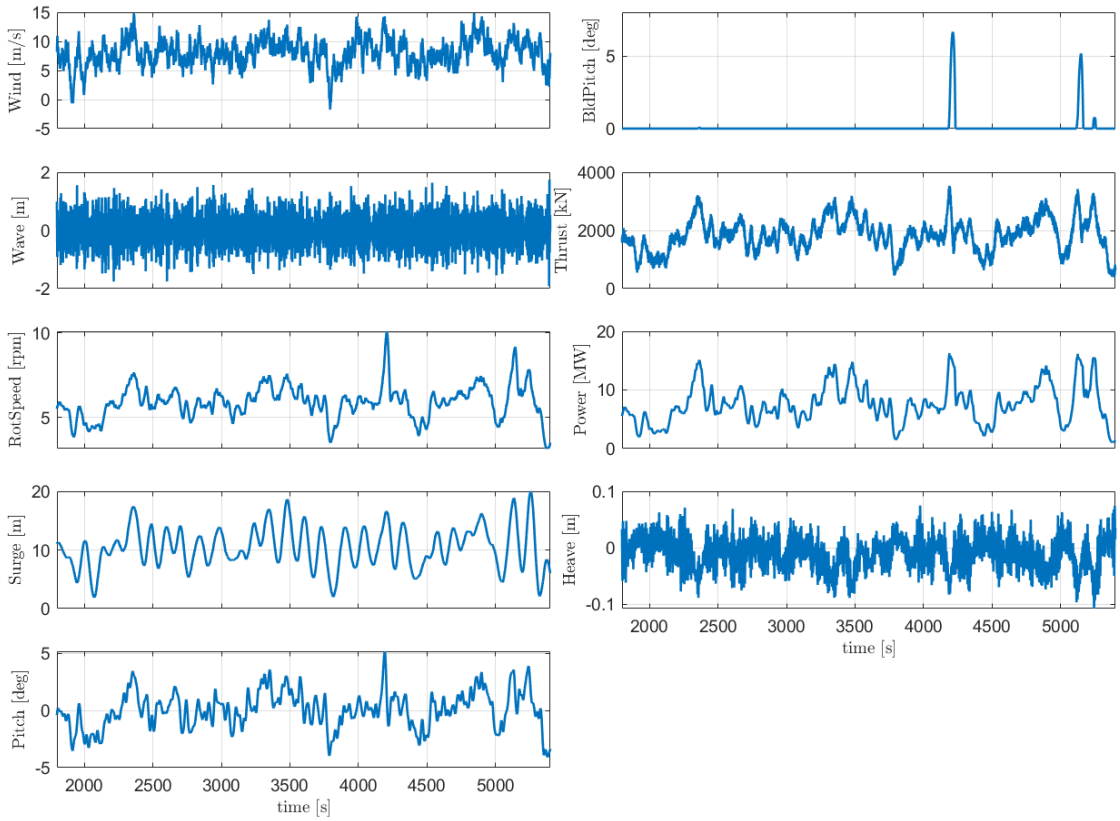
Wind [m/s]
BldPitch [deg]
Wave [m]
Thrust [kN]
RotSpeed [rpm]
Power [MW]
Surge [m]
Heave [m]
Pitch [deg]
time [s]

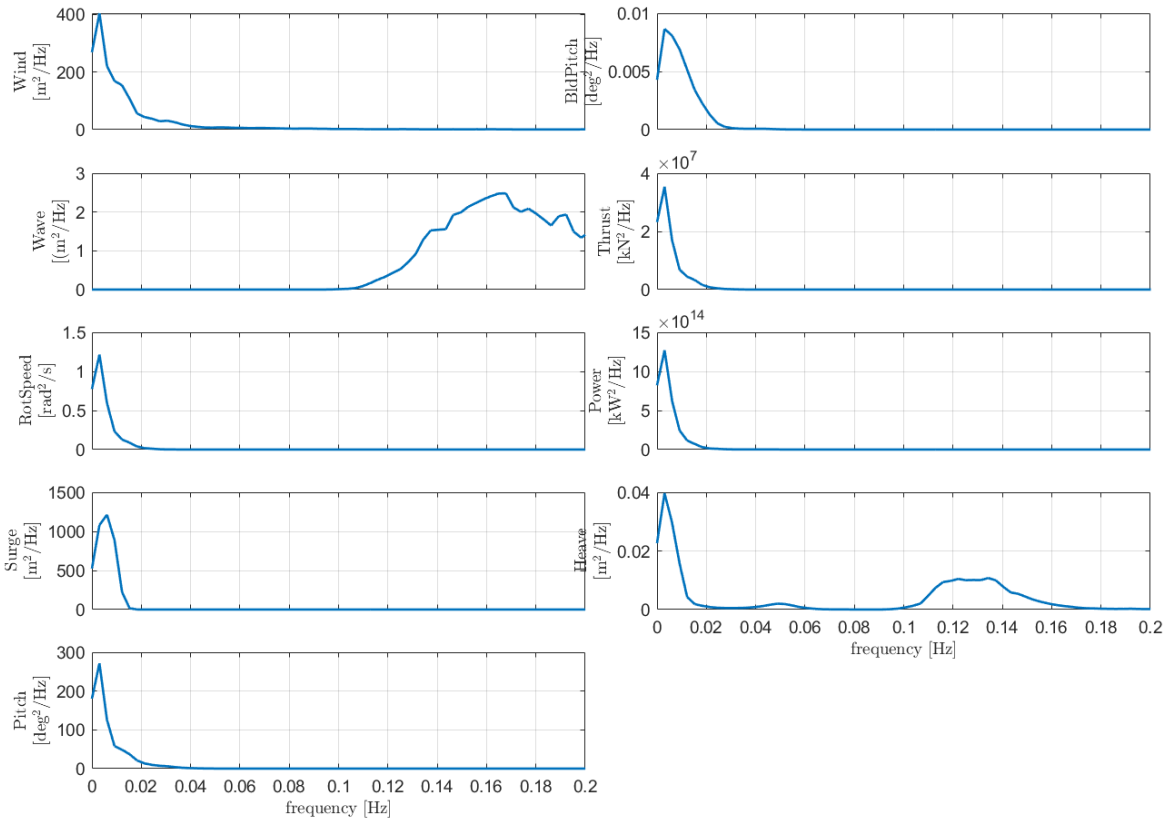
Wind [m²/Hz]
BldPitch [deg²/Hz]
Wave [(m²/Hz]
Thrust [kN²/Hz]
RotSpeed [rad²/s]
Power [kW²/Hz]
Surge [m²/Hz]
Heave [m²/Hz]
Pitch [deg²/Hz]
frequency [Hz]

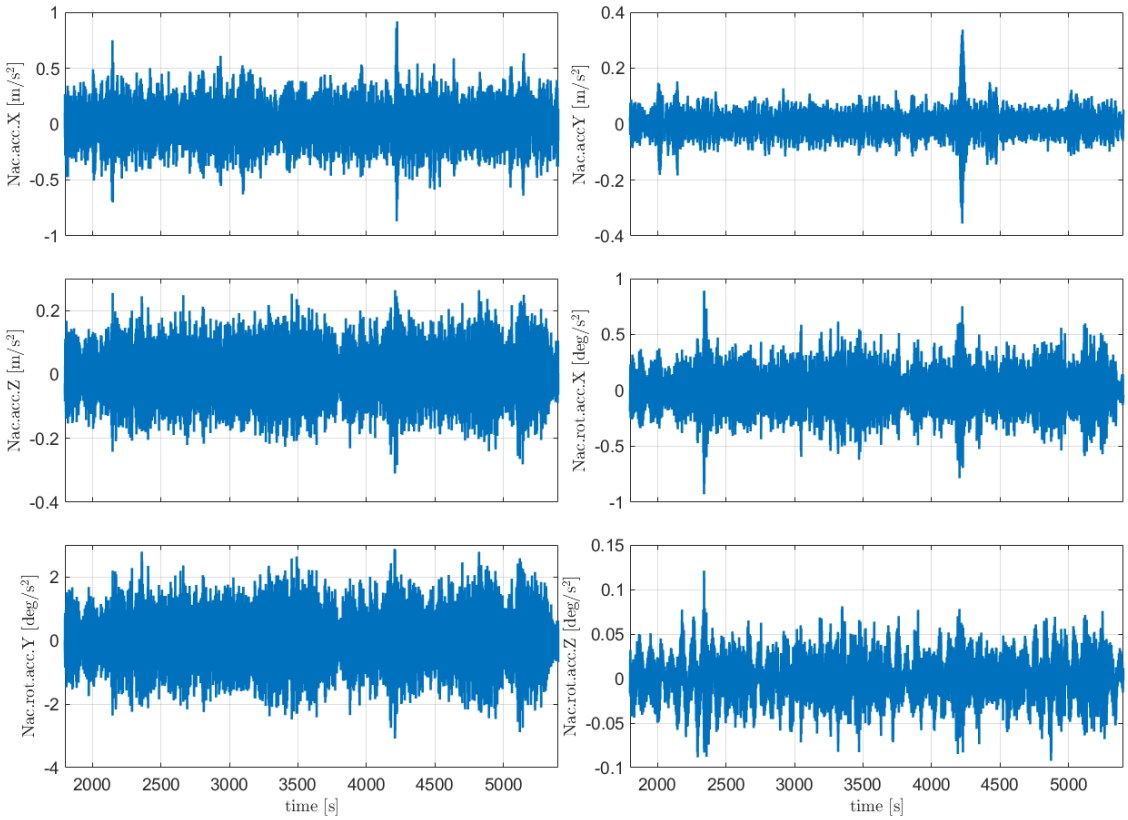
Nac.acc.X [m/s²]
Nac.accY [m/s²]
Nac.acc.Z [m/s²]
Nac.rot.acc.X [deg/s²]
Nac.rot.acc.Y [deg/s²]
Nac.rot.acc.Z [deg/s²]
time [s]
time [s]

- 16m/s

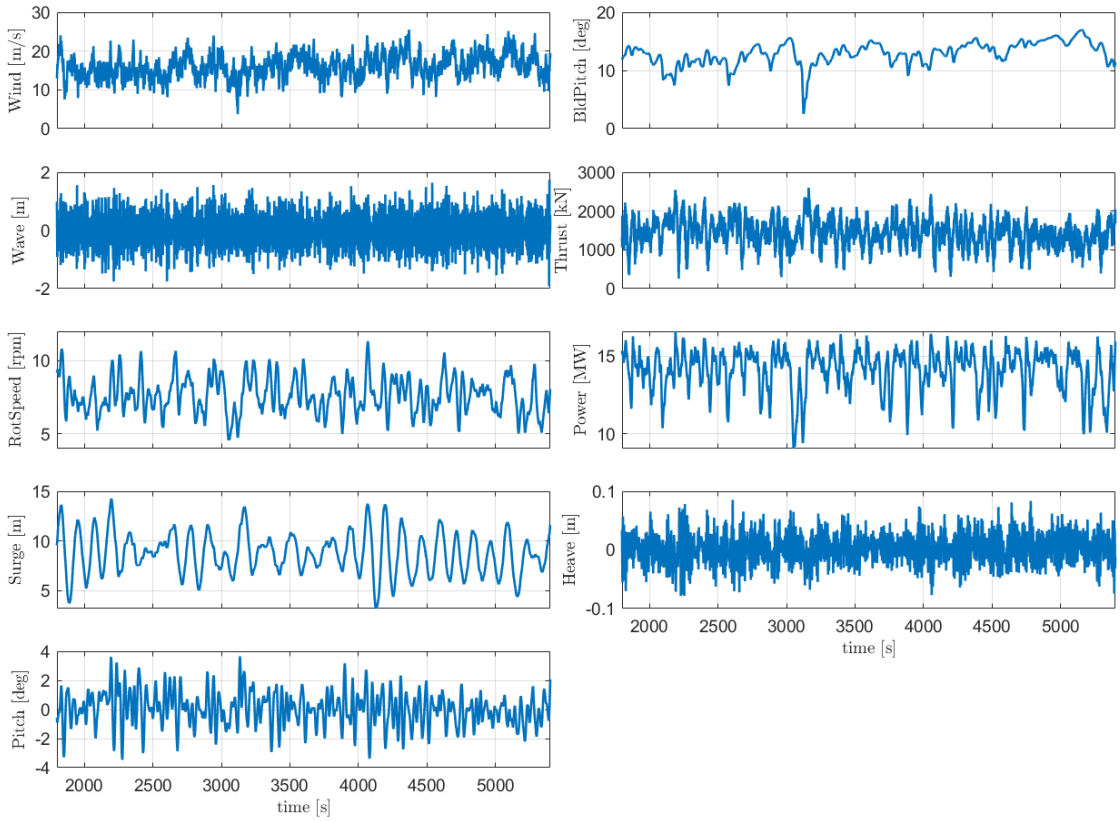
Wind [m/s]
BldPitch [deg]
Wave [m]
Thrust [kN]
RotSpeed [rpm]
Power [MW]
Surge [m]
Heave [m]
Pitch [deg]
time [s]

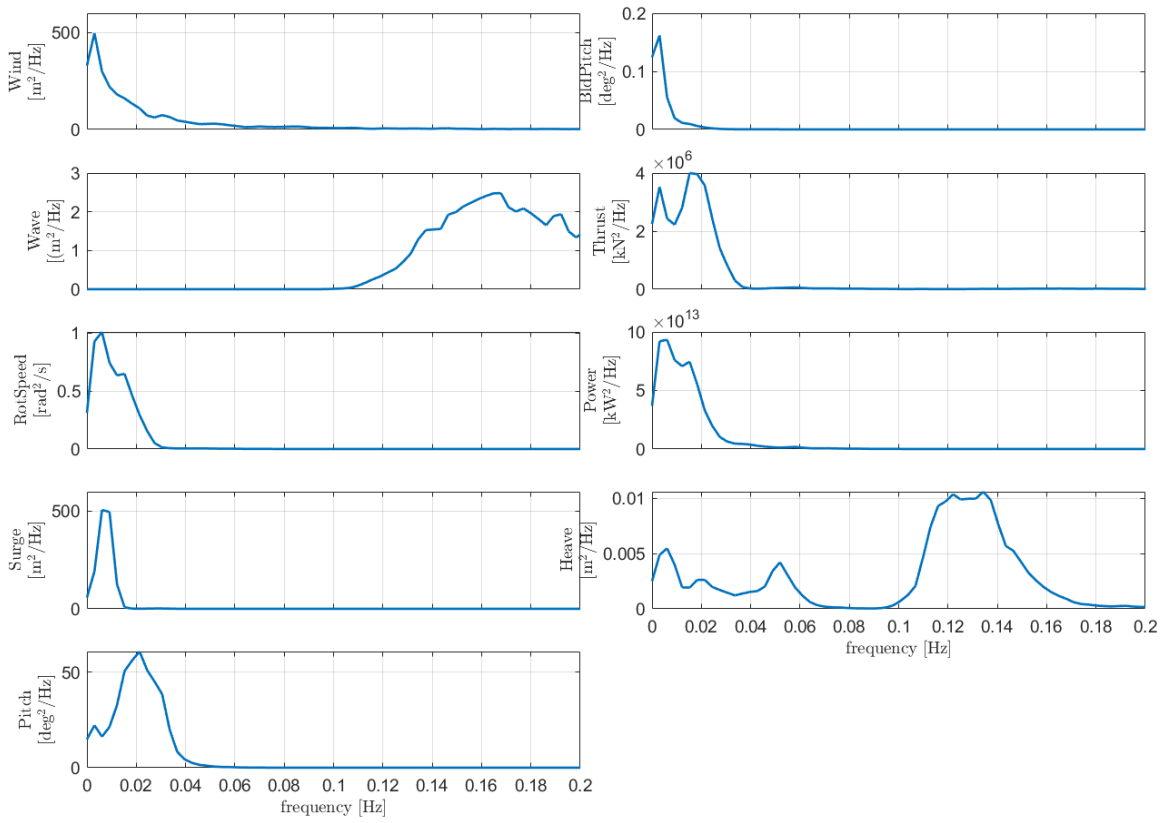
Wind [m²/Hz]
BldPitch [deg²/Hz]
Wave [(m²/Hz]
Thrust [kN²/Hz]
RotSpeed [rad²/s]
Power [kW²/Hz]
Surge [m²/Hz]
Heave [m²/Hz]
Pitch [deg²/Hz]
frequency [Hz]

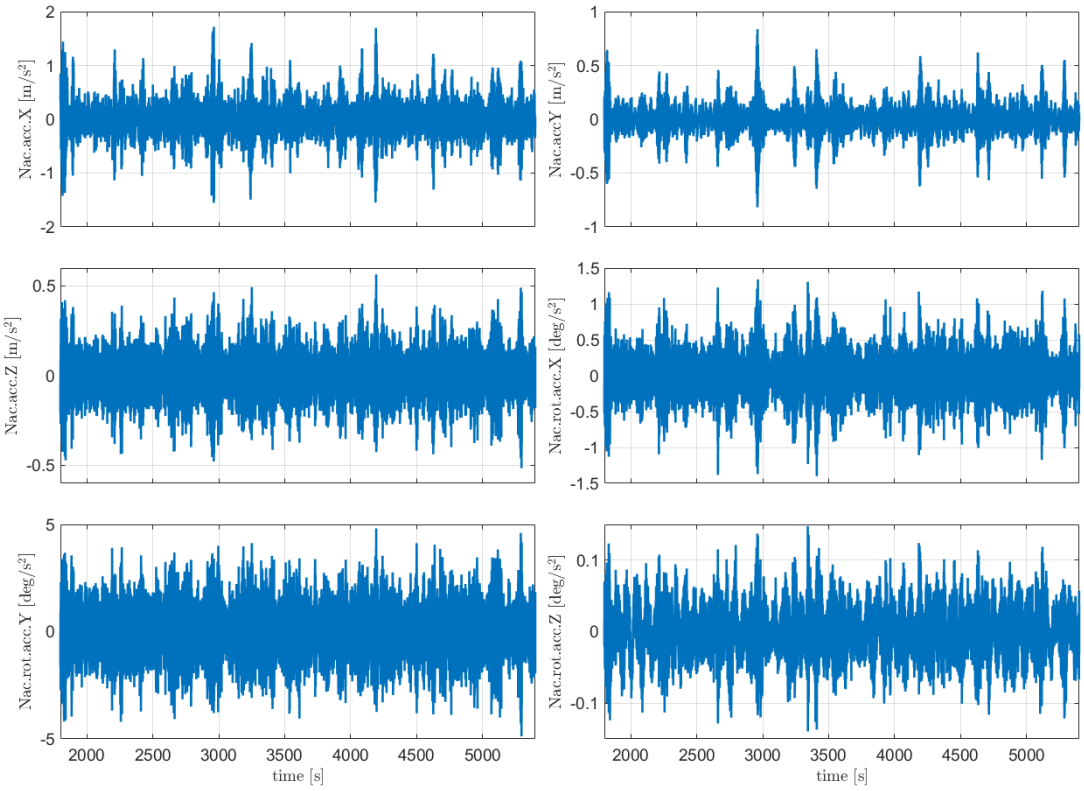
Nac.acc.X [m/s²]
Nac.acc.Y [m/s²]
Nac.acc.Z [m/s²]
Nac.rot.acc.X [deg/s²]
Nac.rot.acc.Y [deg/s²]
Nac.rot.acc.Z [deg/s²]
time [s]
time [s]

- 20m/s

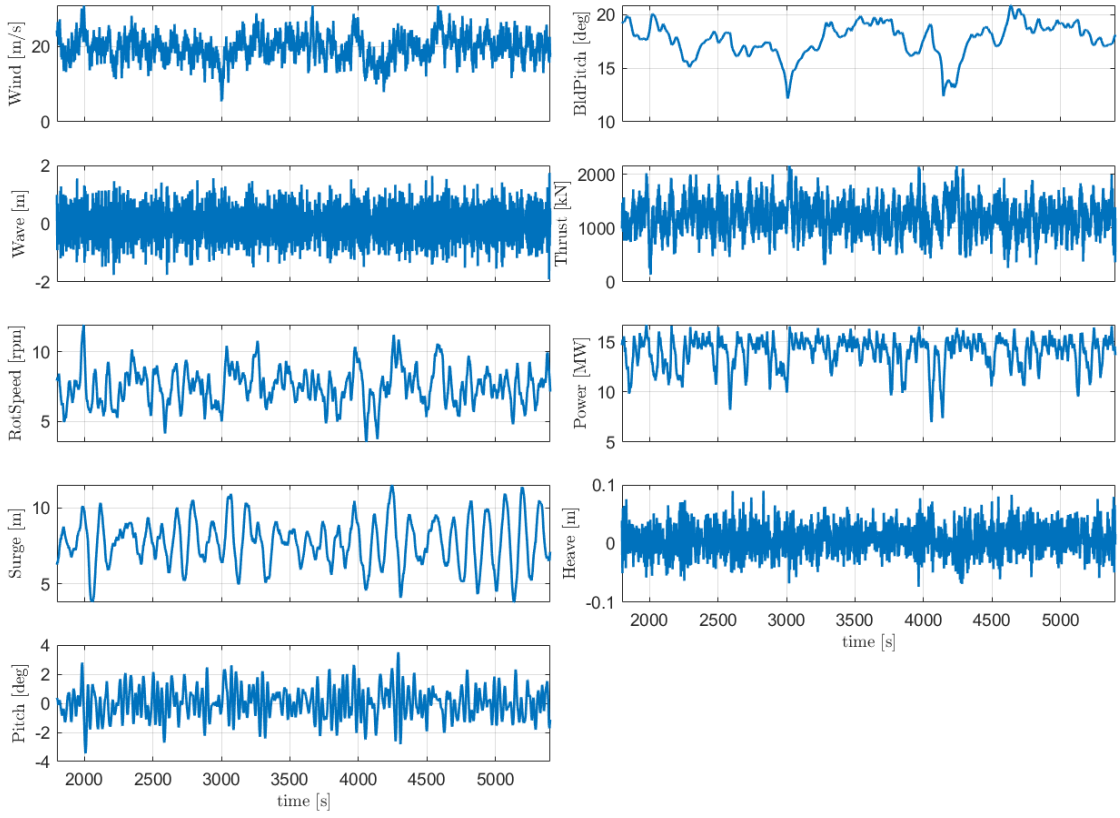
Wind [m/s]
BldPitch [deg]
Wave [m]
Thrust [kN]
RotSpeed [rpm]
Power [MW]
Surge [m]
Heave [m]
Pitch [deg]
time [s]
time [s]

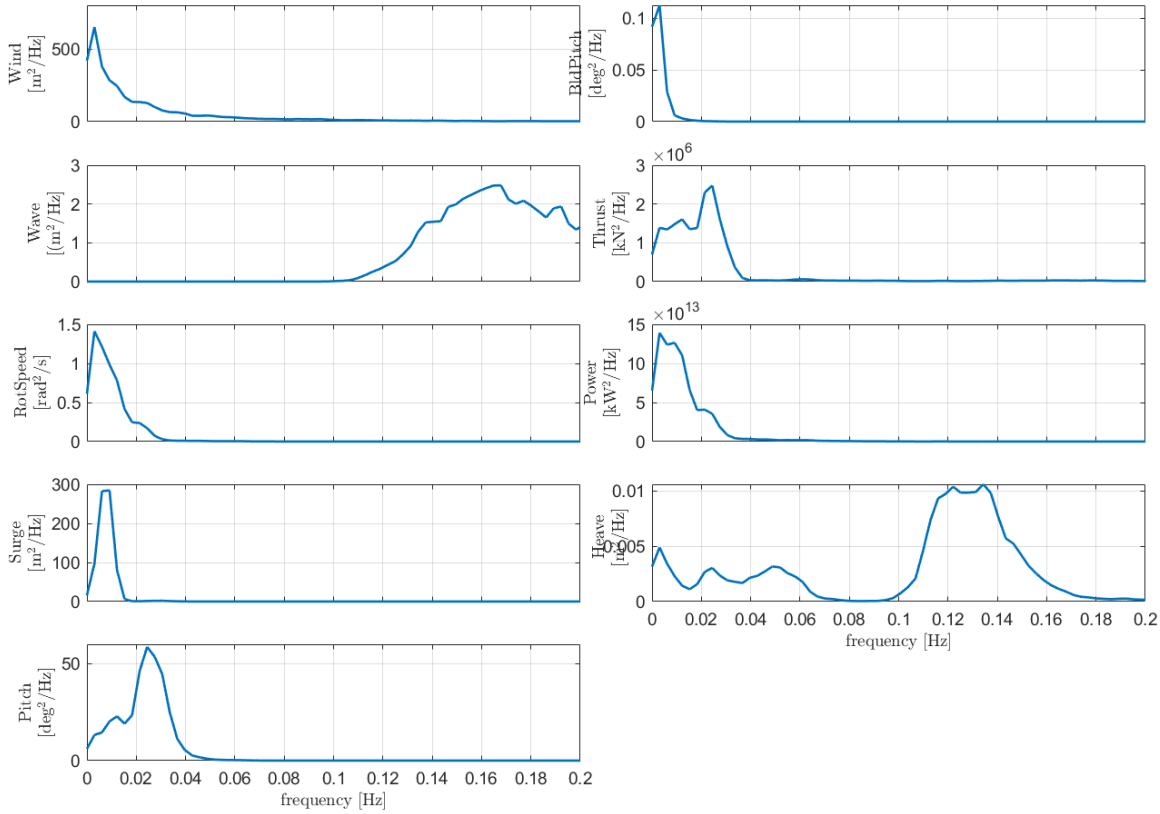
Wind [m²/Hz]
BldPitch [deg²/Hz]
Wave [(m²/Hz]
Thrust [kN²/Hz]
RotSpeed [rad²/s]
Power [kW²/Hz]
Surge [m²/Hz]
Heave [m²/Hz]
Pitch [deg²/Hz]
frequency [Hz]

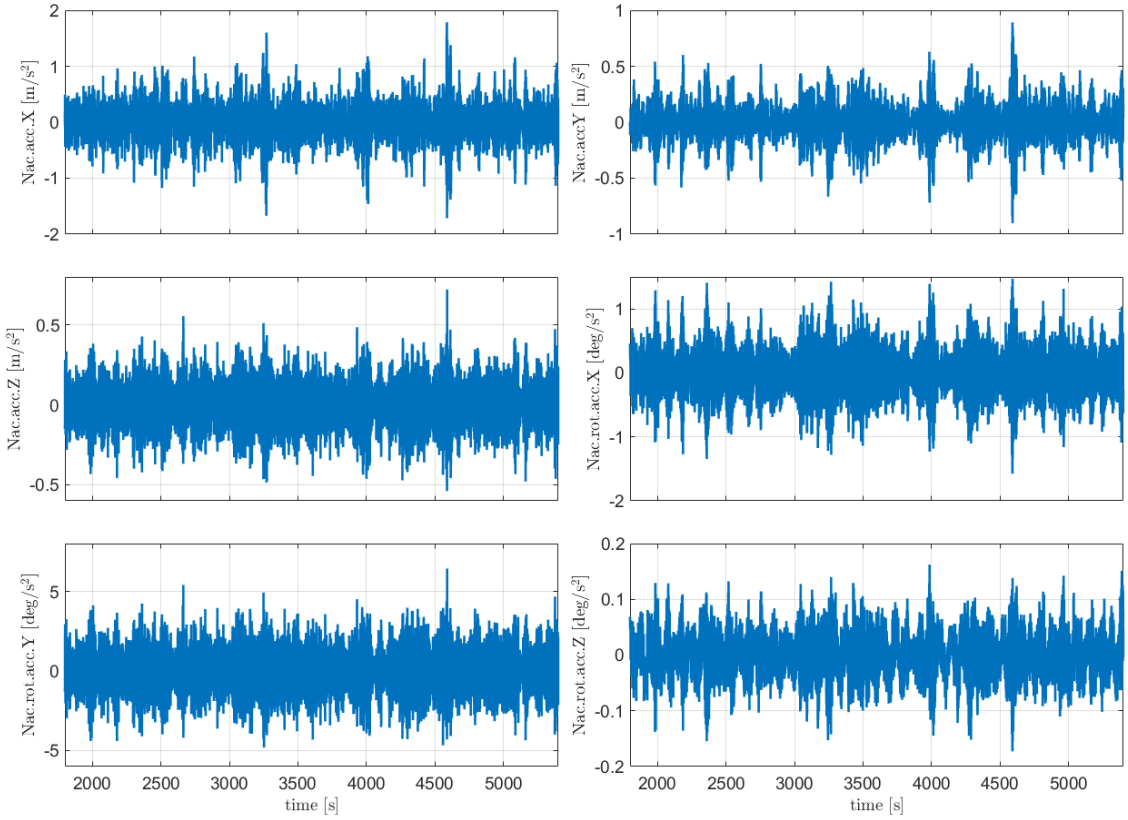
Nac.acc.X [m/s²]
Nac.acc.Y [m/s²]
Nac.acc.Z [m/s²]
Nac.rot.acc.X [deg/s²]
Nac.rot.acc.Y [deg/s²]
Nac.rot.acc.Z [deg/s²]
time [s]

- 25m/s

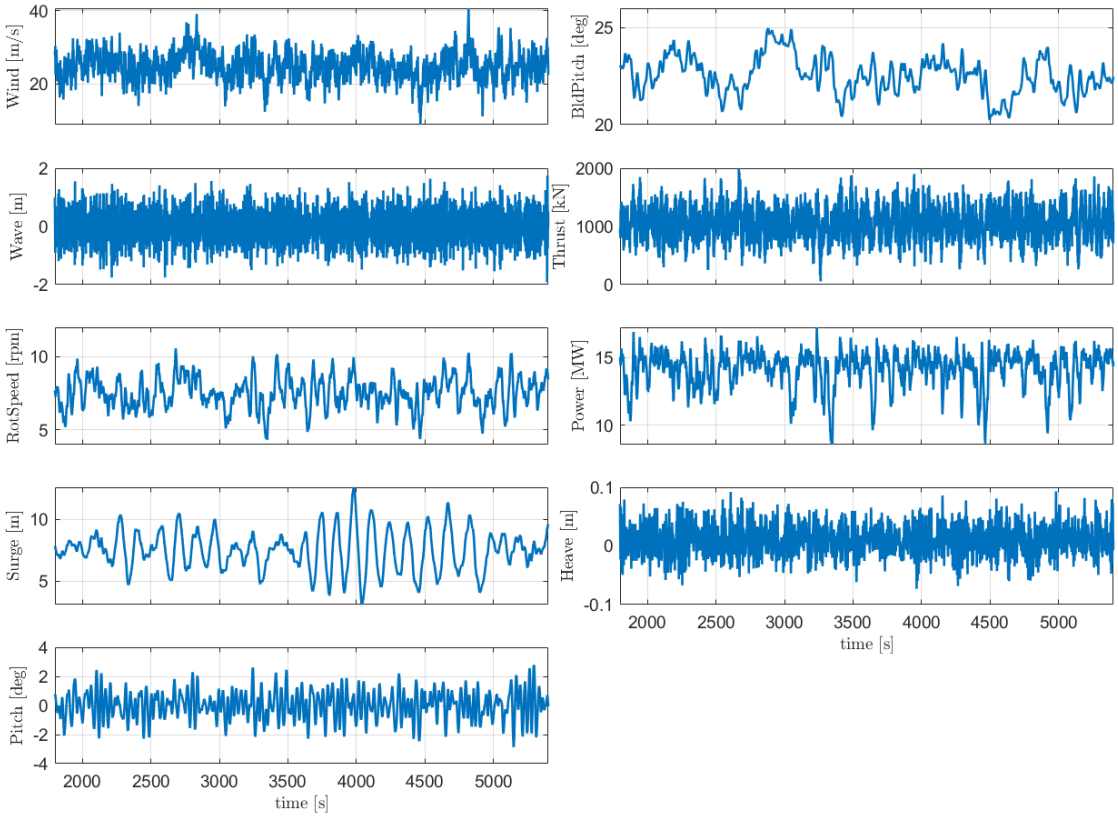
Wind [m/s]
BldPitch [deg]
Wave [m]
Thrust [kN]
RotSpeed [rpm]
Power [MW]
Surge [m]
Heave [m]
Pitch [deg]
time [s]
time [s]

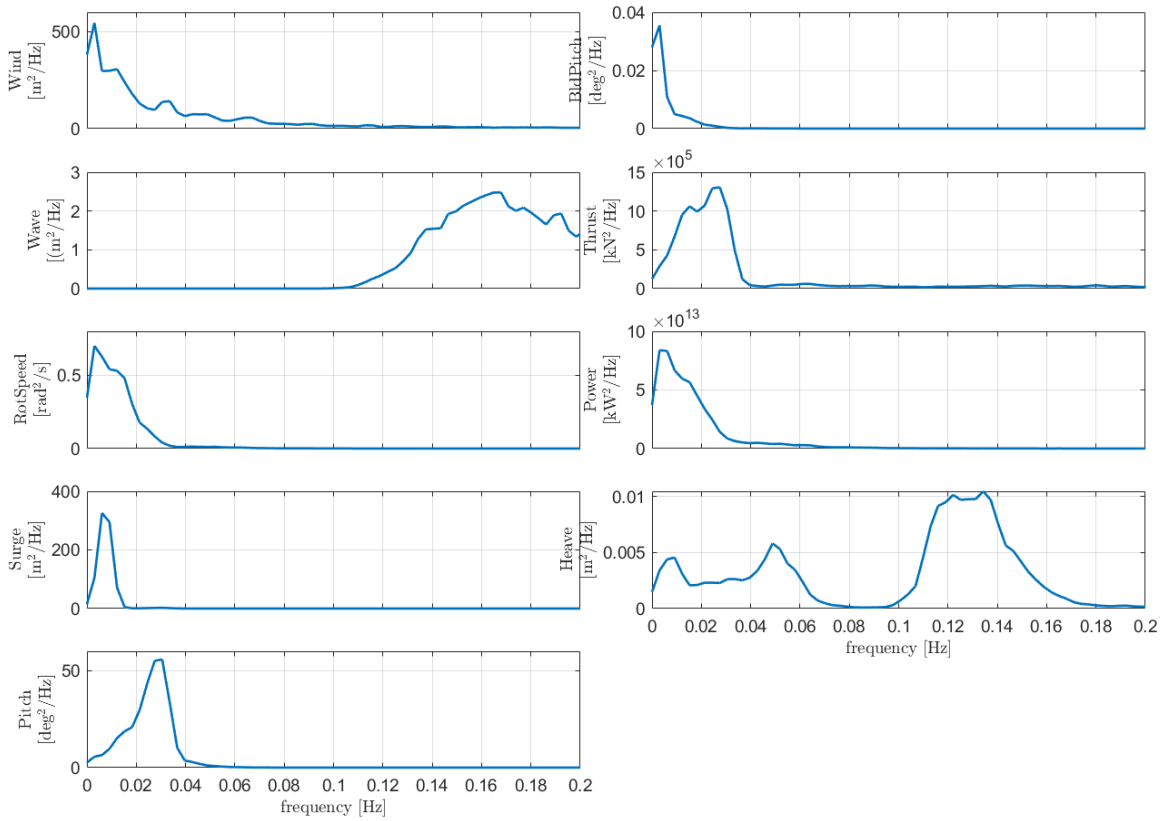
Wind [m²/Hz]
BldPitch [deg²/Hz]
Wave [(m²/Hz]
Thrust [kN²/Hz]
RotSpeed [rad²/s]
Power [kW²/Hz]
Surge [m²/Hz]
Heave [m²/Hz]
Pitch [deg²/Hz]
frequency [Hz]

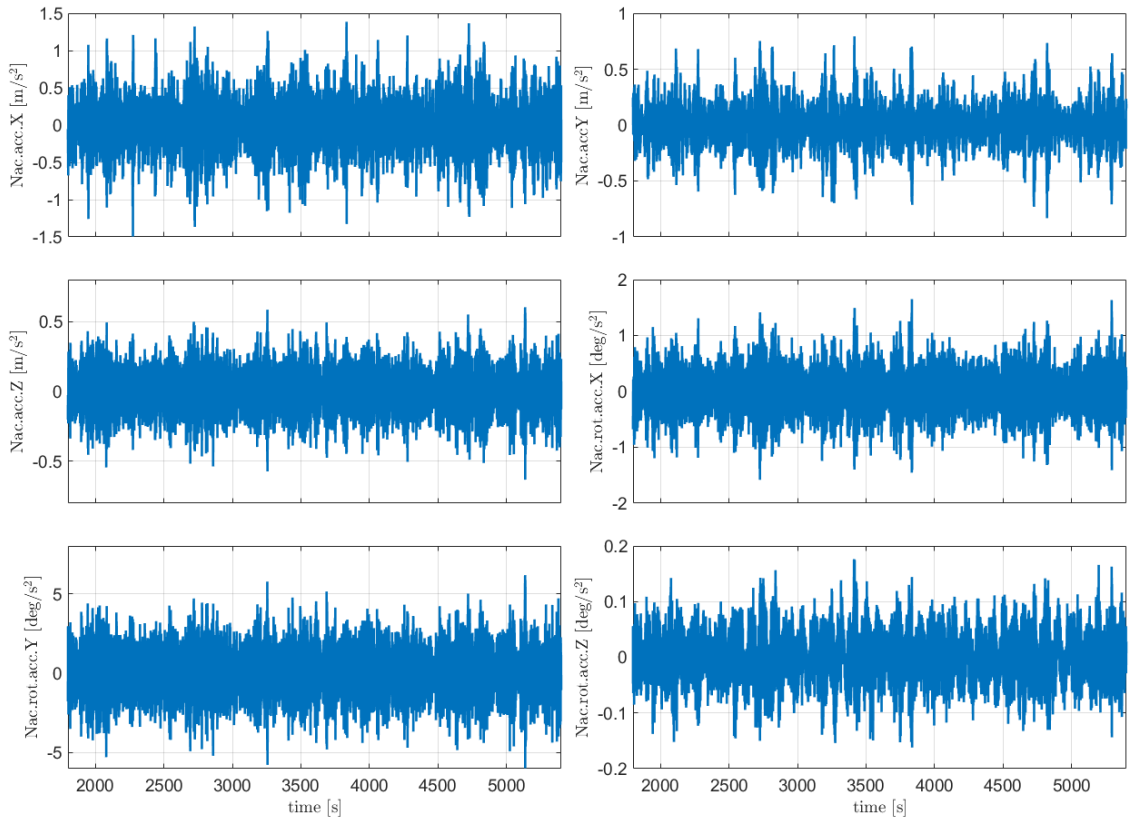
Nac.acc.X [m/s²]
Nac.accY [m/s²]
Nac.acc.Z [m/s²]
Nac.rot.acc.X [deg/s²]
Nac.rot.acc.Y [deg/s²]
Nac.rot.acc.Z [deg/s²]
time [s]

10.2.2 Normal turbulence wind and extreme stochastic waves (DLC 1.6)

- 8m/s

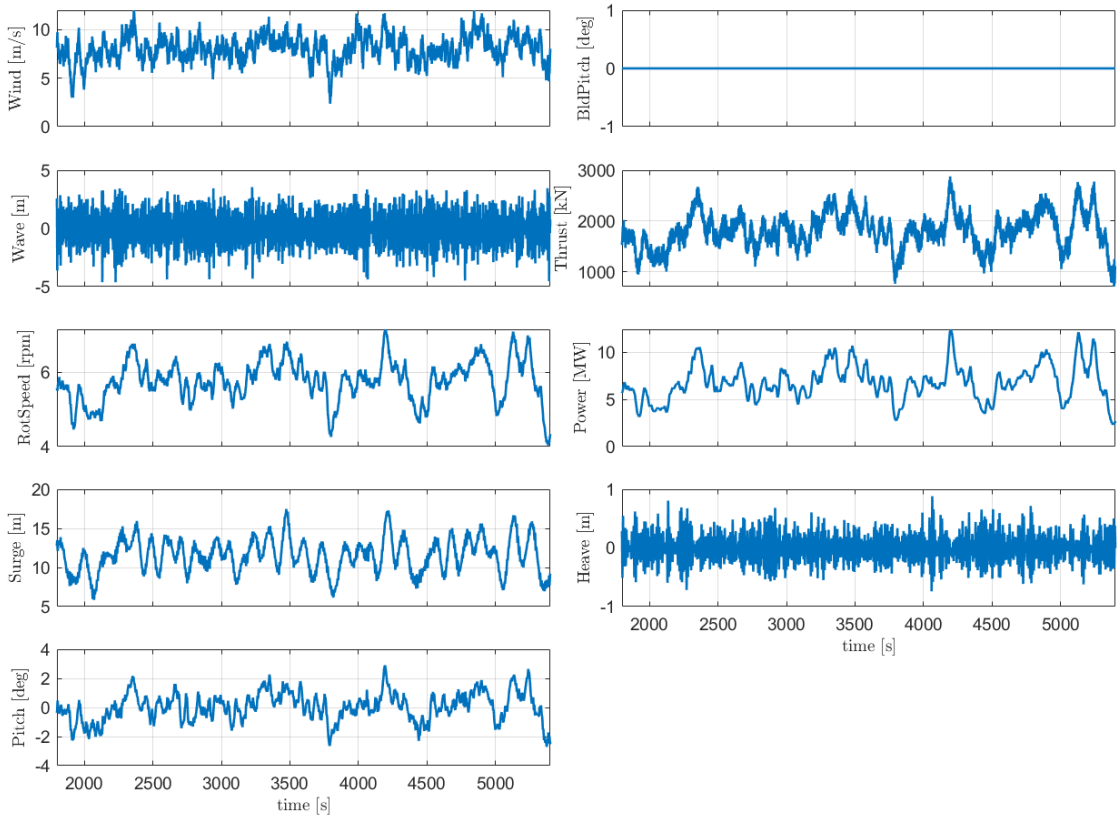

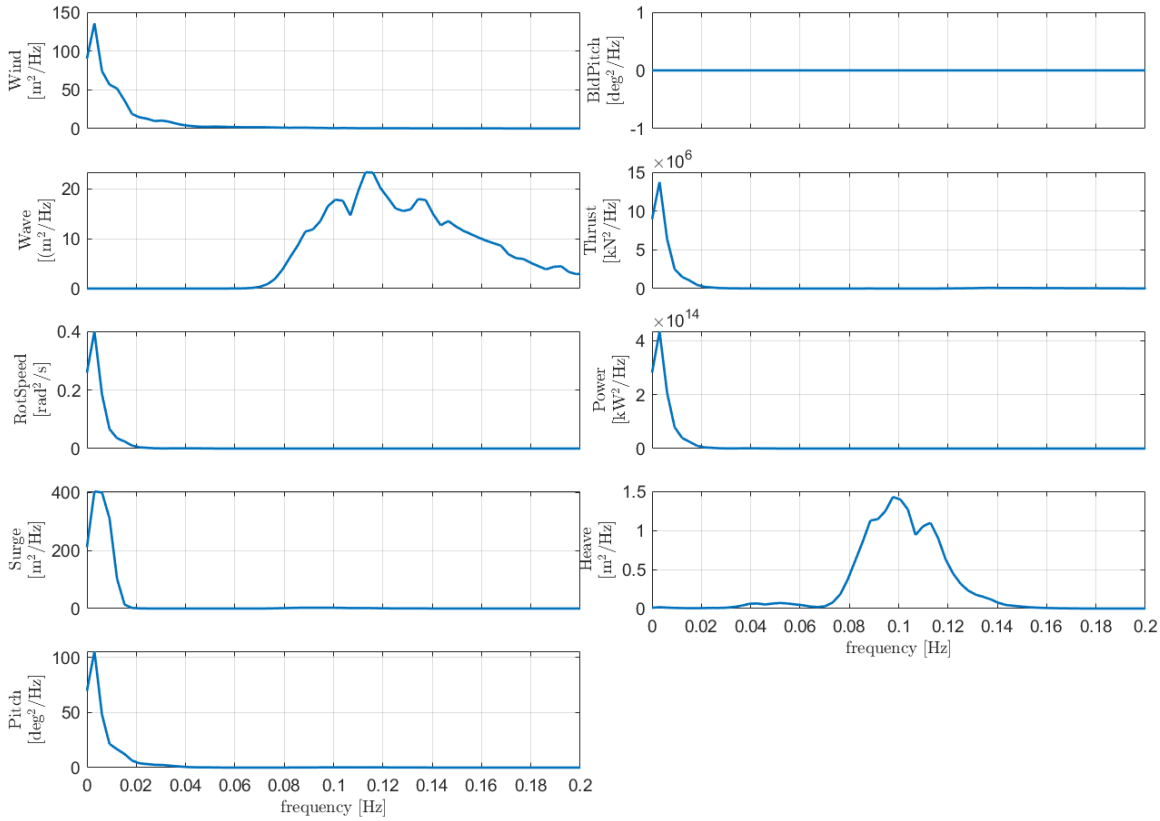
Wind [m²/Hz]
BldPitch [deg²/Hz]
Wave [(m²/Hz]
Thrust [kN²/Hz]
×10^6
RotSpeed [rad²/s]
Power [kW²/Hz]
×10^14
Surge [m²/Hz]
Heave [m²/Hz]
Pitch [deg²/Hz]
frequency [Hz]

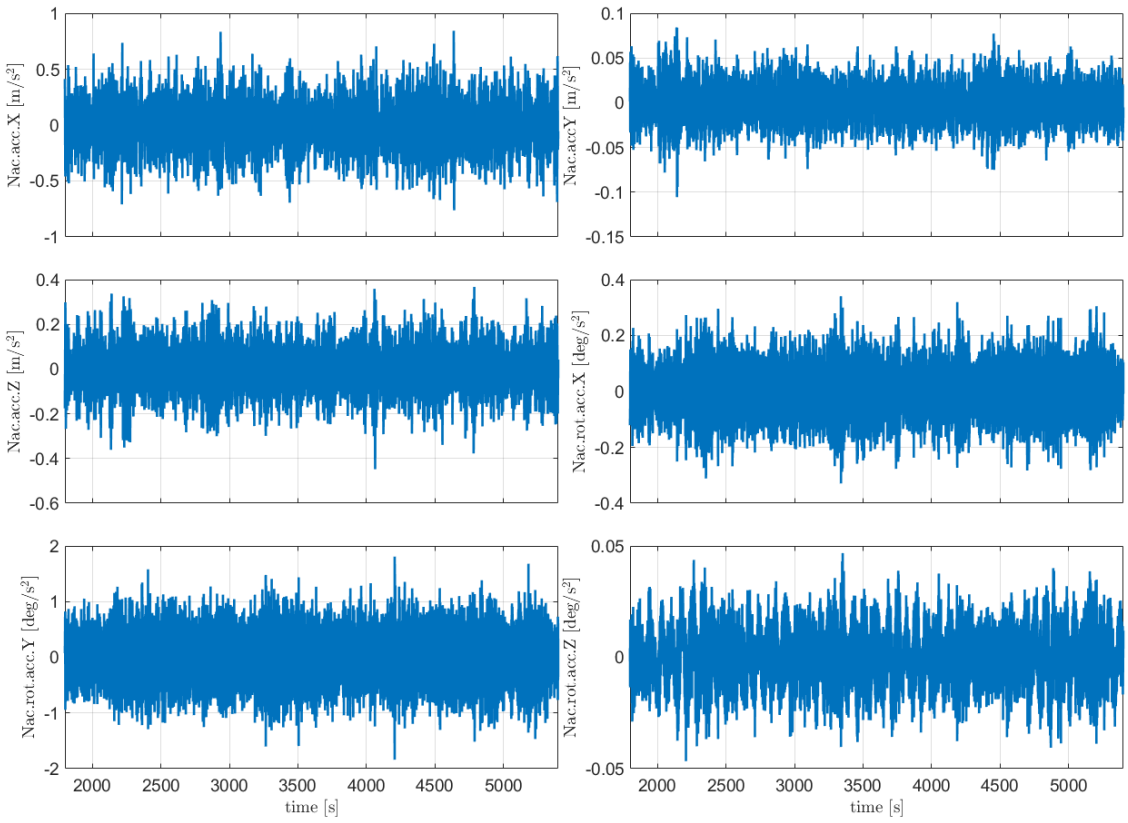
Nac.acc.X [m/s²]
Nac.acc.Y [m/s²]
Nac.acc.Z [m/s²]
Nac.rot.acc.X [deg/s²]
Nac.rot.acc.Y [deg/s²]
Nac.rot.acc.Z [deg/s²]
time [s]

- 16m/s

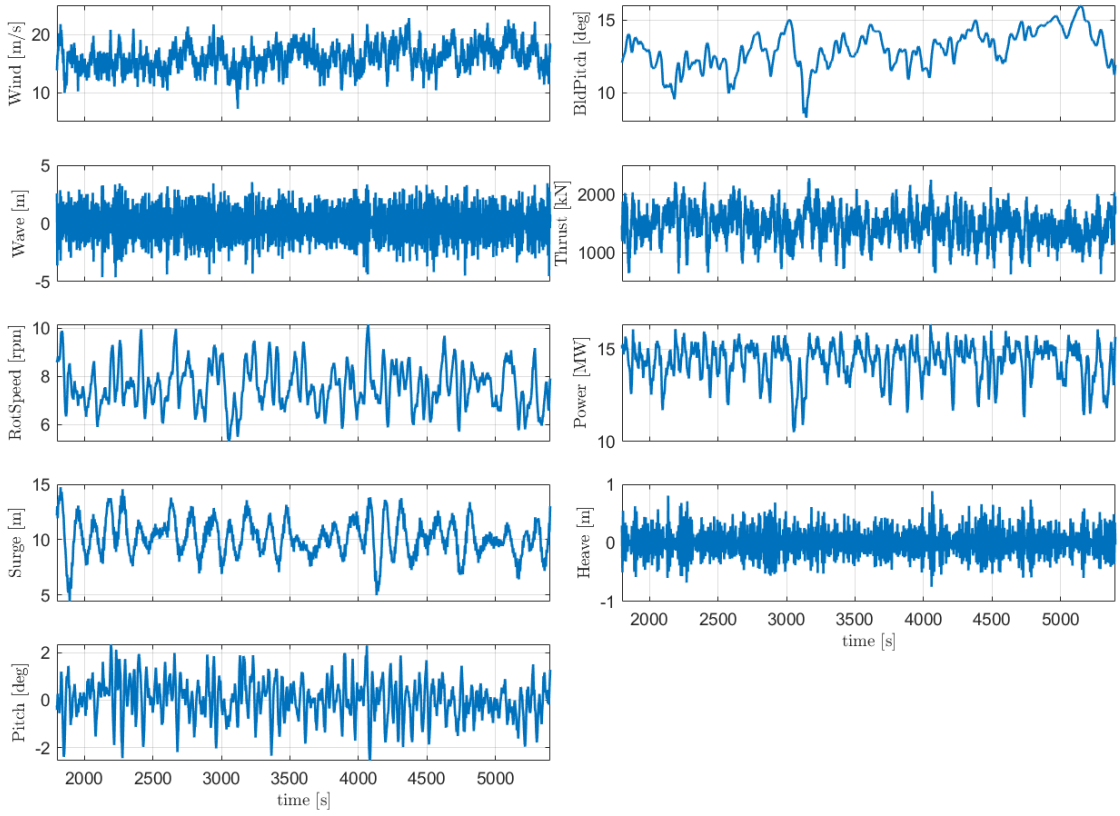
Wind [m/s]
BldPitch [deg]
Wave [m]
Thrust [kN]
RotSpeed [rpm]
Power [MW]
Surge [m]
Heave [m]
Pitch [deg]
time [s]
time [s]

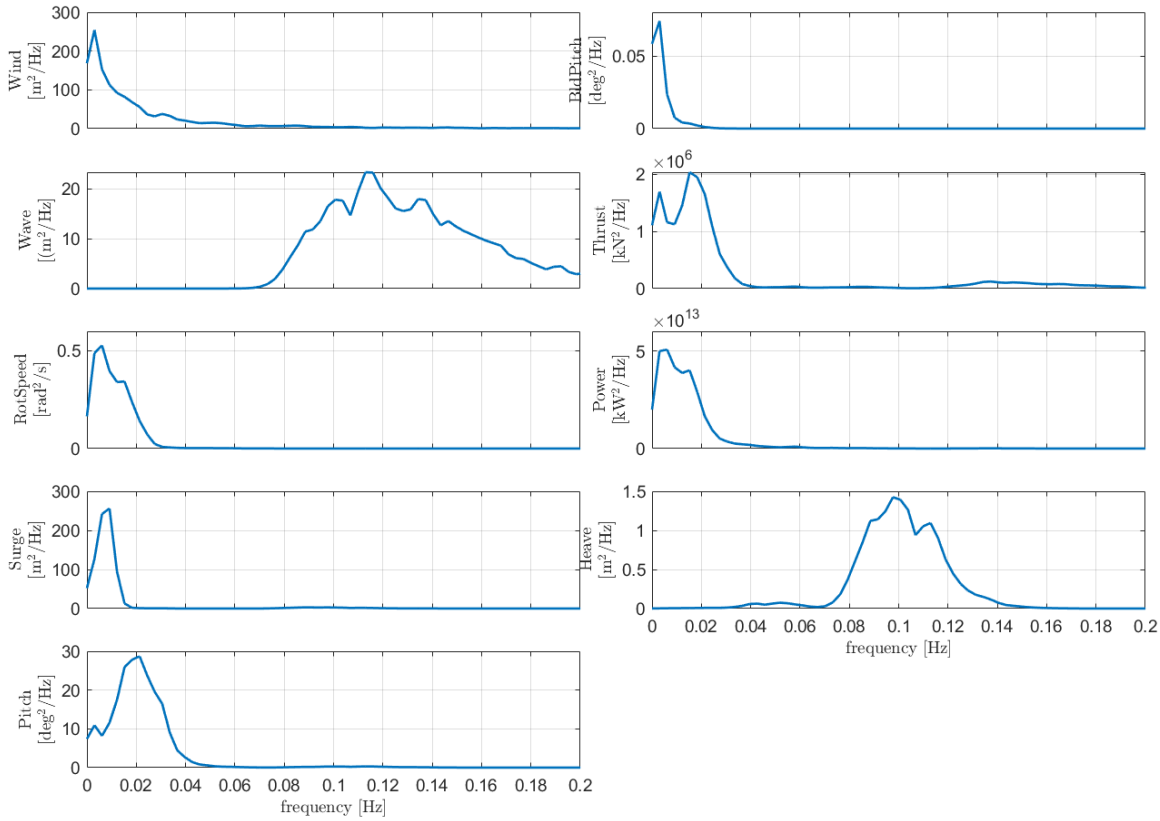
Wind [m²/Hz]
BldPitch [deg²/Hz]
Wave [(m²/Hz]
Thrust [kN²/Hz]
RotSpeed [rad²/s]
Power [kW²/Hz]
Surge [m²/Hz]
Heave [m²/Hz]
Pitch [deg²/Hz]
frequency [Hz]

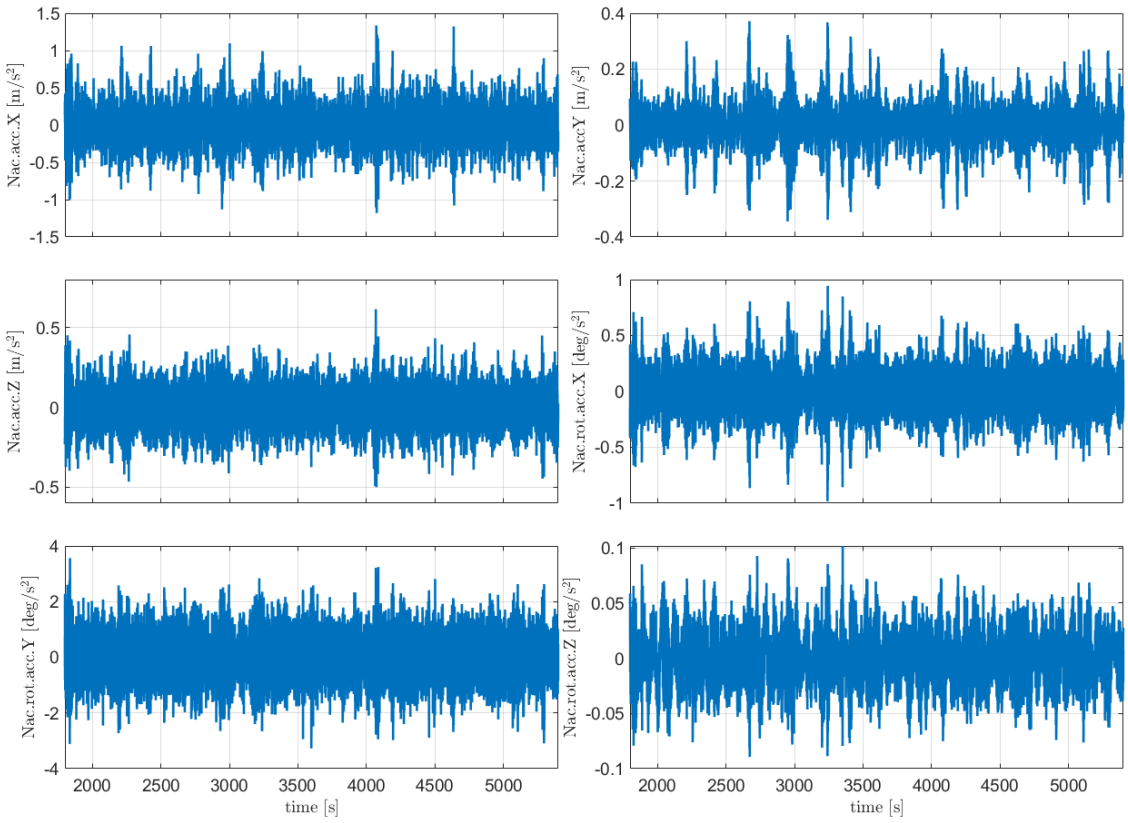
Nac.acc.X [m/s²]
Nac.acc.Y [m/s²]
Nac.acc.Z [m/s²]
Nac.rot.acc.X [deg/s²]
Nac.rot.acc.Y [deg/s²]
Nac.rot.acc.Z [deg/s²]
time [s]

- 20m/s

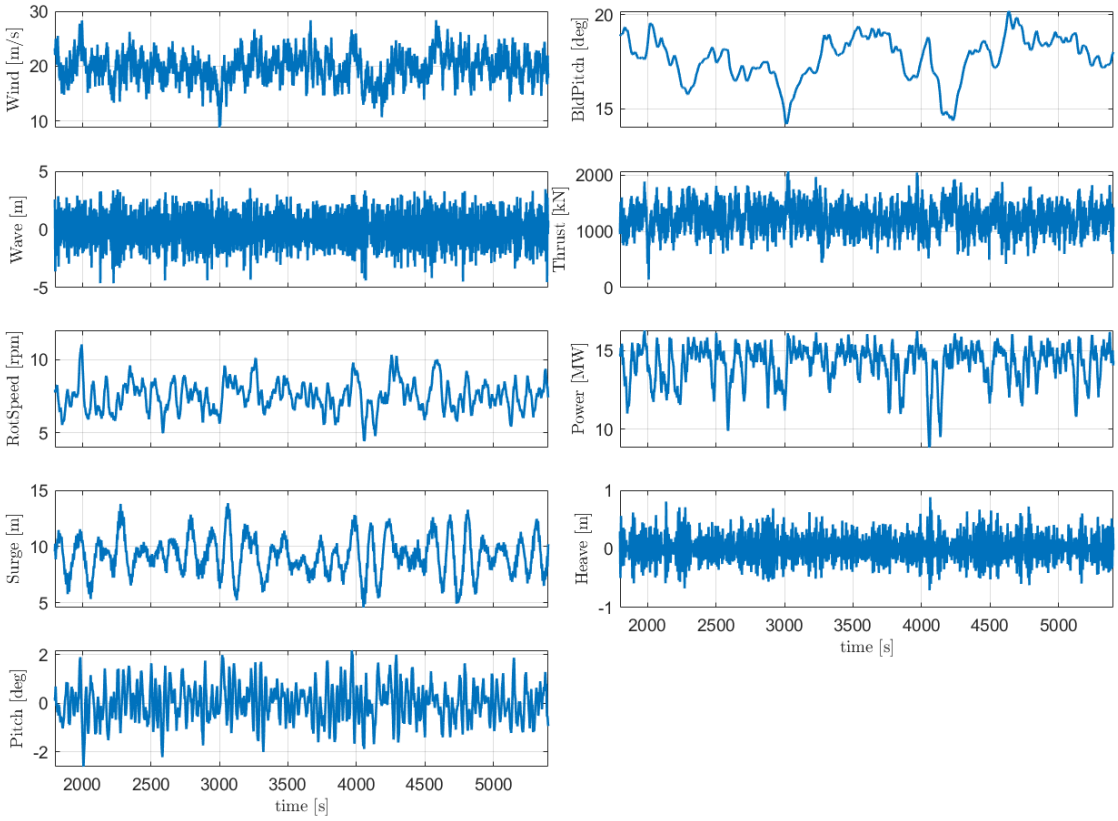
Wind [m/s]
BldPitch [deg]
Wave [m]
Thrust [kN]
RotSpeed [rpm]
Power [MW]
Surge [m]
Heave [m]
Pitch [deg]
time [s]
time [s]

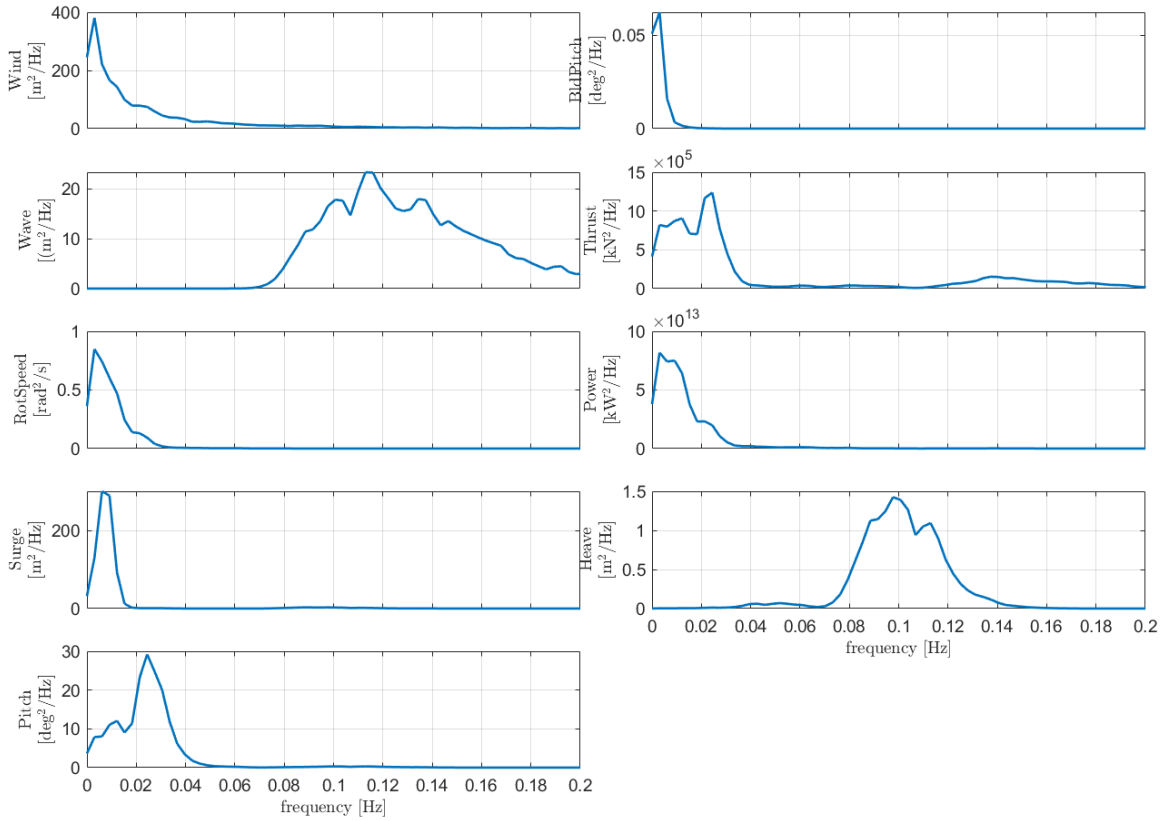
Wind [m²/Hz]
BldPitch [deg²/Hz]
Wave [(m²/Hz]
Thrust [kN²/Hz]
RotSpeed [rad²/s]
Power [kW²/Hz]
Surge [m²/Hz]
Heave [m²/Hz]
Pitch [deg²/Hz]
frequency [Hz]

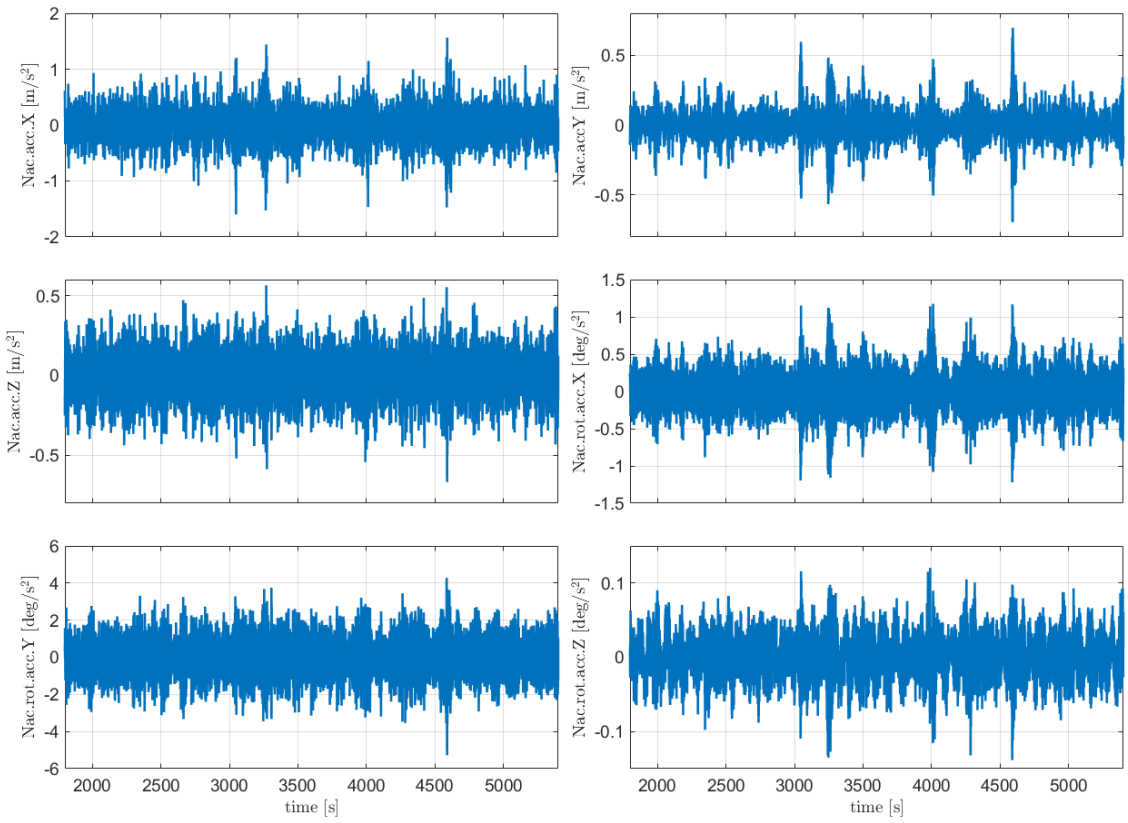
Nac.acc.X [m/s²]
Nac.accY [m/s²]
Nac.acc.Z [m/s²]
Nac.rot.acc.X [deg/s²]
Nac.rot.acc.Y [deg/s²]
Nac.rot.acc.Z [deg/s²]
time [s]

- 25m/s

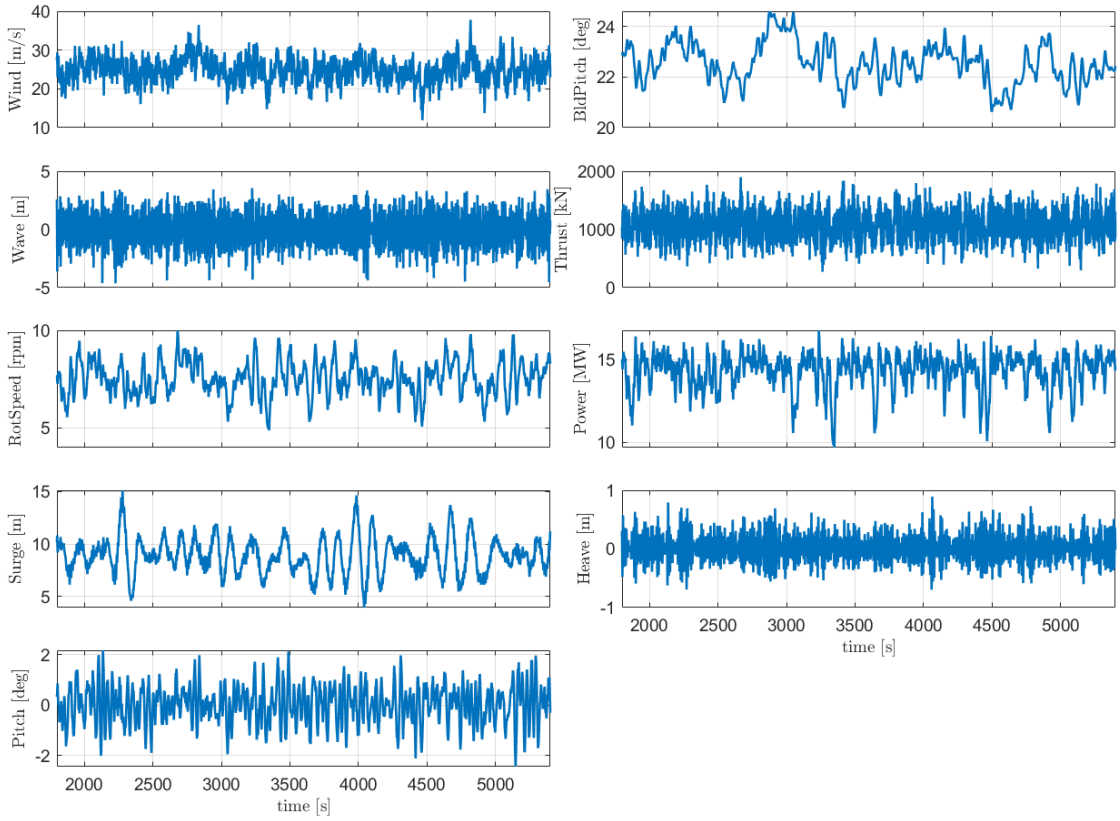
Wind [m/s]
BldPitch [deg]
Wave [m]
Thrust [kN]
RotSpeed [rpm]
Power [MW]
Surge [m]
Heave [m]
Pitch [deg]
time [s]
time [s]

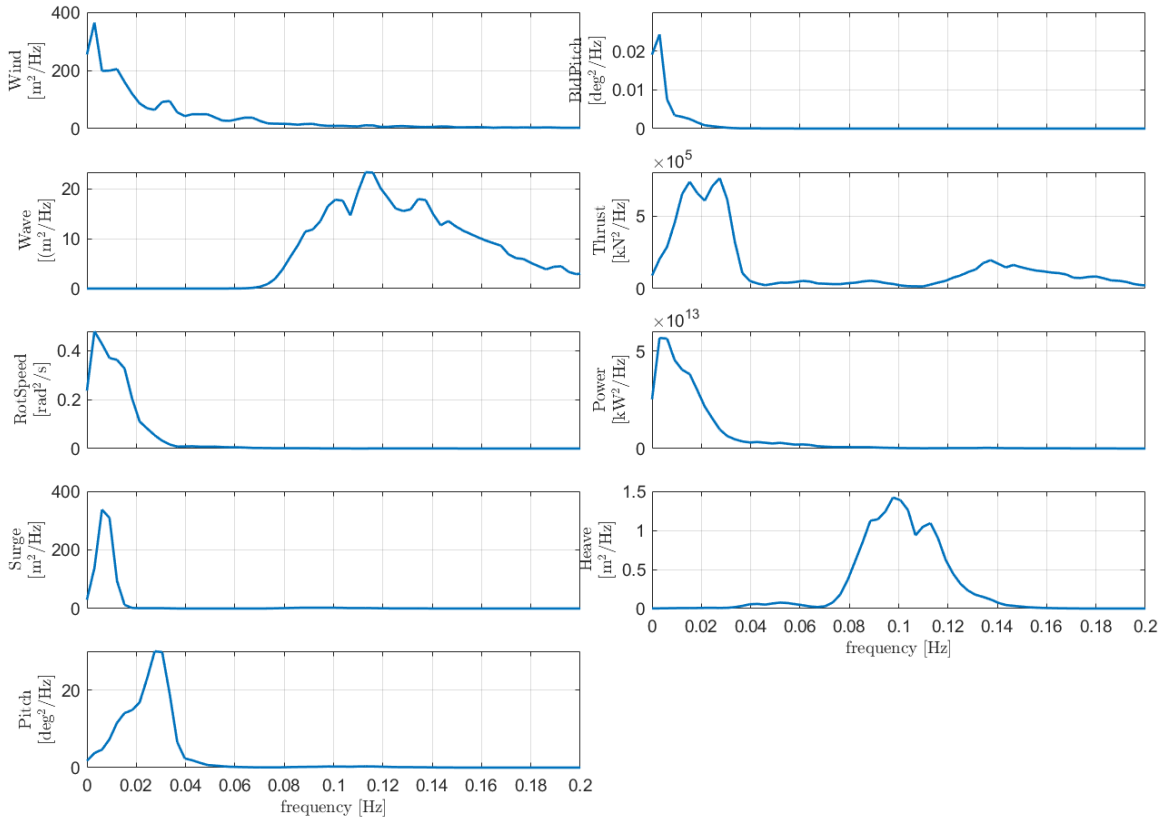
Wind [m²/Hz]
BldPitch [deg²/Hz]
Wave [(m²/Hz]
Thrust [kN²/Hz]
RotSpeed [rad²/s]
Power [kW²/Hz]
Surge [m²/Hz]
Heave [m²/Hz]
Pitch [deg²/Hz]
frequency [Hz]

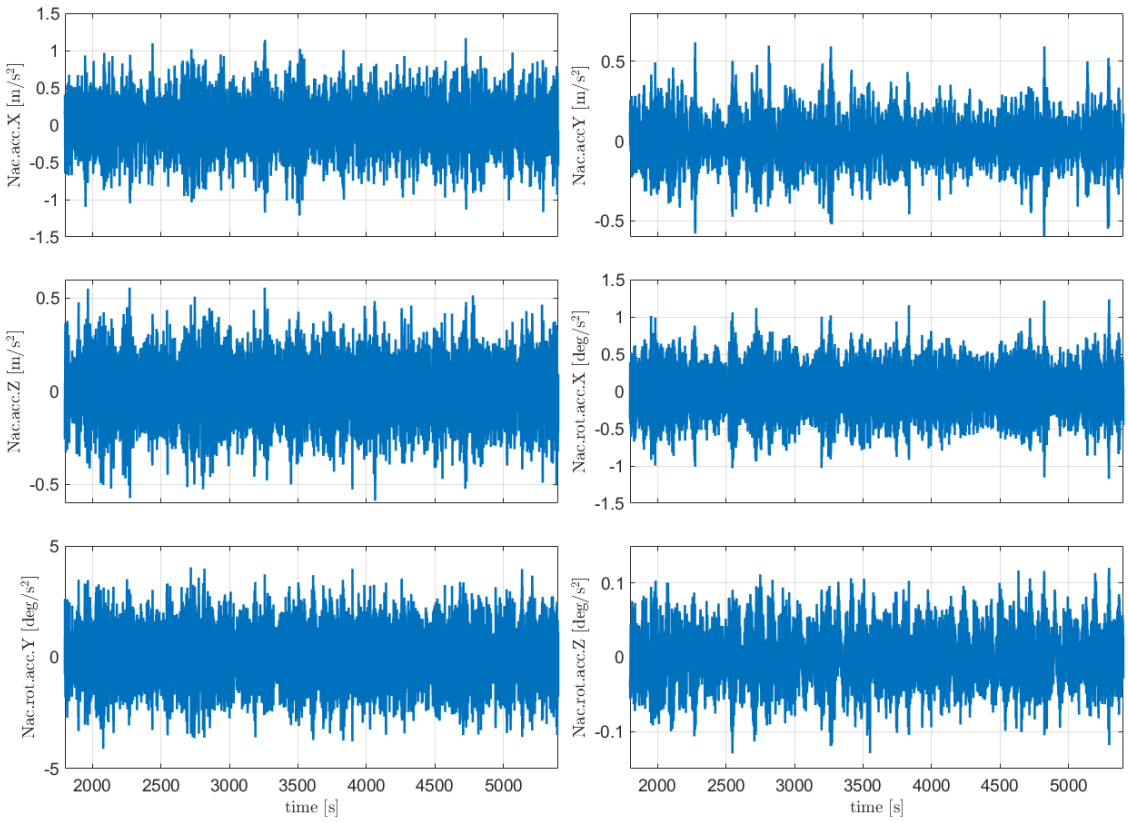
Nac.acc.X [m/s²]
Nac.acc.Y [m/s²]
Nac.acc.Z [m/s²]
Nac.rot.acc.X [deg/s²]
Nac.rot.acc.Y [deg/s²]
Nac.rot.acc.Z [deg/s²]
time [s]